THEORETICAL STUDY OF THE ELECTRONIC STRUCTURE OF COVALENT SOLIDS AND DOPED SEMICONDUCTORS

by

PRADEEP KUMAR KHOWASH

DEPARTMENT OF PHYSICS
INDIAN INSTITUTE OF TECHNOLOGY KANPUR

JUNE, 1985

THEORETICAL STUDY OF THE ELECTRONIC STRUCTURE OF COVALENT SOLIDS AND DOPED SEMICONDUCTORS

A Thesis Submitted
In Partial Fulfilment of the Requirements
for the Degree of

DOCTOR OF PHILOSOPHY

by

PRADEEP KUMAR KHOWASH

to the

DEPARTMENT OF PHYSICS
INDIAN INSTITUTE OF TECHNOLOGY KANPUR
JUNE, 1985

Dedicated to

MY PARENTS

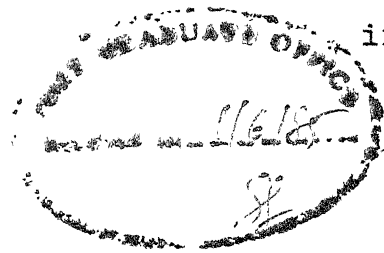

CERTIFICATE

Certified that the work contained in this thesis entitled, "Theoretical Study of the Electronic Structure of Covalent Solids and Doped Semiconductors" has been carried out by Mr.Pradeep Kumar Khowash under my supervision and the same has not been submitted elsewhere for a degree.

Kanpur

June, 1985.

(D.C. Khan)
Professor
Department of Physics
Indian Institute of Technology
Kanpur

ACKNOWLEDGEMENTS

It gives me a great pleasure to express my deep sense of gratitude to Professor D.C.Khan for his able guidance, untiring involvement and his contribution towards my deeper understanding of the problem at hand, Physics in general and what may be called the life of intellect.

I express my sincerest gratitude to Dr.Vijay A.Singh for his involvement and personal interest in the later part of this work. His help and encouragement will always be a pleasant memory.

I thank Dr.J.K.Sharma for helping me in Computer Programming. I am indebted to my teachers both in Visva-Bharati and IIT Kanpur who took keen interest in my academic work.

The warmth and friendship and many stimulating discussions (academic and otherwise), I enjoyed in the company of M/S. S.B.Roy, P.Thakur, G.Mukherjee, T.D.Godhwani and Drs.A.K.Ganguly, D.Chowdhury, Atul Sen, M.Pal and Miss Anshu Agarwal will ever remain in my memory. I cherish with happiness the enthusiastic interest of Miss Mili Datta for the progress of this work.

The affectionate interest of Mrs.S.Khan in my well-being and progress and the warm hospitality I received from Drs.A.Mukherjee, A.K.Majumdar, S.C.Sen and their families during

my stay at IIT Kanpur, shall always remain memorable.

I appreciate the very efficient roles played by M/S. U.S.Misra (typing), A.Ganguly and G.S.Thapa (tracing), H.K.Panda and L.S.Rathore (cyclostyling) in their respective areas to enable me to present the work in a decent form.

I would like to express my deep gratitude to my parents without whose blessings and encouragement I could have never completed this work. The constant emotional support from my brother Kishore and sister Shukla will always remain a happy memory.

PRADEEP KUMAR KHOWASH

CONTENTS

LIST OF TABLES

LIST OF FIGURES

SYNOPSIS

THEORETICAL STUDY OF THE ELECTRONIC STRUCTURE OF COVALENT SOLIDS AND DOPED SEMICONDUCTIONS

by

PRADEEP KUMAR KHOWASH
Department of Physics
Indian Institute of Technology
Kanpur

The aim of the present work is to study theoretically the electronic structure of a number of ionic, covalent and semiconductor solids, using MS X_α SCF method. The valence electron energy levels and the equilibrium charge distribution of all these systems are analyzed to get informations on their bonding characteristics, optical properties and electrical conductivity.

The MS X_α method is briefly described in Chapter I. The method considers a cluster of atoms or ions scopped out of the solid and replaces the effect of the rest of the solid by putting proper charges on the boundary of the cluster (i.e., on the Watson sphere). This is expected to simulate the localized physics in the solid to a good approximation. The cluster is divided into atomic regions, interatomic region and extramolecular region. One assumes a muffin-tin approximation to the potential for each atom in the cluster.

The potential is spherically averaged within each atomic region and in the region outside the Watson sphere. In the interatomic region the potential is volume averaged. The exchange potential is taken in the local X_α approximation ($\rho^{1/3}$) of Slater. The basis wave functions as solutions of Schrödinger equation are obtained in the atomic regions, the interatomic region and in the extramolecular region. The Wronskian on the boundaries are set to zero in order to obtain the energy eigenvalues, and consequently the eigenfunctions. The calculation is performed self-consistently. The name multiple scattering theory comes from the fact that the wave function in the interatomic region is built with the waves scattered from the different atomic sites. The exchange parameter α are due to Schwartz.

In Chapter II, the MS X_αSCF method of calculation is applied to systems like ionic solids (NaCl, LiF, NaF), perovskites (KMF_3 (M = Fe, Ni)), rutiles (MF_2 (M=Fe,Co,Ni,Zn)), metallic oxides (MgO, MnO, VO) and alloys (Fe-Te). Along with the energies the charges within each atomic region are calculated. A charge transfer diagram is defined to understand the chemical bonding (ionic and/or covalent) in these systems. The 3d degenerate level of the cation breaks up into t_{2g} and e_g levels in the ligand field. The crystal field splitting, 10 Dq, is determined for crystals with 3d cation and compared with experiment wherever data are available. The transitions

between two of the valence levels are calculated wherever the corresponding XPS or optical spectroscopic experimental data are available. Finally, the Mössbauer isomer shifts are calculated for iron containing samples.

The self-consistent charge distribution study in ionic solids like NaCl, NaF, LiF shows a transfer of charge from the central ion to the ligands along with some transfer to the interatomic region. This indicate that these well known ionic compounds are not perfectly ionic but show a marginal covalent character. For NaCl the calculated charge distributions are in very good agreement with the experimental results. The energy levels of LiF and NaF bunch into two groups with predominantly F 2s and F 2p character. The energy difference of the F 2s - like and F 2p - like states in LiF is 1.43 Ry as compared to the experimental result of 1.54 Ry obtained by XPS.

The energy levels and the charge distributions are, then, calculated for fluorides and oxides of the different transition metals. The agreement of the energy difference of 1.36 Ry of the F 2s - like and F 2p - like states in FeF_2 with the XPS result 1.54 Ry is encouraging. The crystal field splitting, 10 Dq, is also calculated for the transition metal fluorides. The Mg 2s and Mg 2p levels are identified and their energy difference 2.85 Ry is found to be in fair agreement with the XPS data 2.38 Ry.

The Mössbauer isomer shifts in all the iron containing systems, namely $KFeF_3$, FeF_2 and $Fe_{0.4}Te_{0.6}$ alloy are calculated and compared with the existing results from the experiments.

The first step towards the analysis of the covalent nature of the systems is to calculate the covalency parameter λ_σ from the coefficient of the ligand term in the extended eigenfunction of the uppermost valence level. These values are matched with the λ_σ obtained from the analysis of the neutron diffraction and nuclear magnetic resonance experimental data in terms of the molecular orbital theory. Satisfactory agreements are obtained for $KFeF_3$ and $KNiF_3$. For $KFeF_3$ our results are $\lambda_\sigma = 5.58\%$ as against the neutron diffraction data $\lambda_\sigma = 6.24\%$. For $KNiF_3$ they are 7.55% and 5.11% respectively. The value of λ_σ for MgO is 6.67 percent which is in good agreement with the ENDOR value of 6.50 percent.

The concept of pseudoatoms is then brought in and the charge transfer from and/or to these atoms are calculated to plot the charge transfer diagrams for all the solids studied by us. With the help of these diagrams, the measures of ionic bonding strength and covalent bonding strength for these systems are defined. One finds that the natural state of the non-metallic solid is a mixed ionic-covalent state. In NaCl the ionic is the dominant bonding and covalent bonding is marginal whereas in FeF_2 the covalent bond strength is very large and ionic bonding is marginal. The transition metal

perovskites and rutiles generally fall within these two limits. However, they are predominantly covalent. The oxides of the transition metals also show very large values of covalent bond strength with different degrees of minor ionic character. MgO is an exception to this general character in that it has a small charge transfer from the anion to the cation. This type of charge transfer, referred to as inverse ionic character, is typical of semiconductors. MgO is known to behave as a semiconductor. Inverse ionic character along with large covalency is seen in all semiconductors e.g.Si, InP, GaAs and transition metal impurities in InP.

In Chapter III, the MS X_αSCF method was applied to semiconductors, especially transition metal doped InP, with a view to study the localization of the levels within the band gap. The cluster model has been applied to the canonical semiconductors such as Si and GaAs. It is well known that Cr make GaAs semi-insulating. A similar role played by Fe in InP is expected and so the selfconsistent field energy levels and their eigenfunctions are worked out. Detailed calculations predict a highly localized impurity level for Fe in InP.

For the other transition metal impurities in InP, the impurity levels are either closer to the valence band or conduction band edges. These states thus hybridize with the host and become delocalized as compared to Fe in InP. Very recent experiments on Fe and Co in InP confirms a higher

localization of the former leading to a higher resistivity.

The calculations of the different charge states of Fe in InP are also performed. The t_2^{DBH}-level, arising due to broken bonds, find its place in the mid gap for neutral Fe, whereas it moves closer to the band edges for the other two charged states. The charge transfer is minimum for neutral Fe. The isomer shift for different charge states are calculated but unfortunately no experimental data are available to compare with. However, these results also confirm that neutral Fe makes InP semi-insulating.

The electronic structure of the alkali metals as impurities in InP are also calculated. It is seen that they interact weakly with the host thus pinning the impurity level in the gap.

It is predicted that GaAs may soon supercede Si in technological importance. Since the devices made out of InP are much faster than those of Si, it is expected that InP is going to be a keen competitor to GaAs as a device material. This work forms the theoretical basis for the analysis of the conductivity properties of transition metal doped InP.

In conclusion, we hope that the present work has extended our knowledge of the electronic structure of covalent solids and semiconductors with impurities, especially of their bonding characteristics.

* . . . * . . . . *

...for an atom of N electrons, the solution is a function of 3N variables, and even if it were possible to evaluate such a solution to any degree of numerical accuracy required, no satisfactory way of presenting the results, either in tabular or graphical form, is known. It has been said that the tabulation of one variable requires a page, of two variables a volume, and of three variables a library; but the full specification of a single wave function of neutral Fe is a function of seventy-eight variables. It would be rather crude to restrict to ten the number of values of each variable at which to tabulate this function, but even so, full tabulation of it would require 10^{78} entries, and even if this number could be reduced somewhat from considerations of symmetry, there would still not be enough atoms in the whole solar system to provide the material for printing such a table.

D.R. Hartree, Reports on Progress in Physics, Vol.11 (London: The Physical Society, 1947), p. 113.

* . . . . . * . . . . . *

CHAPTER I
MS X_α SCF METHOD
INTRODUCTION

In the present work we have used the Multiple Scattering X_α Self Consistent Field (MSX SCF) method [1] to study theoretically the electronic structure of covalent solids and semiconductors with transition metal impurities. The valence electron energy levels and their eigenfunctions have been obtained and analyzed to get informations on their bonding characteristics, optical properties and electrical conductivity.

The MS X_αSCF method considers a cluster scooped out of the solid. The effect of rest of the solid is simulated by enclosing the cluster by a sphere, called the Watson sphere, and putting proper charges on the boundary of the sphere to make the cluster electrically neutral. The potential within each non-overlapping atomic sphere is taken in the muffin-tin form. The potential is spherically averaged within each atomic region and in the region outside the Watson sphere and volume averaged in the inter atomic region. The exchange potential is taken as $\rho^{1/3}$ as given by Slater [2]. The basis wave functions for a solution of the Schrödinger equation are obtained in the atomic regions, interatomic region and in the extramolecular region. The Wronskian at the boundaries of the region are then set to zero in order to obtain the energy eigen values. The calculation is performed self-

consistantly.

We applied this method of calculation to systems like perovskites (KMF_3 (M = Fe, Ni)), rutiles (MF_2 (M=Fe,Co,Ni,Zn), ionic solids (NaCl,LiF, NaF), metallic oxides (MgO,MnO,VO) and alloys (Fe-Te). Along with the SCF energies the charges within each atomic region are also calculated. A charge transfer diagram was defined to get an understanding of the chemical bonding (ionic and/or covalent) in these samples. The 3d degenerate level breaks up into t_{2g} and e_g levels in the presence of a crystal field. The splittings are found to be in good agreement with the experiments. The isomer shift was calculated for the iron containing samples.

The transition metals are known to introduce levels deep in the band gap of the host semiconductors [3-5], called the deep impurity states. They play a very important role in modifying the electronic properties of the semiconductor. The III-V materials have a very promising technological future since the devices made out of them are much faster than those made out of silicon. We performed a MS X_α SCF calculation for pure and doped InP for the first time. The transition metals used as impurities were Cr, Mn, Fe, Co, Ni and Cu. The electronic structure shows that the dangling bond hybrid level, t_2^{DBH}, is pulled down as the atomic number increases, owing to the greater attractive potential. This t_2^{DBH} -level is exactly in the middle of the band gap for Fe in InP. This provides a clue to the semi-insulating behaviour of Fe in InP.

A very recent experiment (1984) shows the resistivity of Fe doped InP to be larger than Co doped InP. The different charge states of Fe in InP was studied to have a detailed understanding of the semi-insulating behaviour. The alkali-metals were also doped in InP to find out if they passivate the dangling bonds arising due to vacancy.

I.1 One Electron Approximation Methods

In a system of N electrons and M nuclei (assumed to be at rest), each electron moves in the electric field produced by all (N-1) electrons and all the nuclei. For N greater than a very small number, a rigorous solution is impossible. By averaging the density of (N-1) electrons over their complex motions and finding the electric field from this average density helps one in reducing the many body system to a single body problem. The individual electrons then move in a fixed external field and their wave functions as found from the solutions of Schrödinger equation (SE) are called orbitals - atomic orbitals for atomic case and molecular orbitals for molecules or crystals.

The atomic orbital problem is somewhat simple because of its spherical symmetry. However, the SE for even one of the MO's is difficult to solve. The only basic simplifying feature there is the point group symmetry of the molecule or the cluster which simulates the basic features of the crystal. Consider a system of nuclei with coordinates

$\bar{R}_A$ and charge Z_A and masses M_A and electrons with coordinates $\bar{r}_i$. The time independent SE in atomic units (a.u., $\hbar=e=m_e=1$) is

$$H(\bar{R}_A, Z_A, M_A, \bar{r}_i) U_i(\bar{R}_A, \bar{r}_i) = E\, U_i(\bar{R}_A, \bar{r}_i) \qquad (1.1)$$

We restrict to spin free non-relativistic Hamiltonian. Our basic interest is in the electronic orbitals. Using Born-Oppenheimer approximation

$$H_{el} U_{el}(\bar{r}_i, \bar{R}_A) = E_{el}(\bar{R}_A) U_{el}(\bar{r}_i, \bar{R}_A) \qquad (1.2)$$

where

$$H_{el}(\bar{R}_A) = \sum_i -\frac{1}{2}\nabla_i^2 + \sum_i \sum_A -\frac{Z_A}{r_{iA}} + \sum_{i>j} \frac{1}{r_{ij}} + \sum_{A>B} \frac{Z_A Z_B}{R_{AB}} \qquad (1.3)$$

The electronic wave functions $U_{el}(\bar{r}_i, \bar{R}_A)$ depends directly on the electronic coordinates and parametrically on the nuclear coordinates. Throughout we will assume that there are no 'slow' electrons or 'fast' nuclei which might lead to strong electron-phonon coupling.

The quantum chemical methods for the solution of equation (1.2) can be broadly divided into four classes.

1. Semi Empirical Methods:
   - Model Hamiltonian
   - Adjustable molecular parameters

e.g., . Hückel - Simple tight binding

Extended Hückel

. CNDO

2. Ab-initio methods:

. Choose a form of U (one or many determinants)

. Choose a set of basis function

. No further fundamental approximation

e.g., . LCAO-MO-SCF (Hartree-Fock)

. Configuration interaction (CI)

. Generalized valence bond (GVB)

3. Psudopotential methods:

. Like ab-initio (or local density) but core electrons are replaced by pseudopotentials

e.g., . SCF, CI, GVB.

4. Local density methods:

. Approximate local exchange correlation potential

e.g., . X_α, LSD

. Roots in density functional theory and theory of electron gas

. Various ways of solving the electron SE

e.g., . LCAO, DVLCAO, SW method.

Instead of considering the whole crystal we can focus our attention on a small cluster whose repetition in space reproduces the crystal as a whole. The symmetry properties of the cluster help in simplifying the complexity of the problem. The most effective part of the cluster calculation

is that it can squeeze out the localized physics quite accurately by approximating the effect of the rest of the solid in a suitable manner.

The importance of cluster calculation relating different fields [6-14] are shown in Figure 1.1.

The various X_α LSD are tabulated as

X_α -SW - Scattered wave

X_α -MS - Multiple scattering

- Muffin-tin potential
- Numerical solutions in spheres
- Partial waves
- Most rapid method
- Accurate orbitals and spectroscopic quantities
- Does not yield total energy curves

X_α -DV - Discrete variational method

- LCAO (Slater orbitals)
- Fit ρ and $\rho^{1/3}$ with auxilliary functions
- Numerical sampling for matrix elements
- Quite rapid-work goes up as m^2 (m=No. of basis sets)
- Very large number of sampling points needed for total energy

LCAO X_α - LCAO (Gaussian orbitals)

- Fit ρ and $\rho^{1/3}$ with auxilliary functions
- Analytical integrals

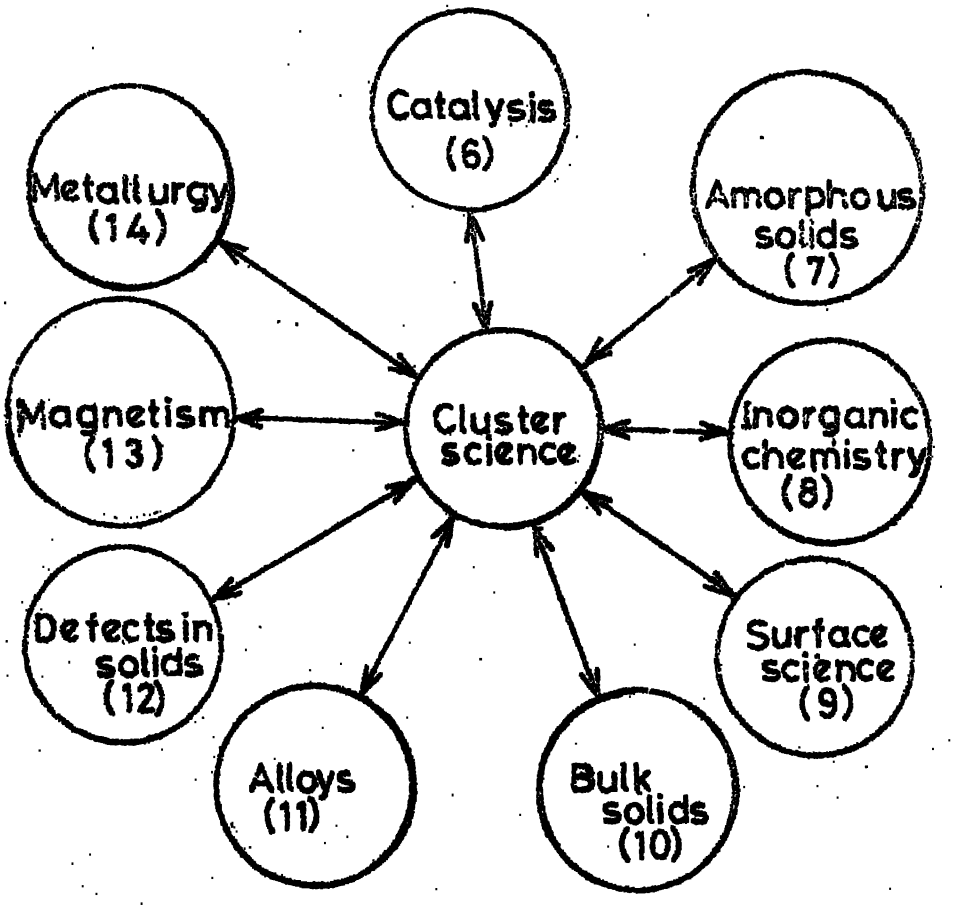

Fig.1.1

Some fields of application of cluster science.

- Slowest of X_α methods - work goes up as m^3
- Accurate total energies

I.2 Hartree and Hartree-Fock Methods

The many electron wave function was written down by Hartree as product of the individual wave functions

$$|U> = \prod_{i=1}^{N} \Phi_i \tag{1.4}$$

The one electron Hartree equation is given by [15]

$$[-\nabla_1^2 + \hat{V}_c(1) + \hat{V}_i(1)]\, U_i(1) = \varepsilon_i U_i(1) \tag{1.5}$$

where,

$$\hat{V}_c(1) = -\frac{2Z}{r_1} + \sum_j n_j \int \frac{U_j^*(2)\, U_j(2)}{|\underline{r}_1 - \underline{r}_2|}\, d\tau_2 \tag{1.6}$$

and,

$$\hat{V}_i(1) = -n_i \int \frac{U_i^*(2)\, U_i(2)}{|\underline{r}_1 - \underline{r}_2|}\, d\tau_2 \tag{1.7}$$

$\hat{V}_c$ is the field arising from the nuclear charge and the total charge density of the electrons in the system and $\hat{V}_i$ corrects the coulombic term for the self interaction of the electron.

The Hartree model ignores the spatial correlation in the motion of any pair of electrons produced by their instantaneous coulomb repulsion. In Hartree-Fock (HF) the coulomb correlations are again ignored but the spin correlation is

introduced through determinantal wave functions in place of equation (1.4). This is called statistical correlation as the electrons obey Fermi-Dirac statistics. This correlation to the coulomb potential made to get an acceptable SCF is called exchange correlation potential which contains those spin dependent exchange effects that are characteristic of anti-symmetry of the wave function and lead to magnetic properties of atomic systems. The neglect of coulomb correlation is corrected in a large measure by the inclusion of statistical correlation.

The Hartree-Fock one electron equation [16,17] is

$$-\left[\nabla_1^2 + \hat{V}_c(1)\right] U_i(1) - \sum_j n_j \int U_j^*(2)\, U_i(2)\, \frac{1}{|\underline{r}_1 - \underline{r}_2|}\, d\tau_2$$

$$U_j(1) = \varepsilon_i\, U_i(1) \qquad (1.8)$$

The last term on the left hand side now includes in addition to self correlation term

$$-\int U_i^*(2)\, U_i(2)\, \frac{1}{|\underline{r}_1 - \underline{r}_2|}\, d\tau_2\, U_i(1), \qquad (1.9)$$

the term

$$-\sum_{i \neq j} n_j \int U_j^*(2)\, U_i(2)\, \frac{1}{|\underline{r}_1 - \underline{r}_2|}\, d\tau_2\, U_j(1) \qquad (1.10)$$

characterized as exchange term. The only non vanishing contribution in equation (1.10) arises from the summation over the orbitals U_j which has the same spin as U_i, owing to the

orthogonality constraints.

This term can be written as

$$\hat{V}_{HFX_i}(1) = \frac{-\sum_j n_j \int U_i^*(1)\, U_j^*(2)\, \frac{1}{|\bar{r}_1 - \bar{r}_2|}\, U_j(1)\, U_i(2)\, d\tau_2}{U_i^*(1)\, U_i(1)} \qquad (1.11)$$

This exchange correlation potential is the potential of a charge whose magnitude is one electronic charge removed from a hole surrounding the location of electron 1. This cnarge which we shall call the "exchange correlation charge", nas the same spin as that of the $i^{\underline{th}}$ spin orbital and has a charge density at the position of the first electron which is just great enough to neutralize the total electronic charge of the spin of the $i^{\underline{th}}$ spin-orbital at that point [18]. This hole termed as Fermi hole [2] accounts for the correlation of the like spin electrons only. So the last term on the left hand side of equation (1.8) should be corrected for the Coulombic correlations of unlike spin electrons.

1.3 Free Electron Exchange Approximation

The Hartree-Fock exchange potential for different occupied orbitals are similar in many respects. So the idea is to form an universal exchange potential by suitably averaging these individual exchange potentials.
The physical nature of average exchange potential avoids calculation of exchange integrals altogether.

Previously the electronic structures were calculated by Thomas-Fermi model where the charge density was treated statistically. Dirac refined the method by adding the exchange terms proportional to the cube root of the charge density. The resulting Thomas-Fermi-Dirac (TFD) model gave a simple good approximation to the potential in an atom. However, it failed to describe binding between atoms in molecules and solids. In practice TFD model was never used as more accurate HF equations could be solved. The major defect of the TFD model was the crude treatment of the kinetic energy (KE) of the electron which is proportional to the 2/3 power of the charge density. Slater in 1951 came up with another model where the KE was treated as in HF model but the exchange term was approximated statistically. This corrects the drawbacks of TFD model and is simpler than HF model.

In a non uniform system Slater proposed the form of exchange potential to be

$$V^{exch}(\underline{r}) = -3\left[\frac{3}{8\pi}\rho(r)\right]^{1/3} \qquad (1.12)$$

The inhomogeneous electron gas problem has been solved using this local electron correlation potential [2,19-21]. A rigorous theoretical justification for such local density potential methods is provided by the theorem of Hohenberg and Kohn [22]. According to them the ground state energy of

an inhomogeneous electron system is a unique functional of density $\rho(r)$. For a given external potential $\hat{V}(r)$

$$E[\rho(r)] = \int \hat{V}(r)\rho(r)\, d^3r + F[\rho(r)] \qquad (1.13)$$

This theorem merely proves the existence of a unique functional and offers no insight into it's exact nature [23]. A number of functionals have been proposed to suit various types of many electron systems [24,25]. Equation (1.13) can be written in detail as

$$E[\rho(r)] = \int \hat{V}(r)\rho(r)\, d^3r + \frac{1}{2}\int \frac{\rho(r)\rho(r')}{|\underline{r}-\underline{r}'|}\, d^3r\, d^3r' + T_s[\rho(r)] + E_{xc}[\rho(r)] \qquad (1.14)$$

Where the second, third and fourth term on the right correspond to the classical Coulomb interaction, KE of the non-interacting many electron system with density $\rho(r)$ and the electron correlation term. A formal similarity between the Hartree equation and equation (1.14) leads to a set of one particle equations [26].

$$\left[-\frac{h^2}{2m}\nabla^2 + \hat{V}(r) + \int \frac{\rho(r)}{|\underline{r}-\underline{r}'|}\, d^3r + V_{xc}(r)\right] U_i(r) = \varepsilon_i U_i(r) \qquad (1.15)$$

With,

$$V_{xc}(r) = \frac{\partial E_{xc}[\rho(r)]}{\partial[\rho(r)]} \qquad (1.16)$$

All the many body effects are included in V_{xc} which, unlike Hartree-Fock potential is local.

As a first approximation the many electron system may be regarded as a homogeneous electron gas. The exchange correlation potential is then the 'exchange only' potential of the homogeneous electron gas [20,21,27] . The exchange energy of the electron gas

$$E_{xc}\ [\rho(r)\ ] = -\int \frac{3}{2}\left(\frac{3}{8\pi}\right)^{1/3}\ [\rho(r)]^{4/3}\ d^3r \qquad (1.17)$$

gives the exchange potential

$$V_{xc}\ [\rho(r)\ ] = -2\ \left[\frac{3}{4\pi}\ \rho(r)\ \right]^{1/3} \qquad (1.18)$$

comparing equation (1.12) (Slater's value), and equation (1.18) (Gasper, Kohn and Sham (GKS) value [26,28]), one finds the difference of a factor 3/2. The difference is due to the fact that in GKS method the electron gas exchange is taken first and then the variation is made while in Slater's method [2] the variation is taken before the approximation is made. So finally a parameter α was introduced such that the final form of V_{xc} was obtained as

$$V_{xc} = -3\alpha\ [(3/4\pi)\ \rho\ (r)]^{1/3} \qquad (1.19)$$

$\alpha = 1$ for Slater and 3/2 for Gasper, Kohn and Sham approximation.

I.4 X_α Method

The approximation of Hartree-Fock method with Slater's exchange (HFS) is called the X_α method. (X = Exchange and α is a parameter introduced in the exchange term). X_α method has gained a wide range of applicability in predicting localized properties through cluster calculation. The earlier approximations were restricted to atoms only. Pratt [29,30], Wood and Pratt [31] worked on transition metal atoms. Results of some non-selfconsistent calculations were found to be in good agreement with experiments but some of the selfconsistent results differred greatly. The method was then applied to molecular systems. Since 1965 much of the energy band calculations have been to determine the values of α, which is unity, 2/3 or something in between [32]. The numerical method for a system which had neither the rotational symmetry of an atom nor the periodic symmetry of a crystalline solid was developed by Johnson [33-36]. The Bloch theorem is missing but some feature of the KKR model of energy band calculation exist.

I.5 The Choice of α

The X_α total energy depends on the exchange parameter α. Unfortunately, the total energy $E_{X\alpha}$ is not a variational with respect to α. In fact, to a good approximation, E_{X_α} is a linear function of α with large negative slope. If $U_i^{X\alpha}$ are the self consistent solutions of the X_α equations then,

$$E\left[U_i^{X\alpha}\right] = \langle \Psi(U_i^{X\alpha}) | H | \Psi(U_i^{X\alpha}) \rangle \qquad (\quad$$

where H is the exact Hamiltonian and $\Psi(U_i^{X\alpha})$ is the wave function derived from $U_i^{X\alpha}$. This expression will be a variational with respect to α

$$\left.\frac{\partial E\left[U_i^{X\alpha}\right]}{\partial \alpha}\right|_{\alpha=\alpha_{min}} = 0$$

Schwartz [37] tabulated the values of α for different atoms and found that its value varied from 0.7 for light atoms to 0.69 for heavy atoms except for hydrogen ($\alpha = 0.9$).

A more practical way of optimising α is to calculate the KE and PE separately for the atom and choose α such that the Virial ratio is equal to unity [38]

$$\eta(\alpha_{vt}) = \left.\frac{-2V\left[U_i^{X\alpha}\right]}{T\left[U_i^{X\alpha}\right]}\right|_{\alpha=\alpha_{vt}} = 1 \qquad (\quad)$$

The α_{vt} defined in this manner shows a similar variation to α_{min}, and the two values are almost equal for most of the atoms. This means that it is possible to choose an α such that $E_{HF}(\alpha)$ is close to HF limit and η_{HF} is close to 1.

By choosing α close to the HF limit $E_{HF}(\alpha)$ and η_{HF} close to unity, we find the PE and KE close to the HF limit. Since these terms are quite sensitive to the changes in $U_i^{X_\alpha}$, this optimization makes X_α and HF orbitals almost identical except for the virtual orbitals.

A third way of optimizing α is to set $E_{X_\alpha}(\alpha'_{HF}) = E_{HF}$. In general α should be different for different orbitals. Schwartz has shown that the values of α vary only slightly as one goes from one atomic configuration to another (as in shifting an electron from the s to the d shell in transition element, or in removing an outer electron). This leads one to hope that it will not be too inaccurate to use the same value of α for an isolated atom and for the same atom incorporated in the crystal. By setting different α for different orbitals no significant effect in the model was observed. Things become complicated and the Virial theorem is not satisfied.

I.6 Method of Calculation

The method is based on the division of complex or solid into polyatomic clusters. Each cluster contains the representative basis atoms of the complex or the solid.

The cluster containing same or different types of atoms is enclosed in a bigger sphere called the Watson sphere. The atomic sites form region I, the space in between the spheres form region II and outside the Watson sphere is termed as region III (Figure 1.2).

To start with, the intra-ionic or atomic potential within each ion or atom of the cluster with 110 mesh points, is interpolated to find the potential at 441 point mesh. Both the ionic potential and the eigen values corresponding to each of the atomic orbitals used as input for interpolation were taken from Hermann and Skillman [39].

The cluster potential at any point $\underline{r}$ is expressed as

$$V(\underline{r}) = \sum_j V^j (|\underline{r} - \underline{R}_j|) \qquad (1.20)$$

where V_j are the free atom SCF-X_α potentials centered at positions $\underline{R}_j$. The potential within each atomic region I can be expanded about its own center in terms of spherical harmonics

$$V_I (\underline{r}) = \sum_L V_L(r)\, Y_L(\underline{r}) \qquad (1.21)$$

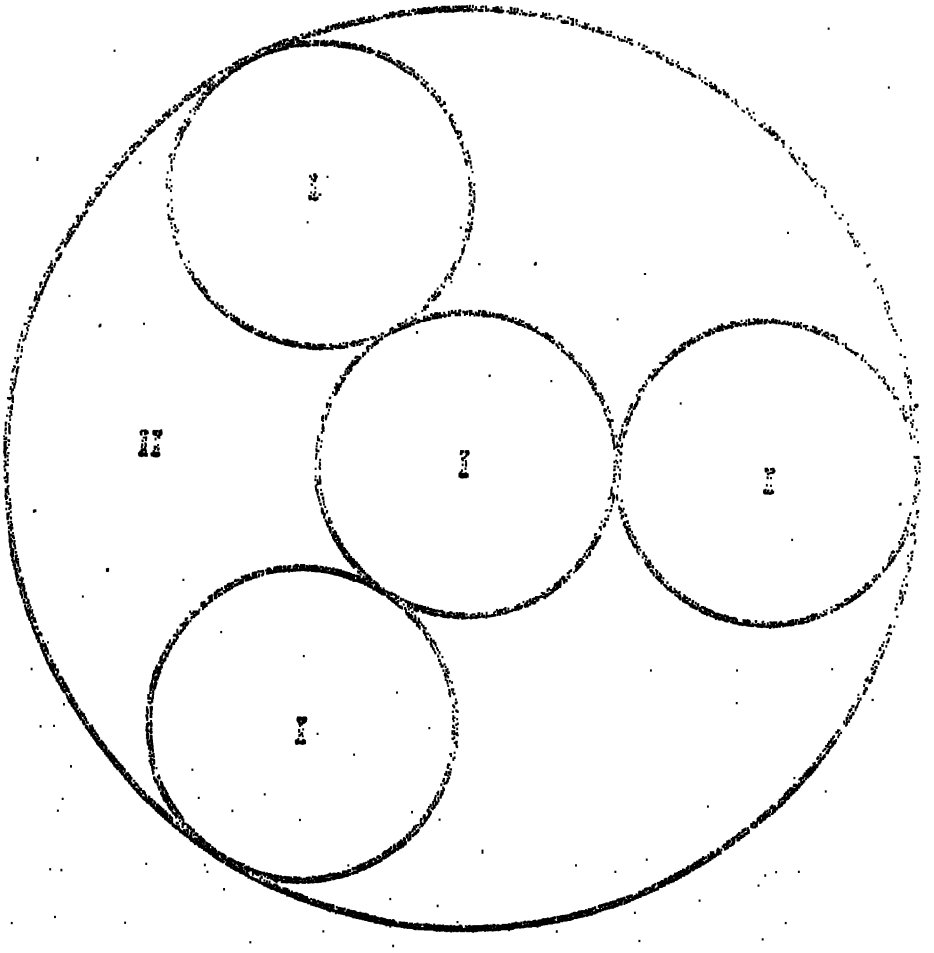

Fig. 1-2

Division of a molcular cluster into (I) atomic, (II) interatomic, and (III) extramolecular regions.

where $L \equiv (l,m)$. The radial component $V_L(r)$ can be evaluated by applying a theorem by Löwdin [44]. We then apply the muffin-tin approximation. According to this approximation we retain only the spherically symmetric term L=0 (l = 0, m = 0) in expansion (1.21) in each atomic region and treat higher order terms as perturbation. Hence the model potential is

$$\begin{aligned} V_I(r) &= V_o(r_i) && r_i \leq b_i \\ &= 0 && r_i > b_i \end{aligned} \tag{1.22}$$

where b_i is the sphere radius. $V_o(r_i)$ includes contributions of all the other atoms to the site i. Thus the effect of the overlapping charge densities is partially included in spherical model. Electron-electron coulomb correlation is not within our model unless we deal with the total wave-function. The potential in the interatomic region is volume averaged

$$\bar{V}_{II} = \frac{1}{\Omega_{II}} \int V(\underline{r})\, d\underline{r} \tag{1.23}$$

We are concerned with the solution of Schrödinger equation

$$[-\nabla^2 + V(\underline{r})]\, \Psi(\underline{r}) = E\Psi(\underline{r}) \tag{1.24}$$

written in Rydberg units in region I, II and III. Within each spherical atomic region I of radius b_j, we expand the

wave function in single centre form

$$\Psi_I^j(\underline{r}) = \sum_L C_L^j R_l^j(E;r)\, Y_L(\underline{r}) \qquad 0 < r \leq b_j \qquad (1.25)$$

where C_L^j are the partial wave coefficients to be determined, and $Y_L(\underline{r})$ are real spherical harmonics. The functions $R_l^j(E;r)$ are solutions of radial equation

$$\left[-\frac{1}{r^2}\frac{d}{dr} r^2 \frac{d}{dr} + \frac{l(l+1)}{r^2} + V^j(r) - E \right] R^j(E;r) = 0 \qquad (1.26)$$

for spherically averaged potential $V^j(r)$. The solutions are generated by outward numerical integration.

In the region outside the Watson sphere, the solution is represented as

$$\Psi_{III}(\underline{r}) = \sum_L C_L^o R_l^o(E;r)\, Y_L(\underline{r}) \qquad b_o \leq r < \infty \qquad (1.27)$$

where b_o is the radius of outer sphere. $R_l^o(E;r)$ are radial wavefunctions for outer spherically averaged potential, and are generated by inward numerical integration.

In the intersphere region, the potential energy is volume averaged and Schrödinger equation is

$$(\nabla^2 - E - \bar{V}_{II})\, \Psi_{II}(\underline{r}) = 0 \qquad (1.28)$$

For $E < \bar{V}_{II}$ its solution in the multicentre partial wave representation is given by

$$\Psi_{II}(\underline{r}) = \sum_j \sum_L A_L^j \, k_l^1 \, (\chi r_j) Y_L(\underline{r}_j) + \sum_L A_L^o \, i_l(\chi r_o) \, Y_L(\underline{r}_o) \tag{1.29}$$

where $i_l(x)$ and $k_l^1(x)$ are modified spherical Bessel function and modified spherical Hankel function, respectively

$$\chi = (\bar{V}_{II} - E)^{1/2} \tag{1.30}$$

and

$$\underline{r}_j = \underline{r} - \underline{R}_j \tag{1.31}$$

Similarly for $E > \bar{V}_{II}$ solutions of equation (1.26) can be written in terms of ordinary spherical Neumann and Bessel functions. We shall consider only $E < \bar{V}_{II}$ case.

In equation (1.29), the first term may be thought of as outgoing spherical wave scattered by regions of spherically averaged potential energy. The second term may be interpreted as incoming spherical wave scattered by extramolecular region.

We can also write the intersphere wave function as

$$\Psi_{II}(\underline{r}) = \Psi_{II}^i(\underline{r}) + \Psi_{II}^s(\underline{r}) \tag{1.32}$$

where,

$$\Psi_{II}^i(\underline{r}) = \sum_L B_L^j \, i_l(\chi r_j) \, Y_L(\underline{r}_j) \tag{1.33}$$

is the incident wave on atom j and

$$\Psi_{II}^s(\underline{r}) = \sum_L A_L^j \, k_l^1(\chi r_j) \, Y_L(\underline{r}_j) \tag{1.34}$$

is the wave scattered from the $j^{\underline{th}}$ atom.

Thus the wave incident on atom j can be related to the waves scattered by all other atoms and interatomic potentials $j' \neq j$ and to the wave scattered by extramolecular potential. Thus we can express the coefficients B_L^j in terms of the coefficients A_L^j and A_L^o. For this, we make use of expansion theorems like

$$k_l^1 (\chi|\underline{r}_2 - \underline{r}_1|)\, Y_L(\underline{r}_2 - \underline{r}_1) = 4\pi \sum_{L'} (-1)^{l+l'} \sum_{L''} I_{L''}(L;L')\, k_{l''}^1(\chi r_1)\, Y_{L''}(\underline{r}_1)\, i_{l'}(\chi r_2)\, Y_{L'}(\underline{r}_2) \qquad r_1 > r_2 \tag{1.35}$$

and

$$k_l^1 (\chi|\underline{r}_2 - \underline{r}_1|)\, Y_L(\underline{r}_2 - \underline{r}_1) = 4\pi \sum_{L'} (-1)^{l+l'} \sum_{L''} I_{L''}(L;L')\, i_{l''}(\chi \underline{r}_1)\, Y_{L''}(\underline{r}_1) k_{l'}^1(\chi \underline{r}_2) Y_{L'}(\underline{r}_2) \qquad r_1 < r_2 \tag{1.36}$$

where integrals

$$I_{L''}(L;L') = \int_0^{2\pi} d\phi \int_0^{\pi} \sin\theta\, d\theta\, Y_{L''}(\theta,\phi)\, Y_L(\theta,\phi)\, Y_{L'}(\theta,\phi) \tag{1.37}$$

are nonzero only for following conditions

$$|l - l'| \leq l'' \leq l + l' \tag{1.38}$$

and

$$l'' + l + l' = \text{even integer} \tag{1.39}$$

Substitution of expansions into (1.29) and comparison with equations (1.32) - (1.34) yields set of equations

$$B_L^j = \sum_{j'} \sum_{L'} G_{LL'}^{jj'}(E)\, A_{L'}^{j'} + \sum_{L'} S_{LL'}^{jo}(E)\, A_{L'}^{o} \tag{1.40}$$

where,

$$G_{LL'}^{jj'}(E) = (1-\delta_{jj'})4\pi(-1)^{l+l'} \sum_{L''} I_{L''}(L;L')\, k_{l''}^{1}(\chi \underline{R}_{jj'})\, Y_{L''}(\underline{R}_{jj'}) \tag{1.41}$$

and

$$S_{LL'}^{jo}(E) = 4\pi(-1)^{l+l'} \sum_{L''} I_{L''}(L;L')\, i_{l''}(\chi \underline{R}_{jo}) Y_{L''}(\underline{R}_{jo}) \tag{1.42}$$

$$\underline{R}_{jj'} = \underline{R}_{j'} - \underline{R}_{j} \tag{1.43}$$

$$\underline{R}_{jo} = \underline{R}_{o} - \underline{R}_{j} \tag{1.44}$$

For the outer spherical boundary, the 'incident waves' and 'Scattered wave' intersphere wave function can be written as

$$\Psi_{II}^{i}(\underline{r}) = \sum_{L} B_L^o\, k_l^1(\chi r_o)\, Y_L(\underline{r}_o) \tag{1.45}$$

$$\Psi_{II}^{s}(\underline{r}) = \sum_{L} A_L^o\, i_l(\chi r_o)\, Y_L(\underline{r}_o). \tag{1.46}$$

Equation (1.45) gives outgoing waves with respect to origin, singular at origin ($r_o = 0$) and equation (1.46) represents incoming waves with respect to the origin. A similar comparison as for different spheres gives

$$B_L^o = \sum_{j'} \sum_{L'} S_{LL'}^{oj'}(E)\, A_{L'}^{j'} \tag{1.47}$$

Now we equate the logarithmic derivatives of the intersphere wave functions with the corresponding values inside the spheres at various sphere radii b_j and b_o, which gives following relations

$$A_L^j = t_l^j(E)\, B_L^j \tag{1.48}$$

$$A_L^o = t_l^o(E)\, B_L^o \tag{1.49}$$

where,

$$t_l^j(E) = - \frac{[i_l(Xb_j),\ R_l^j(E;b_j)]}{[k_l^1(Xb_j),\ R_l^j(E;\ b_j)]} \tag{1.50}$$

and

$$t_l^o(E) = - \frac{[k_l^1(Xb_o),\ R_l^o(E;\ b_o)]}{[i_l(Xb_o),\ R_l^o(E;\ b_o)]} \tag{1.51}$$

The square brackets are used to denote Wronskian

$$[A(x),\ B(x)] = A(x)\ \frac{dB(x)}{dx} - B(x)\ \frac{dA(x)}{dx} \tag{1.52}$$

Using identities

$$[i_l(Xb),\ k_l^1\ (Xb)\ ] = \frac{(-1)^{l+1}}{Xb^2} \tag{1.53}$$

and

$$[j_l(Xb),\eta_l\ (Xb)\ ] = \frac{1}{Xb^2} \tag{1.54}$$

with equation (1.48) and (1.49), following additional relations are obtained between partial wave coefficients;

$$A_L^j = (-1)^{l+1}\ Xb_j^2\ [\ i_l(Xb_j),\ R_l^j(E;b_j)\ ]C_L^j \tag{1.55}$$

$$A_L^o = (-1)^{l+1}\ Xb_o^2\ [\ R_l^o\ (E;b_o),\ k_l^1\ (Xb_o)\ ]C_L^o \tag{1.56}$$

The scattering on a given site of the molecule must be compatible with the scattering at different sites. The set of compatibility relations for the partial wave coefficients are obtained by combining equation (1.48) and (1.50) with (1.40) and (1.47) respectively. We get a set of linear homogeneous equations

$$\sum_{j'}\ \sum_{L'}\ [T^{-1}(E)]^{jj'}_{LL'}\ A_{L'}^{j'} - \sum_{L'}\ S^{jo}_{LL'}\ (E)\ A_{L'}^o = 0 \tag{1.57}$$

$$\sum_{j'}\ \sum_{L'}\ S^{oj'}_{LL'}\ (E)\ A_{L'}^{j'} - \sum_{L'}\ \delta_{LL'}\ [\ t_l^o\ (E)]^{-1}\ A_{L'}^o = 0 \tag{1.58}$$

where,

$$[T^{-1}(E)]^{jj'}_{LL'} = \delta_{jj'}\,\delta_{LL'}\,[t^{j}_{l}(E)]^{-1} - G^{jj'}_{LL'}(E) \qquad (1.59)$$

The secular matrix of the problem is thus

$$\begin{bmatrix} [T^{-1}(E)]^{jj'}_{LL'} & -S^{jo}_{LL'}(E) \\ S^{oj'}_{LL'}(E) & -\delta_{LL'}[t^{o}_{l}(E)]^{-1} \end{bmatrix}$$

The matrix elements are real and symmetric because real spherical harmonics are used and conditions (1.38) and (1.39) are satisfied.

If the cluster has a point group symmetry, instead of spherically symmetrized wavefunctions we construct basis sets of the irreducible representation of this point group. The secular matrix then breaks up into blocks and becomes simpler to solve.

1.7 Advantage and Disadvantages of X_α Method

The main advantage is the simplicity of the model and computational speed. It simulates the self-consistent environment of an electron by a single local potential. The X_α orbitals are as accurate as double zeta basis set of the first and second row atoms and probably better for larger atoms which involve electrons with $l \geq 2$.

The orbital independent potential defined by X_α method leads to a better one electron excitations of a system. Both the occupied and unoccupied (virtual) orbitals of N electron system are under the influence of the potential which simulates the effect of other (N-1) electrons. The X_α ground state virtual eigen values are usually good description of the one electron excitations. A better first order picture of the spectrum is obtained if a transition state calculation [41] is done where one-half the electron is removed from a valence orbital and promoted to an excited orbital.

The X_α method also satisfies Virial theorem, Fermi statistics and the Hellmann-Feynmann theorem independent of α. This is convenient for calculating the force on a nucleus directly in terms of a three dimensional integral rather than through the evaluation of the six dimensional integral necessary for the total energy.

The X_α model can be considered to be an orbital generator which provides a convenient basis to be used as a starting point on a more accurate many body approaches. The method is rapidly convergent. There are no multicentered integrals to be evaluated. It takes care of the orbital relaxations. The energy expansion leads to Fermi-Dirac statistics. The total energy can be found as a function of a steriochemical geometry. For periodic solids, the cluster can

be choosen as an unit cell. Application of Bloch's theorem can lead to band theory.

The disadvantage is that the total energy does not correspond rigorously to a total wave function. The connection is lost with the approximation in the exchange part. The second disadvantage is the presence of α , the exchange parameter, whose choice is not obvious. There is also a numerical disadvantage in this model. The exchange potential is a nonlinear function of the charge density. There are two usual common misconceptions:

(i) Self interaction is disregarded - which is not true.

(ii) Treatment of a free electron gas of constant density - can be had from a simple dimensional argument, quite independent of the perfect gas model [42] .

The application to linear molecules turned out to be poor and the overlapping sphere method was introduced [43].

Nevertheless, since the cluster model is not dependent on the assumption of long range order, problems such as bonding of impurities and defects in crystals and the localized electronic structure of covalent materials are within the scope of the theory.

In general, the method does obtain a good estimate of the wave function and makes the quantitative treatment of any molecule or nonmetallic solid tractable.

I.8 Basic Structure of Program and Inputs

The program consists of four parts:

(i) Generation of atomic potentials

(ii) Calculation of starting molecular potentials

(iii) A non-SCF program to calculate the starting energy levels

(iv) Calculation of self consistent set of energy levels and normalized wave functions.

We shall briefly describe the parameters and various subroutines used for each part.

(i) Atomic potentials:

A Hermann-Skillman program is used to compute the atomic orbitals for the atoms with a slight modification to incorporate for different atoms as given by Schwartz. The potential is read from a 110 point mesh. The number of cores (NCORES) and the valence orbitals (NVALES) are specified

along with the ionicity (ION). The self consistent criterion (TOL) and the eigen value accuracy criterion (THRESH) were fixed at 0.001 and 0.00001 in the 441 integration mesh. The nuclear charge (Z), the state (NNLZ), the occupancy in that particular state (WWNL) and the trial energy for that state (EE) were due to Hermann-Skillman [30]. The input data was in a 110 point mesh. The values at the points not included in the presentation mesh are obtained by interpolation.

(ii) Generation of molecular potential.

The program consists of subroutines for Lagrange interpolation and for calculations of co-efficients of Löwdin's alpha expansion [44-46], used to express potential about any center and a subroutine for integration by Simpson's rule.

(iii) Non-SCF part

Input parameter

(a) The radii of the Watson sphere and the atomic spheres

(b) Charge on the Watson sphere

(c) Molecular potential (output of (ii))

(d) Symmetry input: This consists of a central atom and combinations of ligand atom basis functions,

transforming according to a particular irreducible representation of the cluster symmetry group. The angular momentum quantum number and the magnetic quantum number values along with parity are also specified.

(e) Trial energy values: The deep levels are treated as frozen cores. The valence orbital of the cluster are found by scanning the energy in steps of 0.01 Rydbergs.

The program consists of the following subroutines:

INPUT : Reads and checks the consistency of the input data.

SETUP: Reads and checks the consistency of the symmetry input. Determines the size of the secular matrix in its' reduced form using symmetry.

TMAT and GMAT: Calculates t matrix and G matrix. Radial equation is solved for each energy value. Starting functions are calculated in subroutine FSTART.

SMTX: Using above two subroutines, complete secular matrix is set up.

EIGEN: Solves the secular matrix and finds eigen values and eigen functions.

OSBF: Calculates ordinary and modified spherical Bessel function, Hankel function, Neumann function and their derivatives.

CGC: Evaluates the Clebsch-Gordon co-efficients.

YLM1: Computes radial spherical harmonics.

Other subroutines such as INTEGR, INTERP and LINEQ are used for integration, interpolation and solving simultaneous linear equations respectively.

(iv) SCF Part

In addition to the non-self consistent input the occupancy of each state with the non-self consistent energies are specified here. The maximum number of iterations is also specified in case the self consistency with an accuracy of 0.001 Ry. is not obtained. In addition to the non-self consistent subroutines we have

MSSCF: Controls iterations and stops program after either self consistency is achieved or a specified number of iterations are done.

NRMLIZ: Normalizes the wave functions at every iteration. Calculates charge distribution in different region.

VGEN: Generates potentials for new iterations from normalized charge densities of previous iteration. It also calculates various contributions to the total energy of the cluster.

The selfconsistent energy levels and normalized wavefunctions thus derived form the basis of the analysis made in the present work.

REFERENCES

1. K.H.Johnson, 1966, J. Chem. Phys. 45, 3085.

2. J.C.Slater, 1951, Phys. Rev. 81, 385.

3. L.A.Hemstreet, 1977, Phys. Rev.B 15, 834.

4. A.Fazzio and J.R.Liete, 1980 Phys.Rev. B 21, 4710.

5. G.G.De Leo, W.B.Fowler and G.D.Watkins, 1984, Phys.Rev. B 23, 3193.

6. K.H.Johnson, 1976, In the New World of Quantum Chemistry, B.Pullman and R.Parr (eds.) (Dordrecht, Reidel), p.317.

7. R.P.Messmer, 1981, Phys. Rev. B 23, 1616.

8. E.L.Anderson, T.P.Fehlner, A.E.Foti and D.R.Salahub, 1980, Am. Chem. Soc. 100, 7422.

9. D.R.Salahub, L-C. Niem and M.Roche, 1980, Surf. Sci., 100, 199 and Refs. therein.

10. R.P.Messmer, S.K.Knudson, K.H.Johnson, J.B.Diamond and C.Y.Yang, 1976, Phys. Rev. B 13, 1396.

11. J.Kaspar and D.R.Salahub, 1981, Phys. Rev. Lett. 47, 54.

12. G.G.De Leo, G.D.Watkins and W.B.Fowler, 1981, Phys. Rev. B 23, 1851.

13. D.R.Salahub and R.P.Messmer, 1981, Surf.Sci. 106, 415.

14. C.L.Briant and R.P.Messmer, 1981, Phil. Mag. B 42, 569.

15. D.R.Hartree, 1957, The Calculation of Atomic Structures, John Wiley and Sons, Inc., NY.

16. V.Fock, 1930, Z. Phys. 61, 126; 62, 795.

17. J.C.Slater, 1960, Quantum Theory of Atomic Structure, McGraw Hill, NY.

18. J.C.Slater, 1974, Self Consistent Field for Molecules and Solids : Quantum Theory of Molecules and Solids. V-4 McGraw Hill, NY.

19. D.Pines, 1963, Elementry Excitations in Solids, W.A.Benjamin Inc. NY.

20. L.H.Thomas, 1927, Proc. Camb. Phil. Soc. 23, 542.

21. E.Fermi, 1928, Z. Phys. 48, 73; 49, 550.

22. P.C.Hohenberg and W.Kohn, 1964, Phys. Rev. B.136, 864.

23. N.D.Lang, 1973, Solid State Physics V.28, Ed.H.Ehrenreich, F.Seitz and D.Turnbull, Academic Press.

24. N.H.March, 1975, Self Consistent Field in Atoms, Pergamon Press, London.

25. P.Rennert, 1974, Acta Phys. 37, 219.

26. W.Kohn and S.J.Sham, 1965, Phys. Rev. 140 A, 1133.

27. PAM Dirac, 1930, Proc. Camb. Phil. Soc. 26, 376.

28. P.Gaspar, 1954, Acta Phys., 3, 263.

29. G.W.Pratt. Jr., 1952, Phys. Rev. 88, 1217.

30. G.W.Pratt. Jr., 1956, Phys. Rev. 102, 1303.

31. J.H.Wood and G.W.Pratt Jr., 1957, Phys. Rev. 107, 995.

32. K.Schwartz and Conklin (unpublished).

33. K.H.Johnson, 1967, Int. J. Quantum Chem. 1, 361.

34. K.H.Johnson, 1968, Int. J. Quantum Chem. 2, 233.

35. K.H.Johnson, 1971, Int. J. Quantum Chem. 4, 153.

36. K.H.Johnson and F.C.Smith (Jr.), 1970, Phys. Rev. Lett., 24, 139.

37. K.Schwartz, 1972, Phys. Rev. B 5, 2466.

38. A.Berrondo and O.Goscinski, 1969, Phys. Rev. 184, 10.

39. F.Hermann and S.Skillman, 1963, Atomic Structure Calculations, Prentice-Hall Inc., Englewood Cliffs, New Jersey.

40. K.H.Johnson, 1973, Adv. Quantum Chem., 7, 143.

41. J.C.Slater, J.B.Mann, T.M.Wilson and J.H.Wood, 1969, Phys. Rev. 184, 672.

42. J.C.Slater, 1972, Adv. Quantum Chem. 6, 1.

43. F.Hermann, 1977, Electrons in Infinite Structures Ed. by P.Pharisean and L.Scheire, Plenum Publishing Corporation, NY.

44. P.-O. Löwdin, 1956, Advan. Phys. 5, 96.

45. P.-O. Löwdin, 1962, J. Appl. Phys. 33, 251

46. P.-O. Löwdin, 1960, Ann. Rev. Phys. Chem., 11, 107.

CHAPTER II

Electronic Structure of Covalent Solids

II.1 Introduction

Physicists and physical chemists have a sustained interest in developing quantitative description of chemical bonding of molecules and solids. The systems which have been substantially focussed on are the small molecules [1] and transition metal complexes [2]. Their electronic structures have been determined and the question if their bondings with their ligands are ionic or covalent have been given careful consideration. The present work is an effort to make ab-initio theoretical analysis of the bondings in ionic and covalent solids.

Historically the crystal field model has been extensively used to interpret the absorption spectra [3]. The model proved to be successful as a semi-empirical attempt to calculate the crystal field splittings from pure electrostatics [4]. However, the experimental results indicate that the crystal field approximation is quantitatively very poor, being incorrect even to the first order. The active interaction of the ligands is brought in through the molecular orbital approach. This improved the agreements. But, the coefficients of central atom or ligand wave functions had to be determined by neutron scattering or nuclear magnetic resonance experiments. If the Hartree-Fock

equations are solved exactly along with the relativistic effects then the theoretical results without parametrization are expected to agree sufficiently closely with the experimental results. However, this calculation would take hours even with large computers and hence become very expensive. We have used the multiple scattering X_α self consistent method which is an approximation to the Hartree-Fock method.

II.2 Chemical Bond

When two or more atoms are brought close together, the nuclei and the electrons of these atoms undergo coulomb interactions with each other resulting in fixed internuclear distances at 0°K and a redistribution of the electronic charge density, corresponding to the minimum of the total energy of the system. The atoms do not maintain their exact original identity and, the totality of the nuclei and the electrons form a single system. The system is called a molecule if a small numbers of atoms were originally involved, a complex if it has a total electric charge and a solid if the number of original atoms is very large ($\sim 10^{23}$) and the equilibrium positions of the nuclei form a periodic lattice. However, some semblance of the original atoms are maintained in that the core electrons around each nucleus usually do not change much and what were atoms are now identified as ions in different degree of ionization. In equilibrium, each ion

is located in a position dictated by the total potential minimum. A very small perturbation, leading to a harmonic approximation, will generate collective oscillations of these ions or pseudoatoms. Hence we may form the classical picture of the total system as a collection of pseudoatoms bound with each other by stiff springs. An imaginary spring between two neighbouring pseudoatoms is called a chemical bond.

As we see, the real mathematical problem is the solution of Schrödinger equation for a system of m electrons and n nuclei. However, this is insoluble when m and n are large. Hence different mathematical and physical models are made to describe the binding patterns of various systems. Of these, three models are very prominent: (i) ionic, (ii) covalent and (iii) metallic. In each model we have to define the pseudoatoms, the distribution of the left over electrons which is in some degree of delocalization with respect to the charge distribution for an atomic orbital, and a description of the imaginary entity called the chemical bond in terms of the charge density distribution of the delocalized electrons. In the present chapter we shall be interested in the systems, which are best described either by the covalent model, or by a mixture of covalent and ionic model. Hence we begin with, a brief description of ionic and covalent bonding models. Our description is some what coloured by the historical development of these ideas.

II.3 Ionic Bonding

If we have two kinds of atoms A and B with their electronegativity differing greatly, the transfer of an electron during their interaction converts them into oppositely charged ions

$$A = A^{+} + e + I_A;$$

$$B+e = B^{-} - E_B$$

where I_A and E_B are ionization energy of atom A and electron affinity of atom B, respectively. The electrostatic attraction set up between A and B cause the formation of a molecules

$$A^{+} + B^{-} = A^{+}B^{-} + E$$

where E is the energy change. As a result the ions in the molecules must be at such a distance that the attraction between the electron shells and nuclei is balanced by the repulsion between electron shell themselves or between the nuclei. For a solid, the attraction between the cations and the anions is, at the equilibrium distance, balanced by the repulsion between the cations or anions themselves. We may visualize the cations and anions as pseudoatoms and as if bound by stiff springs and say that an ionic bond is formed. The ions may be considered as spherical balls, since in the process of ionization, the electron shells of the atoms acquire the characteristics of

the noble gases. This view was developed by Kossel in 1916. However, a complete transition of the electron from one atom to anotner to form a pair of cation and anion never takes place [5] —— there is never a cent percent ionic bond.

II.4 Covalent Bonding

Consider a molecule consisting of atoms which have same electronegativity, e.g. H_2. Here the two atoms are equal in their power to attract an electron and hence ionization does not take place. In 1916-1918 Lewis and Langmuir suggested that the chemical bond is formed by a pair of electrons held jointly by two atoms. Such a bond is termed as covalent or homopolar. The sharing of pairs of electrons is conventionally represented by a line or two dots between the symbols of the elements. For example,

H : H ; N : : : N ; S : : S ; Cl : Cl

H - H ; N ≡ N ; S = S ; Cl - Cl

The diagrams are called Lewis structures. The ionic bond can be described rather well in terms of forces between the charged ions, whereas the covalent bond requires a more detailed recognition of the wave nature of the electrons.

In 1927 Heitler and London showed that if a hydrogen molecule consists of two hydrogen atoms a and b in their

1s ground state, the electronic wave function a(1) b(2) gives only a slight minimum for the wrong internuclear distance. Whereas its symmetric component $\frac{1}{2}[a(1)\ b(2)+a(2)\ b(1)]$ shows a deep energy minimum for approximately correct internuclear distance $R = R_0$. Apparently the stabilization of the chemical bond depends on the exchange symmetry of the electrons. This successful work of Heitter and London opened a new field in quantum chemistry and gave rise to the socalled valence Bond theory.

Soon after this Mulliken came up with the idea that the valence electrons of atoms may be considered as belonging to the molecule as a whole. This led to the idea of molecular orbitals. In this MO-LCAO scheme, the molecular orbitals are formed by linear combination of atomic orbitals available for the valence electrons. For the case of hydrogen molecule the two electron wave function is then given by $U = \frac{1}{2}[U(1)$ $+ U(2)]$. Such a wave function is symmetric under permutation of the two electronic coordinates and shows a similar stabilization of the covalent chemical bond to that of the Heitter-London wave function. Both the wave functions have to be supplemented with a spin factor $(\alpha_1\beta_2 - \alpha_2\beta_1)$ corresponding to the antiparallel spins of the electrons in the singlet ground state. The MO idea turned out to be exceedingly fruitful, particularly in molecular spectroscopy, since the molecular orbitals reflected the basic symmetry properties of the molecules involved.

The most physical description of the LCAO approximation is that the electron moves in an orbit which extends to the neighbourhood of both nuclei. In the neighbourhood of one nucleus, e.g., A, the MO resembles an atomic orbital U_a. Similarly in the neighbourhood of the other nucleus B, the MO resembles U_b. Since the complete MO has characteristics separately possessed by U_a and U_b, it is a natural step to adopt the method of linear combinations

$$U = C_a U_a + C_b U_b \tag{2.1}$$

This is most conveniently written as

$$U = N (U_a + \lambda U_b) \tag{2.2}$$

where N is the normalizing factor. The value of N is given by

$$N^{-2} = S_{aa} + 2\lambda S_{ab} + \lambda^2 S_{bb}$$

$$= 1 + 2\lambda S_{ab} + \lambda^2 \tag{2.3}$$

when U_a and U_b are normalized and

$$S_{ab} = \int U_a U_b \, d\tau \tag{2.4}$$

For most purposes, the normalization factor can be dropped to obtain

$$U = U_a + \lambda U_b \tag{2.5}$$

The constant λ measures the polarity of the orbital and may have any value ranging $+\infty$ to $-\infty$, according to the nature of the combining atoms. According to the Ritz variational method this value of λ must be choosen to minimize the energy function

$$E = \frac{\int U H U \, d\tau}{\int U^2 \, d\tau} \tag{2.6}$$

We still have to decide which orbitals U_a and U_b of the two atoms may be combined together. In order to have an effective combination between a given U_a and U_b it is necessary:

(a) that the energies of U_a and U_b in their respective atoms should be of comparable magnitude;

(b) that the charge clouds of U_a and U_b should overlap one another as much as possible;

(c) that U_a and U_b should have the same symmetry relative to the molecular axis ab.

It is difficult to choose pseudoatoms in the case of covalent bonding as well as working out the forces between pseudoatoms since the charge distribution around the nuclear sites are not spherically symmetric. Two extreme cases that could be conjured up are (i) the pseudoatom is a sphere of the same size as the original neutral atom, (ii) the pseudoatom is the ion consisting of the nucleus

and the core shell electrons. The third model, which is the case in between these, has to be defined after the charge distribution is worked out. We draw the charge distribution contour map, identify the outermost contour surrounding each nucleus and define this as the boundary of the pseudoatom. This third model is more realistic, and it forms the basis of talking of bonding in absolute terms, but is rather difficult to handle. Model (i) is simple, allows us to study the charge distributions relative to the neutral atoms, i.e., the charge transfer to reach the molecular or cluster equilibrium with respect to the free atoms and as such permits a simple description of bonding. We may draw the contour map of the relative charge distribution and thus have a visual description of bonding [6] . Or we may determine the charge transfer from each type of pseudoatom and plot them in a charge transfer diagram to get a simple quantitative measure of the ionic, covalent or mixed ionic-covalent bonding. Details of the charge transfer diagram will be discussed when we take up the specific covalent or mixed systems later in this chapter.

II.5 A Critique of Bonding Theory

There is no theoretical foundation for the electron pair bond of Lewis and Langmuir. It is not known why two and not some other number of electrons should be required for a single covalent bond, or how they could act as a bond

between the atoms and at the same time form part of the electronic system of the atoms. Secondly, no explanation was offered of the angles between the bonds formed by an element. The tetrahedral distribution of four, and the octahedral arrangement of six had been deduced for a number of elements from classical stereochemical studies, but these and other symmetrical arrangement of bonds could not be predicted theoretically. Again, considering only the valence electrons there was no way of deciding whether a molecule or complex ion should be formulated with ionic or covalent bonds. For example, F and Cl have the same number of valence electrons, but shows different chemical properties. Also any satisfactory theory of interatomic bonds must take account of the deeper structure of the atom, which plays a part in influencing the chemical individuality of the atom.

II.6 Symmetry and Basis Functions

The symmetry property of the complex helps in reducing the complexity to solve the set of linear equations obtained by applying equation 2.6 in the previous section for different orbitals. If the point group is at hand, we can construct the structurally symmetrized wave functions. These wave functions are used as input in the self consistent process of the calculation.

The LCAO method may be used to construct orbitals of the form

$$\Psi = \Psi(\Gamma) + \sum_i a_i \Psi_i \qquad (2.7)$$

where $\Psi(\Gamma)$ is a wave function of the central atom transforming in the molecular or crystal point group as the irreducible representation Γ and $\Sigma a_i \Psi_i$ is a linear combination of the ligand wave functions transforming as the same irreducible representation Γ. Under this condition only, any smearing out of the electronic orbitals is possible over the whole molecular unit, since only then we can have any cross terms between the two parts of the total molecular wave function.

In this chapter, we concentrate on the octahedral complex where six ligands sit symmetrically on the three orthogonal cartesian axes. The σ-bonds are MO with rotational symmetry about the line joining the nuclei. The combinations of atomic orbitals leading to the σ bond are: s-s, s-p_z, $p_z - p_z$, p_z-d_z etc. π-bonds are MO with nodal plane containing the line between the nuclei ($p_x - p_x$, $p_y - p_y$,...). The MO of δ-bonds posses two nodal planes ($d_{xy} - d_{yx}$,....) [7]. So there can be s, p_z, d_{z^2},..... orbitals in the σ-bonds. Figure 2.1 shows that the z-axis is always pointed towards the central atom. Hence all the σ-bonds are described by using the z-coordinate and the π-bonds by using the x-y coordinates. In addition to this, all the ligand coordinate systems are left handed. This choice has been made because of the fact that two center integrate usually are evaluated by

using one right and one left handed coordinate system [3]. Finally, the positive ends of the twelve x and y axes have been chosen in such a way that only positive signs appear in the linear combinations of the ligand orbitals making up the t_{2g}-π orbitals. This is not necessary but since the most important π-bond is the t_{2g} bond it is convenient to use only plus sign. The six - ligands give rise to six such bonds; consequently, six linearly independent orbitals can be constructed using these wave functions.

Table 2.1 combines linearly the ligand functions with σ- and π- bond characters for an octahedral symmetry corresponding to each irreducible representation of the octahedral symmetry group. The central ion orbitals indicates the functions with same symmetry behaviour as the linear combinations in the same row. The functions in the same row do not have the same irreducible representation, rather they transform as the same column of the appropriate representation matrices [8].

In this chapter we proceed to study the energy levels, charge distributions and bonding of metallic fluorides and oxides. We start with some ionic solids to see the effectiveness of the cluster model.

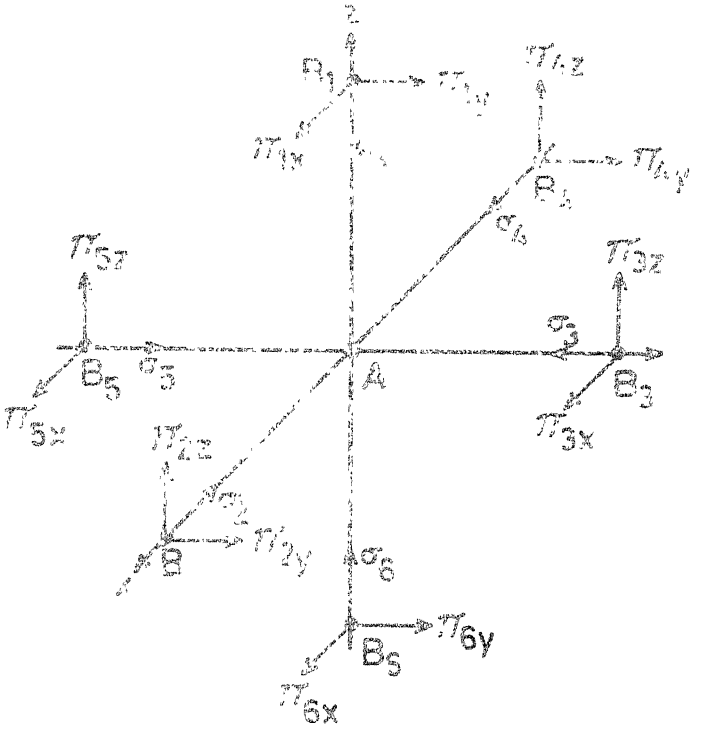

Fig. 2·1

Octahedral complex AB_6

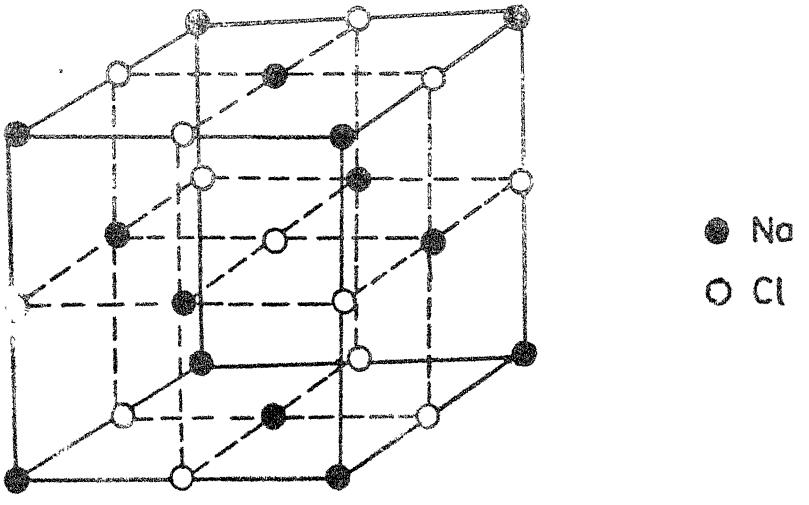

Fig. 2·2

NaCl structure.

TABLE 2.1

II.7 Energy Levels and Charge Distributions

II.7.1 Ionic Solids

II.7.1a Sodium Chloride

NaCl is the archetypal ionic solid of AB type (Figure 2.2). The crystal lattice parameter at 18 and 26°C are 5.6398 and 5.6406 a.u., respectively. A MS $X\alpha$SCF calculation is performed for the 7 atom (Na^+ 6 Cl^-) cluster to find out the one electron energy levels and the charges within each atomic region.

There is bunching of valence levels in groups as seen in the energy level spectra (Figure 2.3). Similar trend is observed by Brescansin et al.[9] . The energy of the last filled level is 0.64 Ry, which corresponds to approximately 8.7 eV. The experimental energy gap which is the difference between first unoccupied and last filled level is found to be 8.97 eV [13].

The charge distribution is compared (in Table 2.2) with a theoretical calculation of a cluster as large as 27 atoms [9] and also with the experimental data [10]. The excellent agreement with the experimental data gives confidence in our calculations.

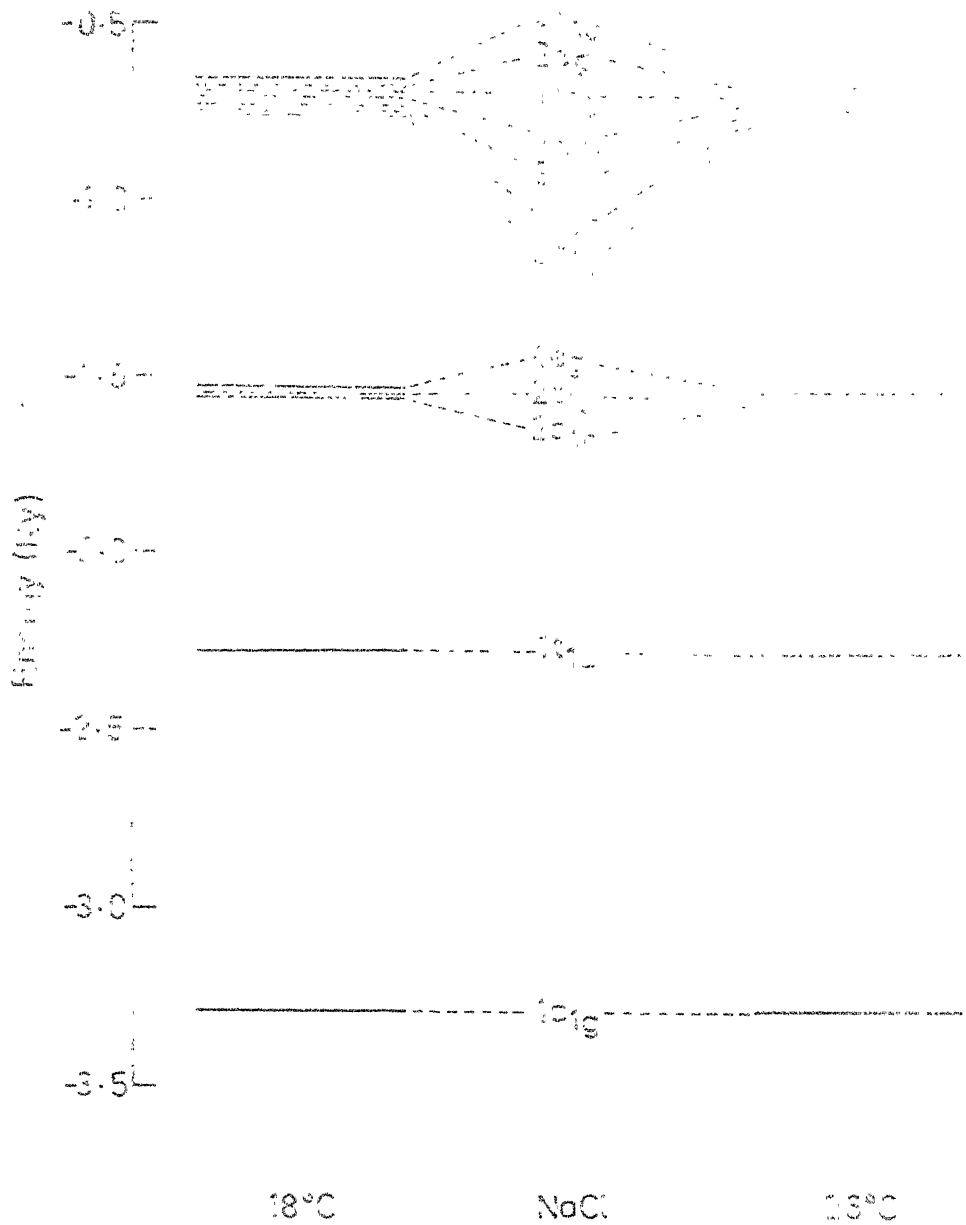

Fig 2-3

One electron energy spectra of NaCl.

Table 2.2

Charge Distribution in the Different Regions of the Cluster of NaCl

Region	1 Na^+ 6 Cl^- (e)	Expt.[9] (e)	1 Na^+ 6 Cl^- 12 Na^+ 8 Cl^- (e)
Central ion	9.9271 (10.1452)	9.9±4%	10.1984
Nearest neighbours (n.n)	17.5362 (17.1142)	17.6±4%	16.9173
Next n.n	-		10.1176
Next next n.n	-		16.7002
Extramolecular region	0.5073 (0.7470)		0.6198
Intersphere	2.3481 (4.4226)		14.3477

The bracketed values are for the second lattice parameter at 26°C.

The information available in the literature is that the lattice parameter of NaCl is 5.6398 a.u. [11] and that the ionic radii of Na and Cl in their closed shell configuration are 1.96 and 3.62 a.u., respectively [12]. We note that the sum of the ionic radii is less than the lattice parameter. Hence some adjustments are possible in the values of the individual atomic radii keeping their sum equal to the lattice parameter. But we know that the ionic radius would affect our results strongly since the basis of our method is matching the logarithmic derivative of the wave

functions at the ionic sphere boundary. Hence we have tried with the various combinations of ionic radii (Table 2.3) and compared the results with experimental values. It is evident that the combinations in which one of the ions has its radius equal to the ionic radius give very close agreement. We choose the 7th combination to find out the charges in the different region of the cluster. The last set of radii in Table 2.3 is obtained by minimizing the volume of the intersphere region. There is a considerable mismatch with the experiments in this case. Thus the concept of minimizing the volume of the intersphere region (a concept used for linear molecules) at the cost of atomic radius fails. The radius of the central ion is also likely to vary with the environment it experiences. Hence an error in the choice of the radius can by no means be removed, but, the ionic radii is a good point to start with.

Table 2.4 shows the percentage ground state charge density population of NaCl corresponding to each of the valence orbitals. q_{int}, q_{os}, q_c and q_l represents the intersphere charge, outersphere charge, central ion charge and the ligand ion charge respectively. IR signifies the irreducible representations of the octahedral point group for our case.

The intersphere charge is found to increase as one goes up in energy for a particular IR. This shows that as we go up in energy, the orbitals take up more and more covalent

Table 2.3

Charges in the Different Region of the Cluster for the Different Ionic Radii

Sl.No.	Central ion radius (a.u)	Ligand ion radius (a.u)	Charge distribution			
			Na ion	Cl ion	Intersphere region	Extramolecular region
1	2.6398	3.0000	10.1532	17.0926	4.5282	0.7629
2	3.6398	2.0000	10.8908	15.3076	13.4557	1.8076
3	4.6398	1.0000	19.7998	10.8477	12.3947	20.2493
4	2.0000	3.6398	9.9900	17.5461	2.3030	0.5013
5	3.0000	2.6398	10.3390	16.6819	6.5546	1.0150
6	2.6176	3.0222	10.1118	17.1080	0.4266	4.8134
7	2.0198	3.6200	9.9271	17.5362	2.3481	0.5073
8	1.9600	3.6798	9.9018	17.5656	2.2147	0.4892
9	3.99482	1.63496	11.4839	14.0050	20.4581	2.0244

Table 2.4

Percentage Ground State Charge Density Population in NaCl

IR	d = 5.6398 (18°C)				d = 5.64056 (26°C)			
	q_{int}	q_{os}	q_c	q_l	q_{int}	q_{os}	q_c	q_l
$1a_{1g}$	0.06	0.00	99.93	0.00	0.06	0.00	99.93	0.00
$1t_{1u}$	0.34	0.00	99.61	0.00	0.35	0.00	99.61	0.00
$2a_{1g}$	3.54	0.14	0.15	16.03	3.53	0.15	0.15	16.03
$2t_{1u}$	2.97	0.12	0.09	16.14	2.97	0.13	0.09	16.14
$1e_g$	2.88	0.00	0.00	16.19	2.60	0.22	0.06	16.19
$3a_{1g}$	15.55	1.40	3.12	13.32	15.47	1.46	3.15	13.32
$1t_{2g}$	19.04	0.00	0.00	13.49	16.96	1.51	0.10	13.57
$3t_{1u}$	5.31	4.54	0.59	14.87	6.41	4.42	0.76	14.73
$1t_{2u}$	13.75	0.00	0.00	14.37	12.54	0.09	0.04	14.42
$1t_{1g}$	10.88	0.00	0.00	14.85	10.18	0.34	0.00	14.88
$2e_g$	12.53	0.00	0.00	14.58	7.78	3.43	0.58	14.70
$4t_{1u}$	11.07	1.93	0.34	14.44	11.03	1.98	0.34	14.44

character. The deep valence levels, e.g., $1a_{1g}$ are hardly affected by the slight change in the lattice parameter. But for the shallow valence levels, e.g., $2e_g$, the charge in the ligand increases slightly at the cost of the inter-sphere region. This indicates that more of the atomic character is maintained at larger lattice parameter.

II.7.1b LiF and NaF

Both LiF and NaF are known to have a structure of NaCl type (Figure 2.2). Table 2.5 indicates the numerical values of the alkali-metal-ligand distance (d), the Watson sphere radius (r_o), the central ion radius (r_c), ligand radius (r_l) and the exchange parameters (α), used in our MS X_αSCF calculations.

Table 2.5

Numerical Values of Different Parameters Used in Our Calculations for LiF and NaF

	d(a.u.)	r_o(a.u.)	r_c(a.u.)	r_l(a.u.)	α_M	α_F
LiF	4.06	6.46	1.66	2.40	0.78087	0.7365
NaF	4.62	6.58	2.66	1.96	0.73044	0.7365

The α values used in our calculations are due to Schwartz [14].

Figure 2.4 shows the energy level diagram of LiF. The feature that immediately attracts attention is the bunching of the valence levels in two groups. Evidently the system is ionic with a small amount of coavalency. The eigen functions of the upper set are fluorine 2p-like and those of the lower set are fluorine 2s-like. The small dispersion in each set is due to covalency effects, the addition with a small coefficient of the Li orbital of symmetry appropriate to the fluorine combination described by the irreducible representation of the level. NaF energy levels also show similar features. The X-ray photoelectron spectrum of LiF finds the F 2p and F 2s energy difference to be 1.54 Ry [15]. Our calculated shift is 1.43 Ry.

The self consistently obtained charges in the different region of the cluster are shown in Table 2.6.

Table 2.6

Self Consistent Charges in Different Regions of the Clusters of LiF and NaF in units of e.

Region	$(LiF)^{5-}$	$(NaF)^{5-}$	$(NaF)^{4-}$
Extramolecular	3.005	1.743	2.344
Central ion	1.993	10.226	9.761
Ligand ion	9.399	8.844	8.511
Intersphere	0.609	4.968	5.828
Watson sphere charge	5.0	5.0	4.0
Constant Potential	-0.654	-0.359	-0.514

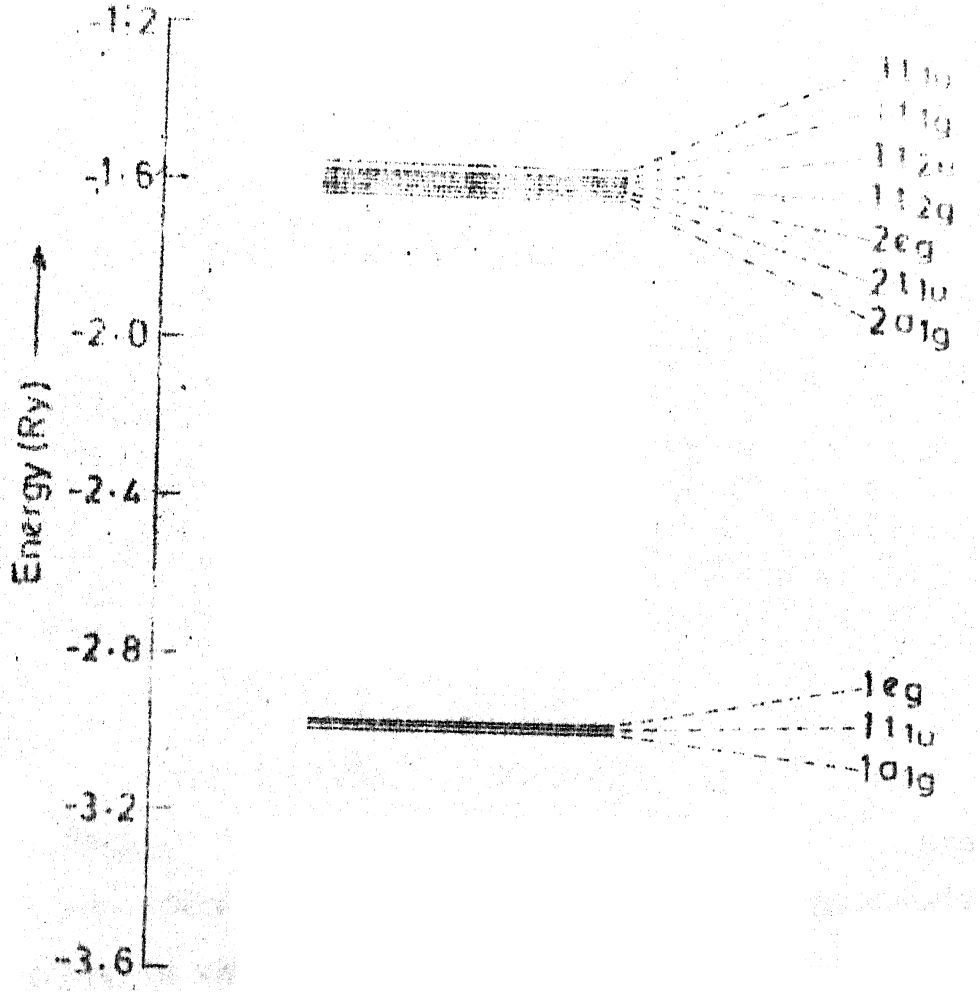

Fig. 2·4

One electron energy spectra of LiF.

be less than the true ionic distribution, shows that the ionic part of the mixed bonding may be in reality "super" ionic where ionicity is overdone. To look further into a theoretical possibility of superionicity, we have solved the MS X_αSCF for a cluster of 1 Na^{++} central ion and 6 F^- ligand ions column 3 of Table 2.6. We see that such a system stabilizes by coming closer to the Na^+ charge distribution and transferring more charge to the intersphere region compared to the standard $(NaF)^{5-}$ case. This means that if one electron of a Na atom is knocked off by a suitable radiation, the local environment will respond by a redistribution of charges corresponding to more covalent character. However, it is to be noted that the charge within the ligand ions is not much affected. But the energy level structure is substantially changed.

Table 2.7 shows that the $1a_{1g}$ and $1t_{1u}$ levels remain core levels of Na^+ for all practical purposes. Levels $2a_{1g}$ and $1e_g$ remain approximately F^- core levels. The level $2t_{1u}$ shows a strong bonding between the cation and the anion. All the higher levels have similar charge distribution pattern: almost empty cation region and large ring like distribution in the anion-annulus, the density slightly stepped up at the boundary as we go from the intersphere region into the anion.

Table 2.7

Percentage Ground State Population Density Distribution For $(NaF_6)^{5-}$ Cluster

IR	q_{os}	q_c	q_l	q_{int}
$1a_{1g}$	0.00	99.94	0.00	0.06
$1t_{1u}$	0.01	91.39	7.26	0.86
$2a_{1g}$	0.21	0.22	15.80	4.78
$1e_g$	0.33	0.15	15.88	4.21
$2t_{1u}$	0.17	8.38	14.58	3.99
$3a_{1g}$	1.08	3.42	13.73	13.13
$1t_{2g}$	1.25	0.23	13.95	14.82
$1t_{2u}$	0.72	0.05	14.52	12.25
$2e_g$	2.44	1.13	14.73	8.01
$3t_{1u}$	1.24	0.65	14.58	10.61
$1t_{1g}$	0.66	0.02	14.80	10.71
$4t_{1u}$	3.12	1.06	14.87	6.59

II.7.2 Transition Metal Compounds

II.7.2a Fluorides of Transition Metal

We shall discuss the different transition metal compounds like $KFeF_3$, $KNiF_3$, FeF_2, CoF_2, NiF_2 and ZnF_2, which are known to have covalent character. The first two of these transition metal compounds have a perovskite structure (Figure 2.5a) while the others have a rutile structure (Figure 2.5b). In the case of perovskites the central atom is a transition metal with six equivalent ligand atoms placed at the face centers of the unit cell. The K atoms occupy the cube corners. We do not consider the K atoms explicitly. But their stabilizing effect is taken care of by putting appropriate charges on the Watson sphere. For the MF_2 ($M = Fe^{2+}$, Co^{2+}, Ni^{2+} and Zn^{2+}) complexes, we find four of the six F atoms to be equidistant from the center while the other two are slightly away. This, thus, distorts the regular octahedral symmetry, generating an axial field. Again, the four equidistant atoms are not at right angles but are at an angle slightly less than 90°. This asymmetry lifts the planer degeneracy in energy.

The α-values of Fe, Co, Ni, Zn and F were taken from Schwartz [14] to be 0.71151, 0.71018, 0.70896, 0.70673 and 0.73732, respectively. The values of the radii used (Table 2.8) are obtained from

$$r_i = d \times \frac{r_i}{r_c + r_l}; \quad i = c,l \qquad (2.8)$$

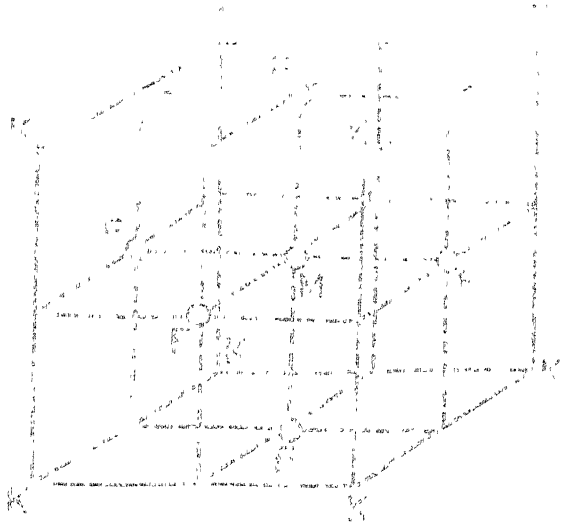

Fig. 2.5(a)

Crystal structure of a Perovskite (KMF_3).

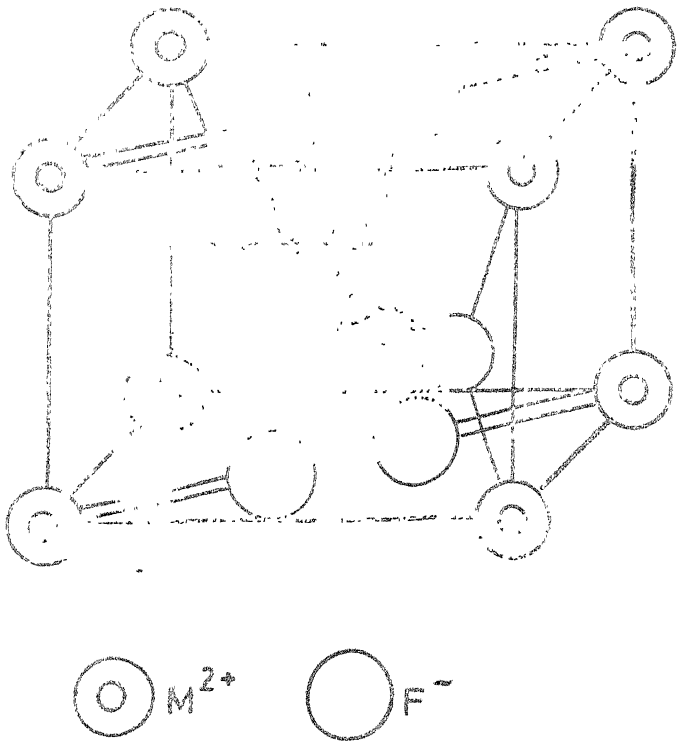

FIG. 2.5b

Crystal structure of a rutile MF_2

where i is the type of ion considered, c and l denote the central and the ligand ions respectively and d is the metal-ligand distance.

Table 2.8

The Value of Radii Used for Different TM Compounds in Atomic Units

Compounds	r_o	r_c	r_l	r_l'
$KFeF_3$	5.617	2.653	1.432	-
*$KFeF_3$	5.258	2.525	1.365	-
$KNiF_3$	5.129	2.456	1.336	-
*$KNiF_3$	5.396	2.584	1.406	-
FeF_2	5.675	2.729	1.331	1.473
CoF_2	5.560	2.640	1.460	1.436
NiF_2	5.571	2.570	1.510	1.389
ZnF_2	5.536	2.624	1.456	1.429

The two values of $KFeF_3$ and $KNiF_3$ correspond to the cases of different central ion-ligand ion distance.

The atomic ten-fold degenerate 3d-level breaks up into a six-fold degenerate t_{2g} level and a four-fold degenerate e_g-level in presence of the crystal field. The e_g-level has a

lower energy as compared to the t_{2g}-level in an octahedral field. The difference in energy between these two levels, called the crystal field splitting, is designated by 10 Dq. Figure 2.6 presents the one electron spectra of FeF_2, CoF_2 and NiF_2. The levels are seen to split due to the asymmetry in their structure. The XPS experiment [15] findsthe F 2s and F 2p energy difference for FeF_2 to be 1.54 Ry which is in very good agreement with our calculated value of 1.36 Ry. The small discrepancy is due to the correlation effects. However, before we start estimating correlation energies of these levels, we should have experimental data on more transitions as also got our calculations more refined to take into account at least the effects of the second nearest neighbours. The 3d occupancy and the crystal field splittings in the different transition metal compounds are tabulated below (Table 2.9). Our results for the perovskites are compared with those of Adachi et al. [17].

The rather good over all agreement for the perovskites shows that the splittings of the d-levels into t_{2g} and e_g should not be thought of as due to the influence of a perturbing electric field as is done in the simple crystal field theory. The only resemblance that the muffin-tin potential used in our approach has the electrostatic potential of the crystal field theory is the octahedral symmetry. The splitting in our case depends crucially on the fact that we are using molecular orbitals

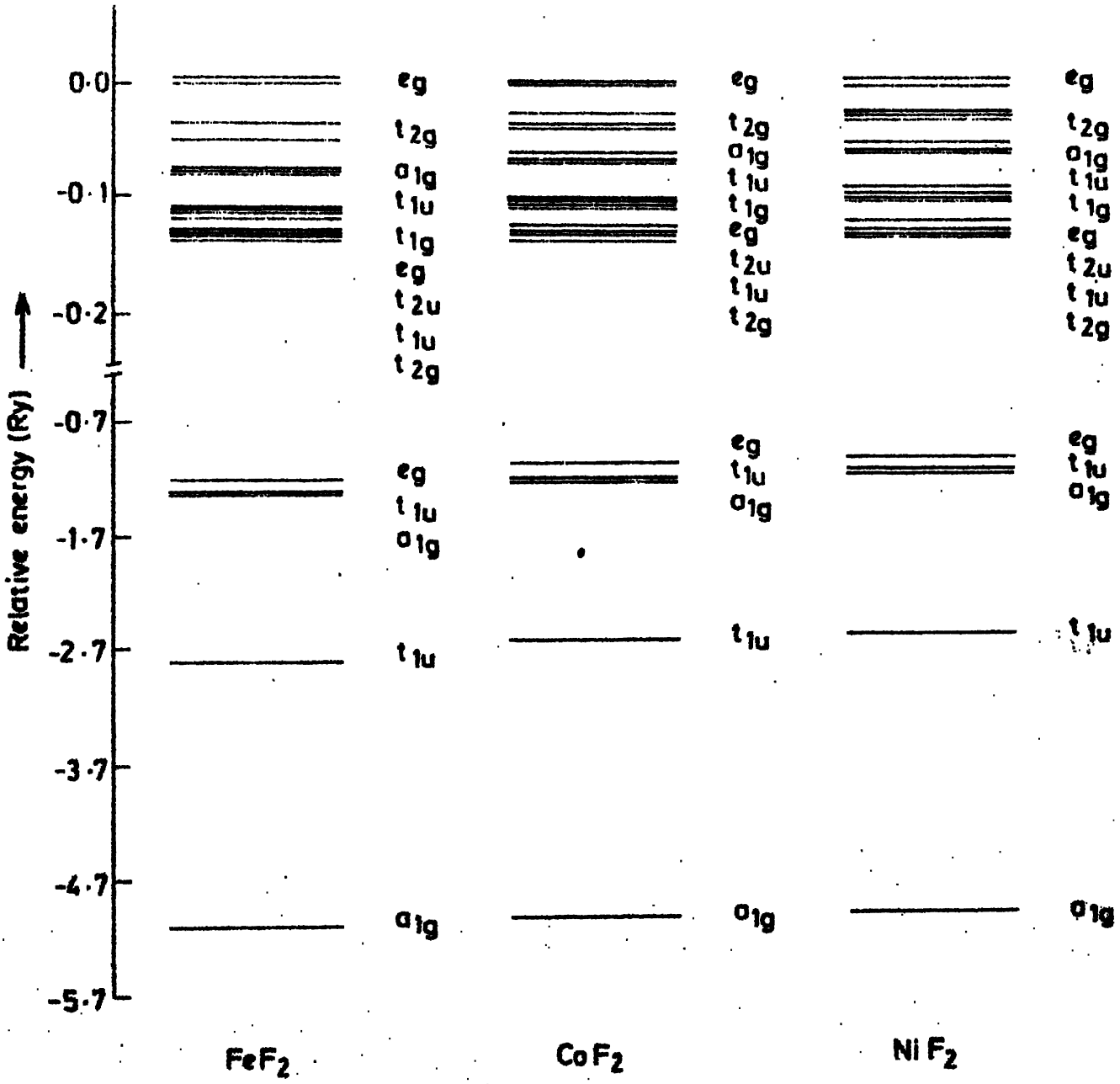

Fig. 2·6

Relative energy in Ry for FeF_2, CoF_2 and NiF_2.

Table 2.9

3d Occupancy and Crystal Field Splittings in the Different Transition Metal Compounds

Compounds	Present work (e)	Adachi et al.[17](e)	10 Dq (present work eV)	Experiment (eV)
$KFeF_3$	5.287	6.147	0.83	
$KNiF_3$	7.715	8.199	0.88	0.9[18]
FeF_2	5.331	-	0.95	
CoF_2	6.389	-	0.68	
NiF_2	7.956	-	0.61	
ZnF_2	9.901	-	-	

which are solutions of the same effective Hamiltonian and occupied in accordance with the Pauli exclusion principle [19].

The charge distributions in the regions of the cluster calculated selfconsistently are shown in Table 2.10. The lattice parameters are 4.085 and 3.893 a.u. respectively for $KFeF_3$ while it is 3.793 and 3.990 a.u. respectively for $KNiF_3$.

Table 2.10

Charge Distribution in the Different Regions of the Cluster for the Transition Metal Compounds in units of e.

Complexes	Extramolecular	Central-ion	Ligand-ion	Intersphere
$KFeF_3$	3.119	23.940	7.741	10.494
*$KFeF_3$	2.574	23.927	7.343	13.440
$KNiF_3$	3.031	24.486	7.547	13.201
*$KNiF_3$	3.022	26.816	7.593	10.603
FeF_2	3.700	25.019	7.141	12.438
CoF_2	3.105	26.029	7.503	10.847
NiF_2	0.599	26.262	8.141	10.299
ZnF_2	1.008	29.622	7.940	10.076

The expected general trend in both the structures is a gradual increase of the total central ion charge as Z increases, in conformity with the simple chemical picture based on the Pauli electronegativity scale. Also, as the interatomic distance increases, there is less mixing of the ligand electrons with that of the central-ion and the charges within the central-ion and the ligand-ion region are expected to be atomic like. The cases of $KFeF_3$ and $KCoF_3$ (see Table 2.10) clearly point this out. The charges

in both the regions increase with distance creating more of atomic environment around their own centers.

The basis functions used in our calculation are the same as those used as molecular orbitals in the ligand field theory. Hence their coefficients, derived from our selfconsistent calculations, are the same as the bonding parameters λ_σ and/or λ_π. In the molecular orbital theory, λ_σ and λ_π can not be calculated from first principles. They have to be deduced by matching the parametrized orbitals form factors with neutron scattering experimental data or their spin-density at the nucleus with NMR experimental data. There are not many experimental data available. But neutron diffraction data for $KNiF_3$ and $KFeF_3$ do exist [20], and they are 5.11 percent and 6.24 percent, respectively. Our calculations give λ_σ equal to 7.55 percent and 5.58 percent for $KNiF_3$ and $KFeF_3$, respectively. The agreement is quite satisfactory. We may note that the neutron scattering data are due to orbitals with unpaired spin only and hence a spin unrestricted calculation is expected to give still better agreements.

II.7.2b Oxides of Transition Metals

Monoxides of the 3d transition elements form a very interesting group of compounds with a wide spectrum of electrical and magnetic properties. In this comparatively small group, ferromagnetics and antiferromagnetics, dielectrics and compounds with high metallic conductivity can be found. Such an unusual combination of properties in a series of iso-structural compounds suggests very strong differences in electronic structure, chemical bonding and energy spectra of compounds. Therefore, it is not surprising that for a long time the electronic structures of the 3d monoxides has been the subject of a large number of experimental and theoretical studies [19,21].

II.7.2b.1 MgO

The one electron energy spectra of MgO is shown in Figure 2.7. We see that the set of occupied orbitals between -0.56 Ry and -0.68 Ry have a predominently ligand 2p character. The energy of the last filled level is 7.62 which is in very good agreement with the experimental energy gap of 7.8 eV [22]. The bonding effects between Mg and O ions and among O ions split the valence band into two groups. One group of $2e_g$, $4t_{1u}$, $1t_{1g}$, $1t_{2u}$, $1t_{2g}$, $3t_{2u}$ and $2a_{1g}$ levels is the set of the non-bonding type levels with nearly complete O 2p character.

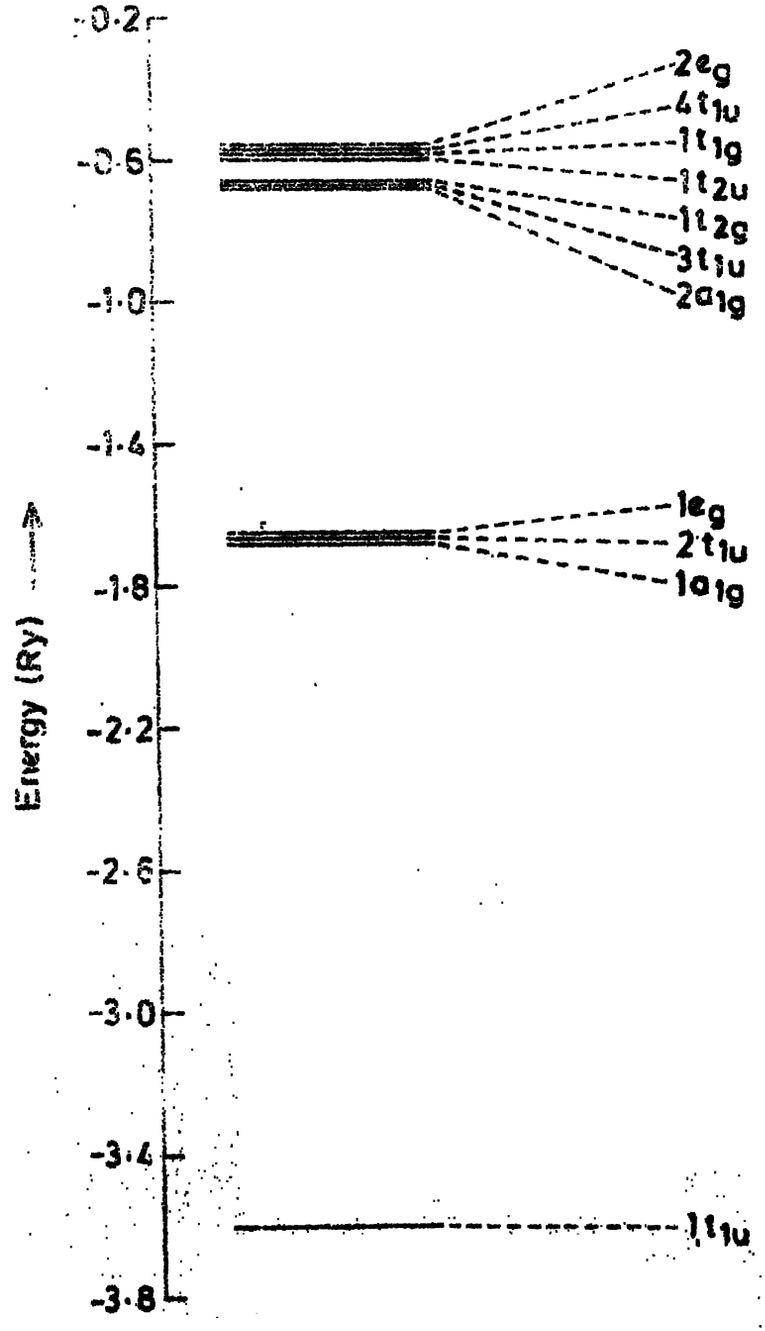

$(MgO_6)^{10-}$

Fig. 2·7

Energy level structure of MgO.

The other group includes $1a_{1g}$, $2t_{1u}$, $1e_g$ levels. The wave function of the $1a_{1g}$, $2t_{1u}$ and $1e_g$ levels correspond to the ligand 2s orbitals mixed with the Mg 3s orbitals. A DV X_α calculation was performed by Satoko et al.[23]. The energy level structure shows a similar sequence except for the inversion of $3t_{1u}$ and $1t_{2g}$ levels. Our self-consistent orbital energies are also compared with those of Satoko et al. [23] (Table 2.11). Any difference encountered could be due to the different lattice parameters used. Our lattice constant is 4.2 a.u. in contrast to 3.98 a.u. of Satoko et al. The XPS confirms the Mg 2s and Mg 2p levels [15] at 6.69 and 3.84 Ry, respectively. They are in fair agreement with our calculated values of 5.8 and 3.42 Ry, respectively.

Table 2.11

Self Consistent Orbital Energies in Ry for MgO

Ions	Orbital	Present work	Satoko et al.[23]
Mg	1s	92.2	91.8
O	1s	37.37	37.13
Mg	2s	5.80	5.37
Mg	2p	3.42	3.02
O	2s	1.67	1.49
O	2p	0.51	0.51

If the MgO were a perfect ionic crystal, the charges on the Mg and O ions would equal +2e and -2e, respectively. Table 2.12 shows the selfconsistently obtained charge distributions in the different regions of the cluster. Because of the partial covalency, however, some amount of electrons flow back into the cation region from the anion region. The net charge transferred from the ligand ion is 1.86e, while that from the central ion is 1.65e. One can assume that the central ion looses 2e and then an amount of charge equivalent 0.35e flow back. Since the anions only give away electrons, the charge flowing back into the cation region can be thought of from the ligands. Thus MgO has an inverse ionic character (discussed in detail in Section II.8).

TABLE 2.12

Charge Distribution in the Different Regions of the Cluster of MgO in units of e

Region	$(MgO)^{10-}$	$(MgO)^{10-}$ [23]
Central-ion region	10.35	10.33
Ligand-ion	6.14	6.06
Intersphere	18.36	-
Extramolecular	4.47	-
Net charge transfer from Mg	1.65	1.67
Net charge transfer from O	1.86	1.94

The covalency parameter, λ_σ, as obtained from ENDOR [24], is 6.50%, has an excellent agreement with our calculated value of 6.67%.

The DV X_α method does not approximate the potential within each atomic region to be in the muffin-tin form as in MS X_α method. But again, to obtain a better result with DV method one needs a large number of sample points. To conclude, we say that even with this MS X_α method one can obtain sufficiently good results so long as the potential is not highly asymmetric.

II.7.2b.2 VO and MnO

Vanadium monoxide and Manganese monoxide have a simple crystal lattice of NaCl type, in which each metal atom, in the defect free lattice, is surrounded by a regular octahedron of oxygen atoms. The length of the metal-oxygen bond are set at 4.48 and 4.20 a.u., respectively [11]. In accordance with the formal valence of the elements and the filling of the energy levels of the compound, the octahedral cluster in VO and MnO should contain 10 excess electrons as in the case of MgO. The V and Mn radius were set at their muffin-tin value of 2.40 and 2.31 a.u. [25], respectively. The α-values of V, Mn and O were set at 0.71556, 0.71279 and 0.74447, respectively [14].

The energy level diagrams corresponding to $(VO_6)^{10-}$ and $(MnO_6)^{10-}$ clusters are shown in Figure 2.8. The results are plotted in a relative scale. $(VO_6)^{10-}$ shows a similar clustering of levels as in the case of MgO whereas in MnO the upper levels are somewhat spread out. The O 2p level lies 6.12 eV below the t_{2g} level (Fermi level) which is in contrast with the available XPS data with an energy 4 eV [26]. for MnO.

Table 2.13 shows the charge distribution of VO and MnO. Our calculated values for VO are compared with that of Gubanov et al. [27,28] for a different metal-ligand distance of 4.08 a.u. The table also includes the $(MnO_4)^{1-}$ cluster calculation results of Johnson [29] which has a tetrahedral symmetry.

Table 2.13

Charge Distribution in VO and MnO Clusters (in units of e)

Region	$(VO_6)^{10-}$	$(VO_6)^{10-}$ [27]	$(VO_6)^{10.5-}$ [28]	$(MnO_6)^{10-}$	$(MnO_4)^{-}$ [29]
Central-ion	22.121	21.884	21.917	24.362	22.462
Ligand-ion	7.023	6.805	6.809	7.370	6.274
Intersphere	7.262	13.573	13.689	11.248	9.456
Extramolecular	9.423	4.721	4.535	2.720	0.968

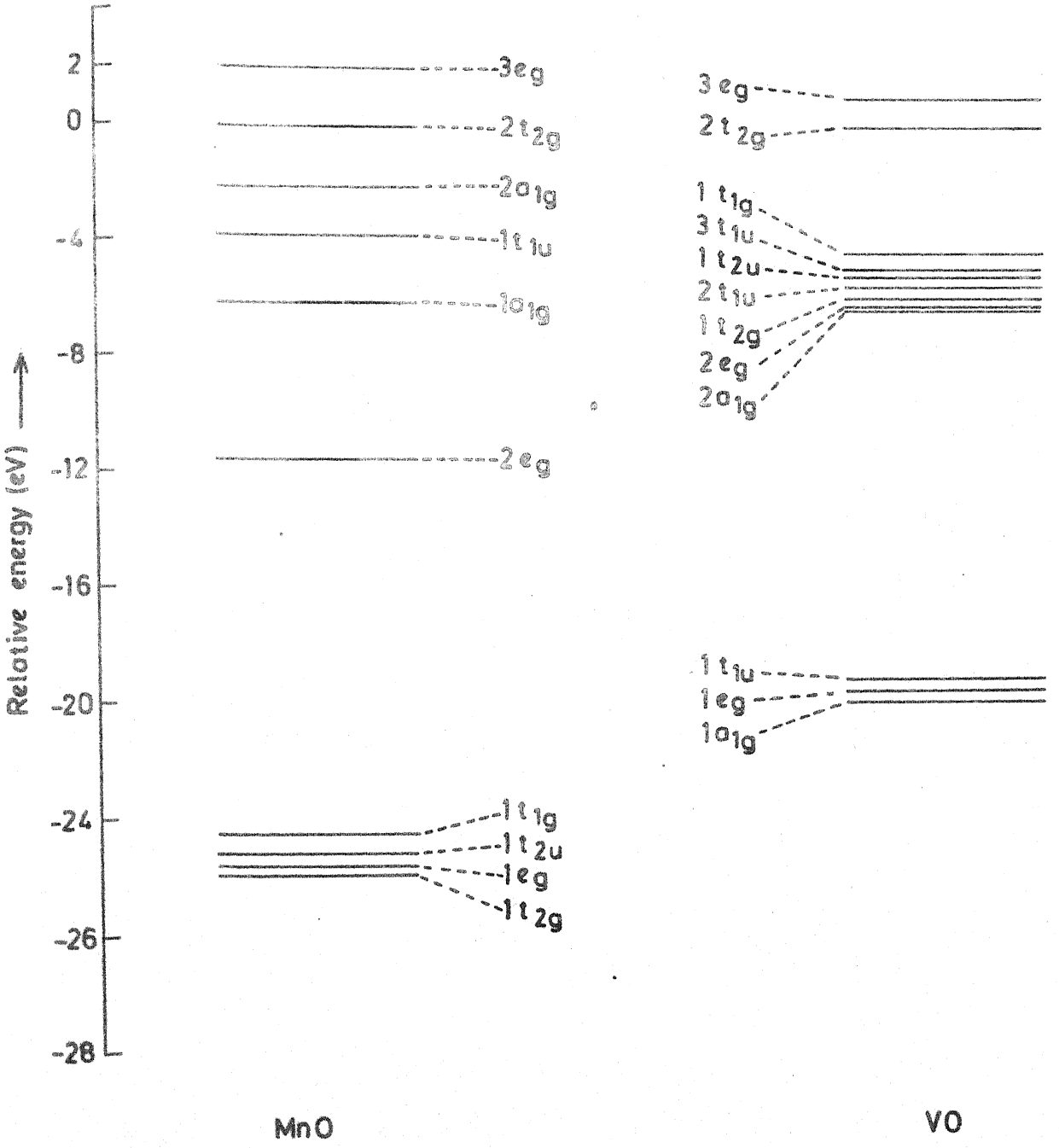

Fig 2·8

One electron energy spectra of MnO and VO in eV in relative scale.

The present work shows a loss of charge equal to 0.879e and 0.638e from V and Mn as compared to the value of +2e as considered to start with. Alternatively, we can think that the ligand charge has contributed partly to the central-ion region and a major part to the intersphere and extramolecular regions. In $(MnO_4)^{1-}$ cluster both Mn and O loose charge to the intersphere region. For a purely ionic case the net charge on V or Mn should be +2e with -2e charge on O ion. So a cnarge of 1.121e and 1.362e arrive at the V^{2+} ion and Mn^{2+} ion. The results of Gubanov et al. shows an increase of 0.884 only for the $(VO_6)^{10-}$ cluster. The charge deviation from O^{2-} ion in our case are 2.97e and 2.63e for VO and MnO while that of Gubanov et al. is 3.19e for VO and that of Johnson is 3.72e. The matching of $(MnO_6)^{10-}$ and $(MnO_4)^{1-}$ cluster results are never expected since the symmetry of the later is tetrahedral. This gives a feeling about the structure dependence of the charge distribution. In $(MnO_4)^{1-}$ cluster, the Mn is in Mn^{7+} state. So a charge of 22.462 - (25-7) = 4.462e is pulled into the Mn region out of (10-6.276)x4 = 14.896e of the ligands. Since $(MnO_6)^{10-}$ cluster has six nearest neighbours, the total charge given out by all the O^{2-} ions is (2.63x6=) 15.78e of which only 1.36e goes to the central ion. This shows that $(MnO_4)^{1-}$ is more inverse ionic (discussed in II.8) as compared to $(MnO_6)^{10-}$.

II.7.2b.3 $BaTiO_3$ and $SrTiO_3$

We repeated the calculations for the electronic structures of $BaTiO_3$ and $SrTiO_3$ for utilization in the charge transfer diagram later in connection with the discussion of the bonding characteristics of covalent solids. Our results agree closely with the existing calculations [30,31].

II.7.3 Alloys: Fe-Te Cluster

The present method may be easily extended to the vast area of the localized electronic structure in alloys. The alloys usually have short-range structural order. We may form a cluster of such a locally ordered unit and work out the MS X_α- SCF energy states and charge distribution. These may be used for the determination of a physical property of localized nature, e.g. the electric field gradient at the nucleus of a Mössbauer atom. Here we initiate the calculation for Fe-Ni-Te ternary alloy as an example.

Experimental Mössbauer studies of Fe-Ni-Te alloys have been done in detail in our laboratory [32]. The crystal structure changes at several critical concentrations of the metal-metalloid ratio. The typical structures are tetragonal, orthorhombic, rhombohedral and defect Ni-As. The spectra could be analyzed in terms of two or three or four quadrupole doublets with isomer shifts. Each doublet

was linked with an Fe-site in the crystal and the QS and IS data were analyzed to obtain detailed information about the first, second and the third neighbour environment of this Fe atom, and the complex bonding in this cluster. The most dominant bonding was the Fe-Te covalent bonding. Each Fe atom is octahedrally coordinated with six Te atoms and as such forms a cluster with octahedral symmetry as studied in the present chapter.

For $Fe_{.4}Te_{.6}$ alloy (Ni = 0) the Fe-Te distance is 5.24 atomic units [33]. The Fe and Te radii are 2.23 and 3.01 a.u. respectively with the Watson sphere radius 8.25 a.u. As initial inputs we put neutral Fe and Te atoms with exchange parameters 0.71151 and 0.7000 respectively. The electrical neutrality of the cluster is maintained by putting zero charge on the Watson sphere. The calculated charge distribution in the cluster is tabulated below (Table 2.14).

Table 2.14

Charge Distribution in Fe-Te Cluster in units of e.

Extramolecular region	1.3586
Central Fe region	23.8292
Ligand Te region	50.2941
Intersphere region	11.0144

The charge in the central region indicate that Fe pseudoatom has approximately the Fe^{2+} character. The Mössbauer study in our laboratory [32] show that Fe atoms form layers in the crystal and confirm that iron as in Fe^{2+} state.

The occupied one electron energy level structure of Fe-Te cluster is shown in Figure 2.9. It is seen that the intermediate levels have a predominantly Te 5p character.

The charge transfer diagram (Figure 2.11) to be discussed later, show that Fe-Te bonding is strongly covalent.

II.8 Measure of Covalency

For charge transfer analysis we divide the molecule or the cluster in a solid into several regions: One atom representing each type of atom or ion in the molecule or cluster, e.g., hydrogenic pseudoatom and fluorine pseudoatom in HF, and an interatomic region. The basis of the charge transfer analysis is the fact that the neutral atoms, when brought close to each other, reorganize their internuclear distance and redistribute their charges to come to energy minimum and the corresponding electrostatic equilibrium. In our cluster calculation we have used the

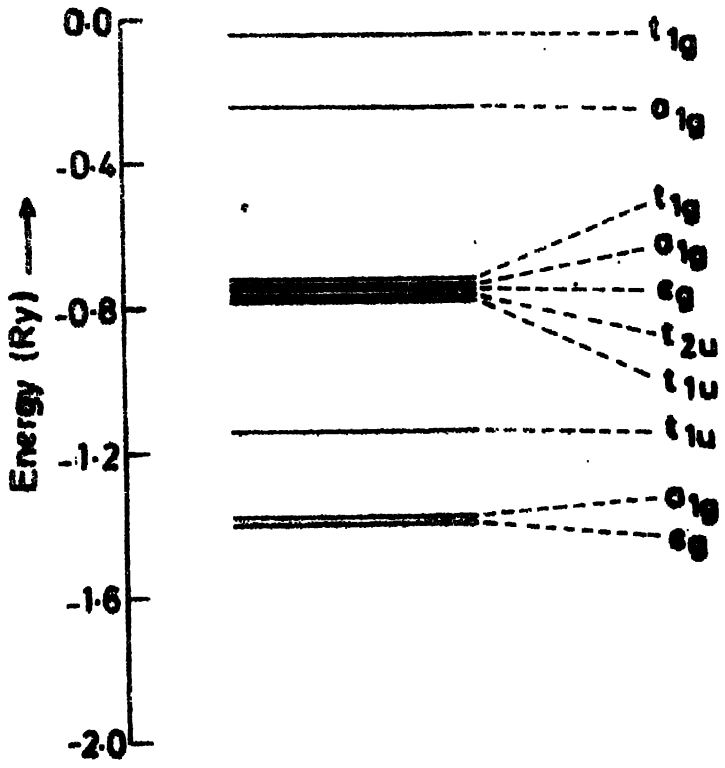

(Fe - Te)

Fig. 2·9

One electron energy level of Fe-Te cluster.

inter-nuclear distances obtained experimentally, that is the equilibrium distances. Hence our calculation determines the equilibrium charge distribution in the different regions. Contrasting with the neutral atom charges in each region we can find how much charge is flown in or out of each region to reach electrostatic equilibrium. If the charge gone out of the cation is exactly equal to the charge entering the anion, the system is obviously ionic. Any deviation from this process involves charge being transferred to the inter-atomic space, a charge belonging to both the ions or pseudo-atoms and hence covalent in nature. Hence from the charge transfer diagram we may get a measure of the covalent bonding. Probably a more satisfactory measure of covalent bonding would be to (use model (iii) as discussed in II.4) calculate the total electrostatic force on each pseudoatom for various interatomic distances and calculate the constant for the imaginary spring binding the pseudoatoms. But then the calculations would be far more elaborate than the present one. We use the charge transfer diagram to analyze our data.

To construct the charge transfer diagram, we note that the available electrons in the cluster are solely from the central ion and the ligand ions. Since the total number of electrons is conserved, we can write

$$\Delta\rho_c + \Delta\rho_l + \Delta\rho_{ei} = 0 \qquad (2.9)$$

where $\Delta\rho_c$ is the charge transferred to or from the central pseudoatom in forming the equilibrium cluster from the neutral atoms. $\Delta\rho_l$ is the charge transferred to or from the ligand pseudoatom in forming the cluster from the neutral atoms. $\Delta\rho_{ei}$ is the charge in the extramolecular and intersphere region in equilibrium state of the cluster.

Equation (2.1) is the equation of a plane passing through the origin. The general equation of a plane is

$$ax + by + cz + d = 0 \qquad (2.10)$$

If $d = 0$ and $a = b = c = 1$, then the plane passes through the origin making an angle 45° with all the three coordinate axes. The angle, thus depends on the ratios of the coefficients. In our charge transfer diagram this depends on the charge transfer ratio between the cations and the anions. The charge transfer ratio is again a function of the electropositivity and electronegativity of the anions and cations and also the structure of the complex.

Since only two of the three variables $\Delta\rho_c$, $\Delta\rho_l$ and $\Delta\rho_{ei}$ are independent, the description of the charge transfer process could be considered complete with the knowledge of any two of them. We plot our data in the $\Delta\rho_c$ and $\Delta\rho_l$ space. The intersection of the charge transfer plane in three dimensions with the $\Delta\rho_c - \Delta\rho_l$ plane is the straight line dealing with the charge transfer between the anion and the

cation only and correspond to the ionic case of various kinds. The amount of charge transferred from the cation to the anions is governed by their electropositivity and electronegativity, respectively. The line from the origin to the ideal ionic point ($\Delta\rho_c = +1$; $\Delta\rho_1 = -1$ for NaCl), is named as the true ionic region (Figures 2.10 and 2.11). The extension of this line in the same quadrant is termed as super ionic region. If the electrons are taken up by the cations from the anions then we call it an inverse ionic system. The inverse ionic line is an extension of the true ionic line in the opposite quadrant. The inverse ionic character is seen in III-V semiconductors where the ligands first give away one electron to the central ion and redistribution takes place for reaching the equilibrium. For the solids considered by us, there are two types of ionic lines, one for the charge transfer ratio 1:1 (e.g., NaCl, MgO) and the other for the charge transfer ratio 2:1 (e.g., FeF_2, NiF_2).

Most systems are mixed ionic and covalent and as such their charge transfer points fall off the ionic line. If any point is joined to the center of the coordinate system then the length $\sqrt{(\Delta\rho_c)^2 + (\Delta\rho_1)^2}$, called the root mean squared charge transfer, gives a measure of the total charge transfer for the charge redistribution to take place. Again we may determine the coordinates of this point along the ionic line and normal to the ionic line. The former gives the

root mean charge transfer between the cation and anion only and may be called the ionic bond strength whereas the latter is the root mean square charge transfer to the interatomic and extramolecular region from the central and the ligand atoms and is a measure of covalent bond strength. The unit of the each bond strength is an electron. Both ionic and covalent bond strength can also be described as a combination of charge transfer ($\Delta\rho_c$, $\Delta\rho_1$).

Figure 2.10 shows that NaCl has the shortest line normal to the ionic line, identifying its basic ionic and marginally covalent character. LiF and NaF show similar characteristics, with somewhat more augmented covalencies. The transition metal perovskites and rutiles could be considered as typical covalent compounds. The ionic bond of each of them is much smaller than its ideal ionic limit. But the covalent bond strength of each is distinctly large, being in each case substantially greater than its ionic bond strength. For the rutiles we note that the covalent bond strength decreases as we go from Fe to Zn. It is also evident that the ratio of the covalent to ionic bond strength decreases as we go from Fe to Zn. Hence according to the present analysis, FeF_2 is the archetype of a covalent compound with large covalent bond strength in absolute terms as well as in relation to the ionicity. The ionic part of ZnF_2 shows an inverse character, though small in value.

Table 2.15 shows the numerical values of the covalent bond strength of all the systems studied in the present work.

Table 2.15

Covalent Bond Strength for Different Systems in Units of Electrons

NaCl	0.2	$KFeF_3$	2.04	FeF_2	2.09	MgO	2.51	Si	2.40
LiF	0.3	$KNiF_3$	1.78	CoF_2	1.78	VO	1.33	InP	3.18
NaF	0.65			NiF_2	1.52	MnO	0.85	GaAs	1.13
				ZnF_2	1.12	$BaTiO_3$	3.25		
						$SrTiO_3$	2.83		

In Figure 2.11 the results of our calculations for the oxides of metals are plotted. We also include here the data for a few semiconductors worked out in the next chapter. All the systems show very large absolute values of the covalent bond strength. MnO, $BaTiO_3$ and $SrTiO_3$ show 'normal' ionic bond strengths of different degrees. VO is, again, a truely covalent system with almost zero ionic bond strength. MgO, which is known to have semiconducting properties, lies in the inverse ionic region. Other semiconductors like Si, InP [34] and GaAs [35] also lie in the inverse ionic region. The case of InP and GaAs were expected to be so, since they start with a charge transfer from the group V to group III elements. For Si this is partly due to the fact that the central atom and the ligand atom in the

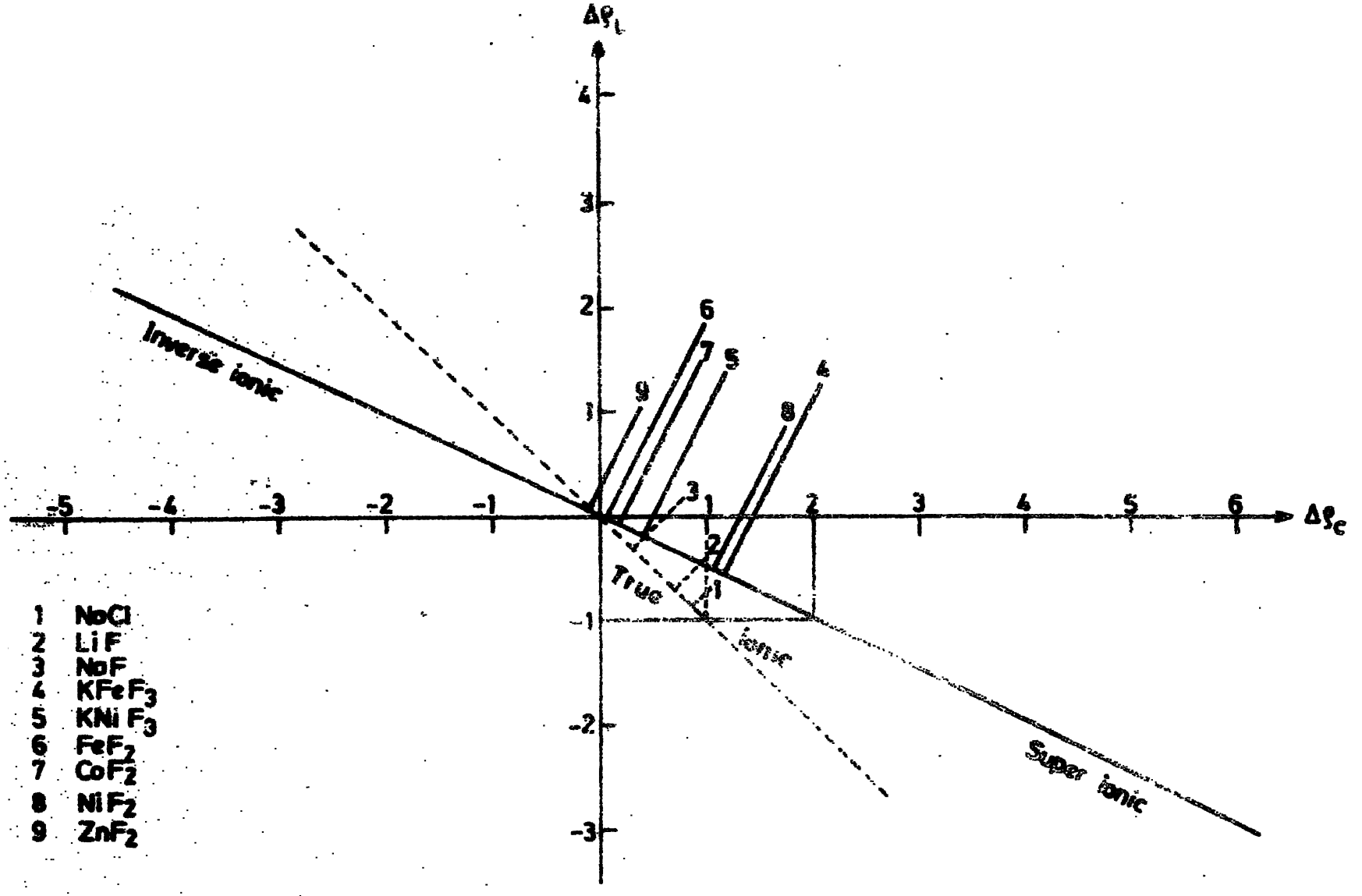

Fig. 2·10

Charge transfer diagram for NaCl and fluorides of metals.

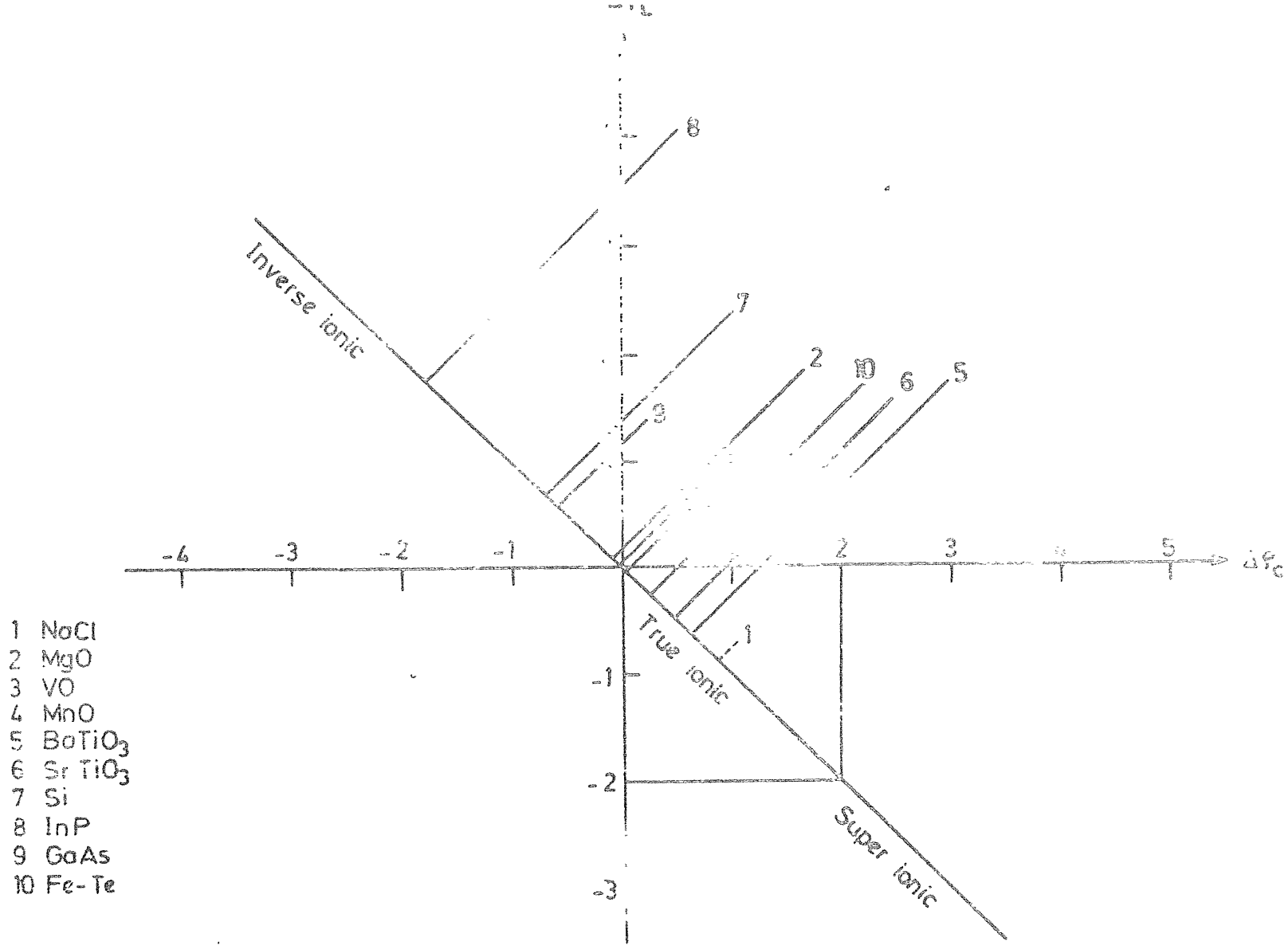

Fig. 2.11

Charge transfer diagram for oxides of metals, semiconductors and an alloys.

cluster are treated as different, though in real solid no two Si atoms could be considered as different in their properties. However, the fact that emerges is that, within the framework of the present analysis, the semiconductors could be categorized as a group of substances with large covalency combined with inverse ionicity.

The present work makes an effort for the analysis of the structure of a large number of solids, showing that most systems are mixed ionic and covalent, with NaCl in one extreme with large ionic and marginal covalent character and the semiconductors at the other extreme, with large covalent and inverse ionic character. This analysis bridges the gap between the purely ionic theories and the band structure calculations.

II.9 Isomer Shift

Isomer shift is the manifestation of a very specific feature of the hyperfine interaction between nuclear and electronic charges, namely the finite nuclear size on Coulomb energy. The interaction between total electronic charge $e\rho_e(r)$ and the electrostatic potential generated by nucleons, $V_n(r)$, is

$$U = -e \int \rho_e(r)\, V_n(r)\, d\tau \qquad (2.11)$$

For a point nucleus $V_n(r) = \frac{Ze}{r}$ (2.12)

and $$U_p = -Ze^2 \int \rho_e(r)\, V_n(r)\, d\tau = -Ze \langle r^{-1} \rangle_e \quad (2.13)$$

where $\langle r^{-1} \rangle_e$ is the average over all electrons present. Since U_p depends only on Z, the energy of all nuclear states of a certain nuclide will be same. But for a finite nuclear size, the Coulomb interaction between the electronic charge and the nuclear potential will be different for the ground state and for the excited state. This is indicated by the observed energy shift in the Mössbauer spectrum. Considering the nuclear charge to be uniformly distributed over the nuclear sphere of radius R we have

$$V_n(r) = \frac{Ze}{R} \left[\frac{3}{2} - \frac{1}{2} \left(\frac{r}{R}\right)^2 \right] \qquad r < R \quad (2.14)$$

$$= \frac{Ze}{r} \qquad r > R \quad (2.15)$$

So the change in potential from that of a point nucleus is

$$V_n(r) = \frac{Ze}{R} \left[\frac{3}{2} - \frac{1}{2} \left(\frac{r}{R}\right)^2 - \frac{R}{r} \right] \qquad r < R \quad (2.16)$$

$$= 0 \qquad r > R \quad (2.17)$$

The energy shift is now given by

$$\Delta U_v = -e \int \rho_e(r)\, \Delta V_n(r)\, d\tau \quad (2.18)$$

Assuming $\rho_e(r)$ to be constant over the nuclear volume, we obtain by integrating the above expression

$$\Delta V_n = \frac{2}{5} \pi Ze^2 \rho_e(0) R^2 \qquad (2.19)$$

Such differences were encountered long ago by the experimentalists in optical spectroscopy as isotope shift. To obtain the isotope shift one measures the optical transition for two different isotopes of an element. The Coulomb energy, which is part of the transition energy, will change slightly for the two isotopes since R^2 changes with the change in nuclear number.

Now if the source and the absorber consists of two chemically different materials then $\rho_e(0)$ will be different for the source and absorber. Hence the final expression for isomer shift is then given by $(\Delta\rho_e(0) = \rho_e(0)^{absorber} - \rho_e(0)^{source})$

$$IS = \frac{2}{5} \frac{\pi c}{E_\gamma} Ze^2 (\Delta R)^2 \Delta\rho_e(0) = \alpha \rho_e(0). \qquad (2.20)$$

where $(\Delta R)^2 = (R^2)^* - (R^2)$ refers to two isomeric states of a given nucleus. If the relativistic corrections are made the above expression for IS is then multiplied by $S'(Z)$ which is 1.29 for ^{57}Fe.

In our transition metal compounds like $KFeF_3$, FeF_2 and Fe-Te alloy, the isomer shift is calculated theoretically using the above expression. Since in all these experiments ^{57}Fe is used as the source $\rho_e(0)$ of metallic iron is needed.

This value was taken from Walker et al.[36]. The calibration constant α has the term $(\Delta R)^2$ was choosen to be 0.51 [36] and 0.12 [37], respectively. Table 2.16 shows the charge density at the origin and the calculated isomer shift as compared to the experimental data.

Table 2.16

Charge Density at the Origin Used to Calculate Isomer Shift and Compared with Experimental Data

System	$\rho(0)$(a.u.)	α (a.u.mm/sec)	IS(mm/sec)	S'(Z)IS	Expt. (mm/sec)
$KFeF_3$	6.5232	0.51	1.008	1.301	1.38 [38]
FeF_2	6.5971	0.51	0.971	1.253	1.36 [38]
Fe-Te	3.9670	0.12	0.544	0.701	0.518 [32]

It may be noted that the value of α as tabulated in the literature ranges from 0.11 to 0.51 a.u. mm/sec. The only way of finding a better α from experiments is muonic X-ray [39] which is drawing attention these days. The calculated results show satisfactory agreement with experiments. Our results could be improved by taking into consideration the effect of the second nearest neighbour also.

REFERENCES

1. B.M.Dev, 1981, Force Concepts in Chemistry, Van Nostrand Reinhold Company, New York.

2. C.K.Jorgesen, 1971, Modern Aspects of Ligand Field Theory, North Holland, Amsterdam.

3. C.J.Ballhausen, 1962, Introduction to Ligand Field Theory, McGraw Hill Book Company, Inc. NY, Toronto, London.

4. W.H.Kleiner, 1952, J. Chem. Phys. 20, 1784.

5. M.Karapetyants and S.Drakin, 1974, The Structure of Matter, Mir Publisher, Moscow.

6. R.F.W.Bader, 1981, The Nature of Chemical Bonding in Force Concepts in Chemistry, p.39 Ed. B.M.Dev, Van Nostrand Reinhold Company, New York.

7. T.Matsubara, 1982, The Structure and Properties of Matter, Springer-Verleck, Berlin.

8. H.L.Schläfer and G.Gliemann, 1969, Basic Principles of Ligand Field Theory, Wieley Interscience, London.

9. L.M.Brescansin and L.G.Ferreira, 1979, Phys. Rev. B 20, 3415.

10. V.G.Schoknecht, 1957, Z. Naturforschg, 12a, 983.

11. R.W.G.Wyckoff, 1960, Crystal Structure, Interscience Publishers, Inc., New York.

12. C.Kittel, 1977, Introduction to Solid State Physics, p-100, Wiley Eastern University Edition, New Delhi, Bangalore.

13. D.W.Roessler and W.C.Walker, 1968, Phys. Rev. 166, 599.

14. K.Schwartz, 1972, Phys. Rev. B5, 2466.

15. S.Hüfner, 1979, Photoemission in Solids II, p-173, Ed. L.Ley and M.Cardona, Springer Verlag, Berlin, Heidelberg, New York.

G.K.Wertheim and H.J.Giggenheim, 1973, Phys.Rev.Lett., 30, 1050.

16. J.W.Stout and S.A.Reed, 1954, J.Am.Chem.Soc., 76, 5279.

17. H.Adachi, S.Shiokawa, M.Tsukado, C.Satoko and S.Sugano, 1979, J. Phys. Soc. Jpn. 47, 1528.

18. R.G.Shulman and S.Sugano, 1963, Phys. Rev. 130, 506.

19. J.C.Slater, 1974, Quantum Theory of Molecules and Solids V-4, McGraw Hill, New York.

20. B.C.Tofield, 1975, Structure and Bonding V-21 Springer-Verlag, Berlin, Heidelberg, New York.

21. K.H.Johnson, R.P.Messmer and J.W.D.Connolly, 1973, Solid State Comm. 12, 313.

22. R.C.Whited and W.C.Walker, 1969, Phys. Rev. Lett., 22, 1428.

23. C.Satoko, M.Tsukado and H.Adachi, 1978, J. Phys. Soc. Jpn. 45, 1333.

24. P.Freund, 1974, J. Phys. C 7, L33.

25. V.L.Moruzzi, J.F.Janah and A.R.Williams, 1978, Calculated Electronic Properties of Metals, Pergamon, New York.

26. D.Adler, 1968, Solid State Physics V-21 Ed.F.Seitz, D.Turnbull, H.Ehrenreich, Academic Press, New York.

27. V.A.Gubanov, D.E.Ellis and A.K.Chirkov, 1976, Zhurnal Strukturnoi Khimii, 17, 955.

28. V.A.Gubanov & D.E.Ellis, 1976, Zhurnal Strukturnoi Khimii, 17, 962.

29. K.H.Johnson, 1973, Advan. Quantum. Chem. 7, 143.

30. F.M.M.-Calendini, H.Chermette and P.Pertosa, 1979, Solid State Comm. 31, 55.

31. M.Tsukado, C.Satoko and H.Adachi, 1980, J. Phys. Soc. Jpn. 48, 200.

32. Atul Sen, Ph.D. Thesis, IIT Kanpur, unpublished.

33. F.Gronvold, H.Haraldsen and J.Vihovde, 1954, Acta Chem. Scand. 8, 1927.

34. Chapter III of this thesis (See III.3 and III.4).

35. A.Fazzio, J.R.Leite and D.L.De Siqueira, 1979, J. Phys. C 12, 513, 3469.

36. L.R.Walker, G.K.Wertheim and V.Jaccarino, 1961, Phys. Rev. Lett. 6, 98.

37. P.Ruegsegger and W.Kündig, 1972, Phys. Lett. 39 B, 620.

38. R.Ingalls, F.Van Der Woude and G.A.Sawatzky, 1978, Mössbauer Isomer Shifts, Ch-7, Ed. G.K.Shenoy and F.E.Wagner, North Holland Publishing Company, Amsterdam, New York, Oxford.

39. R.M.Steffen (private communication).

CHAPTER III

Electronic Structure of Doped Semiconductors

III.1 Introduction

In this chapter we shall be dealing with structures of terrahedral symmetry. Most of the II-IV and III-V semiconductors possess this symmetry. The electronic structure of semiconductors with impurities in substitutional and interstitial position nas many unresolved aspects and is the focus of attention of many groups of scientists. The translational symmetry of the crystal is broken by the impurity and the defect levels deep in the band gap of the semiconductors are difficult to investigate by ab-initio analytical theory, though they are important in understanding the electronic properties of the semiconductors. Hence, earlier attempts to apply this approach have been restricted to semi-empirical methods, specially the Extended Hückel Method, which is a nonself consistent procedure. It was proposed by Messmer and Watkins [1] and Larkin [2]to surround the impurity by a cluster of substrate atoms and apply methods from molecular theory. One might expect that such a description could handle deep defect levels in semiconductors, which have localized orbitals and states associated with extended impurity complexes. Usually, levels in the band gap with the position $> \frac{E_g}{10}$ from any one of the band edges, valence or conduction, is called a deep level. A level close to the

conduction band edge ($<\frac{E_g}{10}$) is called a donor level and a level close to the valence band edge is called an acceptor level. E_g is the band gap.

The cluster model is known to account well the electronic structure of substitutional or interstitial impurities present in the solid. Since Messmer, Watkins and Larkin many authors have demonstrated the effectiveness of the cluster approach to deep impurities in semiconductors. Of the various methods applied, MS X_α SCF method stands out.

In this chapter we will first tabulate the symmetry formed by the ligands and then go over to the MS $X\alpha$ SCF calculations for systems like Si and InP. The impurities in Si have been extensively studied by other authors [3-7]. In our work the transition metal impurities in InP are considered along with the different charge states of Fe in InP. The effect of alkali-metal impurities in InP is also studied.

III.2 Symmetry and Basis Functions

The elements of the IV^{th} group are in a special situation, since their electropositivity and electronegativity are both 4. This comes from the configuration of their outer shell electrons $(ns)(np^3)$. All elements except for Pb crystallize into diamond structures (Figure 3.1a), in which four electrons per atom take part in

the electron pair bonds, and each atom extends four chemical bonds in the tetrahedral directions forming a three dimensional network. Such crystals are named as covalent crystals or homopolar-bonded crystal or valence bond crystal.

The one s and the three p orbitals can be linearly combined, if the energy difference between these orbitals is small, to obtain [8]

$$\Psi_{111} = \frac{1}{2}(s + p_x + p_y + p_z)$$

$$\Psi_{\bar{1}\bar{1}\bar{1}} = \frac{1}{2}(s + p_x - p_y - p_z)$$

$$\Psi_{\bar{1}1\bar{1}} = \frac{1}{2}(s - p_x + p_y - p_z)$$

$$\Psi_{\bar{1}\bar{1}1} = \frac{1}{2}(s - p_x - p_y + p_z)$$

These functions have a large amplitude in the direction denoted by the subscripts. From these tetrahedral hybrid orbitals one can construct bonding orbitals and anti-bonding orbitals by linear combination with similar hybrid orbitals of the neighbouring atoms. When a pair of electrons with opposite spins is accommodated in a bonding orbital, a covalent bond is completed.

The above feature may also be described in terms of band theory. For a large lattice parameter the s and p orbitals of the valence electrons in all atoms are degenerate, at the level of an isolated atom. With decreasing lattice parameter, the s and p level each form an energy band: the s and

p bands can accommodate 2 and 6 electrons per atom, respectively. For a smaller lattice constant, the s-band and p-band cross each other and they mix into two bands of completely different character. The lower band corresponds to the band of bonding orbitals of sp^3 hybridization and the higher to that of the anti-bonding orbitals (Figure 3.1b). Each of them contains four electrons per atom.

Considering only the first nearest neighbours, we now construct the symmetry with respect to the center of a cluster or molecule. The irreducible representation of the tetrahedral symmetry group is indicated on the left-most column of Table 3.1. The second column shows the central atom orbitals which form the basis of this representation. Third and fourth columns show the σ- and π-combinations of the ligand atoms which have the same symmetry as the central atom orbital in the same row.

III.3 Silicon

The characteristic of Si is its strong covalency with a large pile up of charge in the bonds between atoms. This raises two essential questions on the applicability of MS X_α SCF method to the molecular description within the cluster: whether the muffin-tin approximation of the potential is sufficient for the representation of real strongly non-spherical potential, and whether the local potential

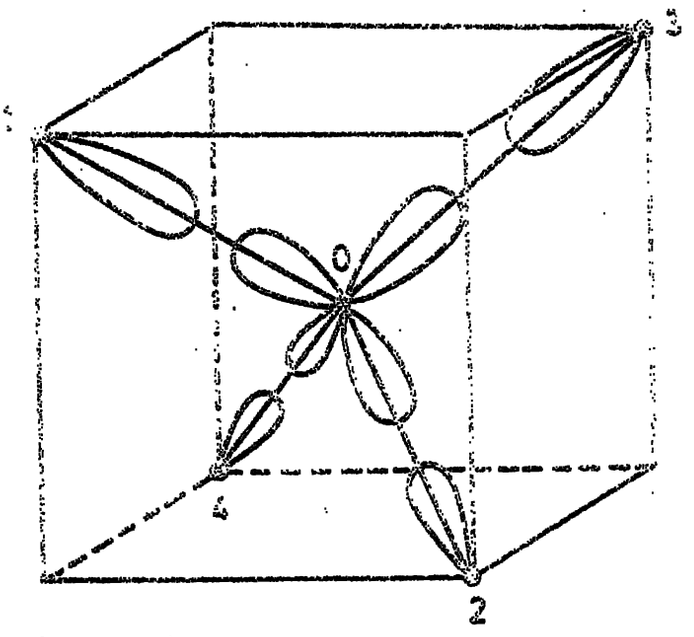

Fig. 3·1a

Diamond structure

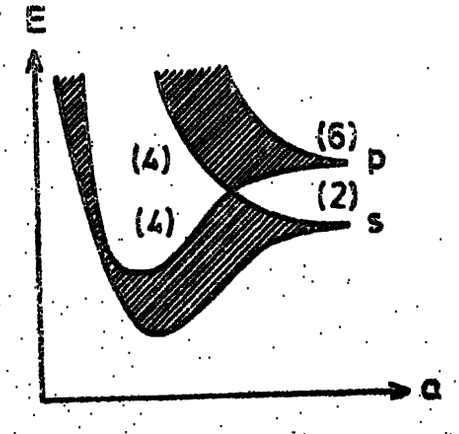

Fig. 3·1b

Energy band of diamond structure as a function of a lattice constant.

TABLE 3.1

Orbitals for Tetrahedral Complexes

Representation	Metal Orbital	Ligand σ	Ligand π
A_1	s	$\frac{1}{2}(\sigma_1 + \sigma_2 + \sigma_3 + \sigma_4)$	
E	d_{z^2}		$\frac{1}{4}[\pi_{1x} + \pi_{2x} + \pi_{3x} + \pi_{4x} - \sqrt{3}(\pi_{1y} + \pi_{2y} + \pi_{3y} + \pi_{4y})]$
	$d_{x^2-y^2}$		$\frac{1}{4}[\pi_{1y} + \pi_{2y} + \pi_{3y} + \pi_{4y} + \sqrt{3}(\pi_{1x} + \pi_{2x} + \pi_{3x} + \pi_{4x})]$
T_2	p_x, d_{yz}	$\frac{1}{2}(\sigma_1 + \sigma_3 - \sigma_2 - \sigma_4)$	$\frac{1}{4}[\pi_{4x} + \pi_{2x} - \pi_{1x} - \pi_{3x} + \sqrt{3}(\pi_{4y} + \pi_{2y} - \pi_{1y} - \pi_{3y})]$
	p_y, d_{xz}	$\frac{1}{2}(\sigma_1 + \sigma_2 - \sigma_3 - \sigma_4)$	$\frac{1}{4}[\pi_{1x} + \pi_{2x} - \pi_{3x} - \pi_{4x}]$
	p_z, d_{xy}	$\frac{1}{2}(\sigma_1 + \sigma_4 - \sigma_2 - \sigma_3)$	$\frac{1}{4}[\pi_{3x} + \pi_{2x} - \pi_{1x} - \pi_{4x} + \sqrt{3}(\pi_{4y} + \pi_{1y} - \pi_{2y} - \pi_{3y})]$
T_1			$\frac{1}{4}[\pi_{2y} + \pi_{4y} - \pi_{3y} - \pi_{1y} + \sqrt{3}(\pi_{1x} + \pi_{3x} - \pi_{2x} - \pi_{4x})]$
			$\frac{1}{4}[\pi_{1y} + \pi_{2y} - \pi_{3y} - \pi_{4y}]$
			$\frac{1}{4}[\pi_{2y} + \pi_{3y} - \pi_{1y} - \pi_{4y} + \sqrt{3}(\pi_{3x} + \pi_{2x} - \pi_{1x} - \pi_{4x})]$

approximation of exchange and correlation is appropriate for a system with such large density fluctuations. However, this method has successfully been applied to a number of molecules with covalent bonds [9]. To improve upon the charge density to a large extent, spheres without nuclear charge can be introduced in the interstitial position, where the potential is spherically averaged instead of assigning a constant potential to this region [10,11]. The local potential approximation of exchange and correlation in Si as compared with screened exchange shows an error of approximately 15% in the self-energy while the error in exchange gap enhancement is 2-3% [12].

Our calculated one electron energy levels for Si, by MS X_α SCF method are indicated in Figure 3.2. The levels are filled according to the Pauli exclusion principle and are designated by the irreducible representation of the tetrahedral point group. The $2t_2$-level is the last filled level and $3a_1$ is the first empty state corresponding to the valence band and the conduction band edges, respectively. The energy difference between these two band edges, called the band gap, is found to be approximately 2.0 eV which is in fair agreement with the experimental value of 1.14 eV [13].

We tried to look at the band gap by changing the exchange parameter α. The value 0.72751 for α is taken from Schwartz [14]. The next two values were obtained by increasing α in

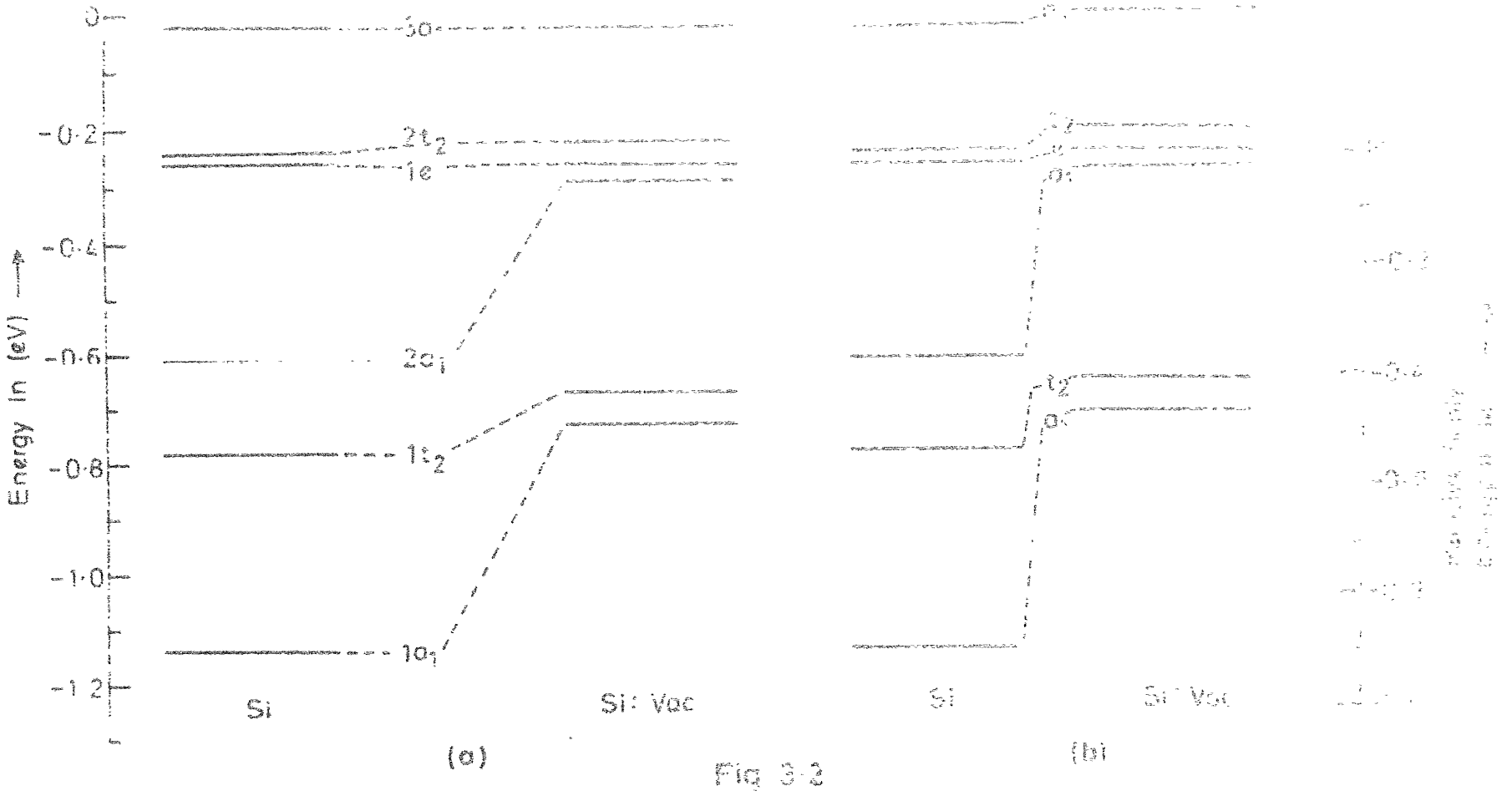

Fig 3·2

One electron energy level spectra for Si and a vacancy at the central Si - site in (a) absolute scale and (b) relative scale.

steps of 0.1. The band gap is found to increase and the levels in the valence band goes deeper as the value of α is increased. The charge distribution for different α in the different regions is indicated in Table 3.2. The corresponding one electron spectra is presented in Figure 3.3. In the process of calculation of Cartling et.al. [3],four interstitial spheres were introduced in addition to the five Si spheres. There were 12 hydrogen atoms to saturate the dangling bonds. In the present calculation neutral Si atoms are put together to form the cluster and hence the charge on the Watson sphere was set at zero.Table 3.2 points that

TABLE 3.2

Charge Distribution in Si for the Different Exchange Parameters

Region	α=0.72751	α =0.82751	α=0.92751	Cartling[3]
Extramolecular	2.5876	1.2537	1.7870	0.19
Central ion	12.9365	12.4702	12.9573	13.2
Ligand ion	11.6007	13.7056	12.6590	12.3
Inter sphere	8.0695	1.4505	4.6163	8.39

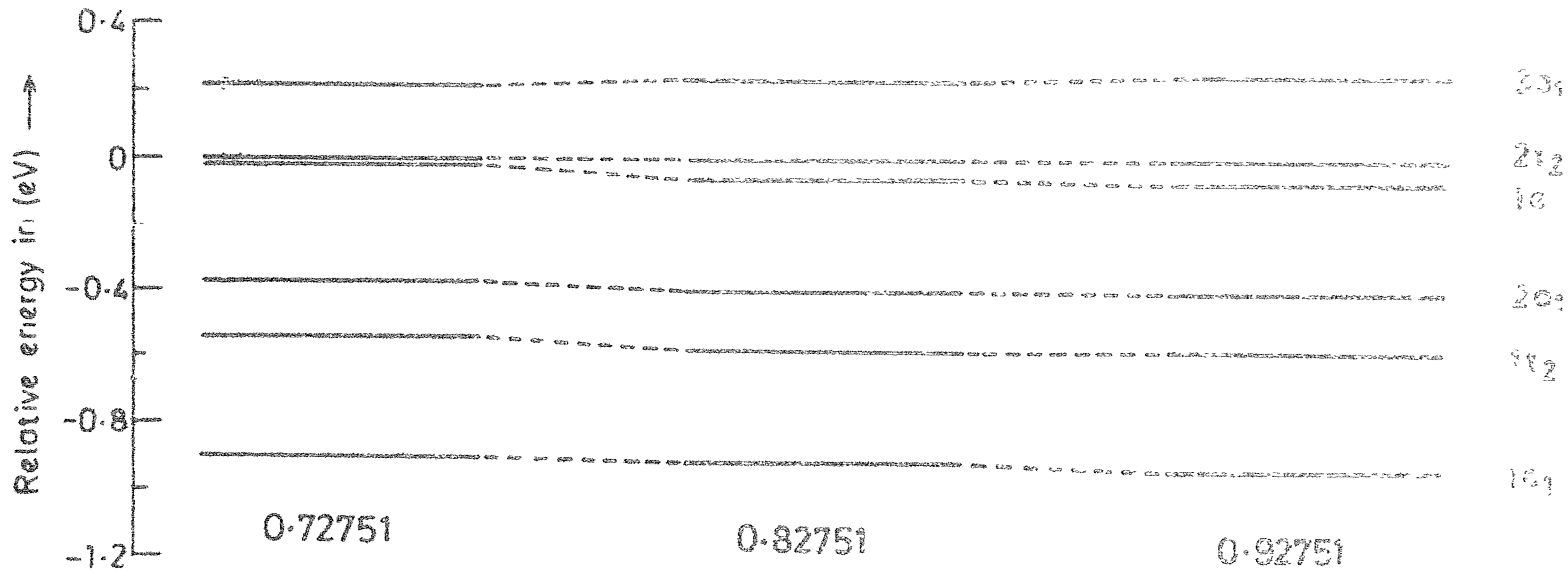

Fig. 3·3

The variation of one electron energy spectra of Si with the different exchange parameter α.

the charge on the central ion is nearly the same. This shows that the central ion charge is not affected much for a slight change in the boundary condition, after the self consistency has been achieved.

A vacancy is then created by removing the central Si atom. It is seen that the t_2-level moves into the band gap. This is because of breaking of bonds between the central atomic site and its neighbours. So this $2t_2$-level in the band gap of Si spectrum is associated with the broken bonds at the vacancy site. An impurity may be inserted in the vacancy to study the other defects in the sample. A simple argument for why the a_1-state ought to be lower than the t_2-state [15] is illustrated in Figure 3.4. Here the atomic valence s and p states are considered to interact with the a_1- and t_2-states of the lattice vacancy into which the impurity is inserted [5]. In the present calculation a shallow impurity level in the gap at E_v + 0.55 eV is obtained. The results are shown both in absolute and relative scale in Figure 3.2. In the relative scale the upper most completely filled levels are matched together. The $1a_1$- and $2a_1$- levels move up towards the valence band edge with the e-level forming the valence band edge. In this five atom cluster no effect of dangling bonds was considered.

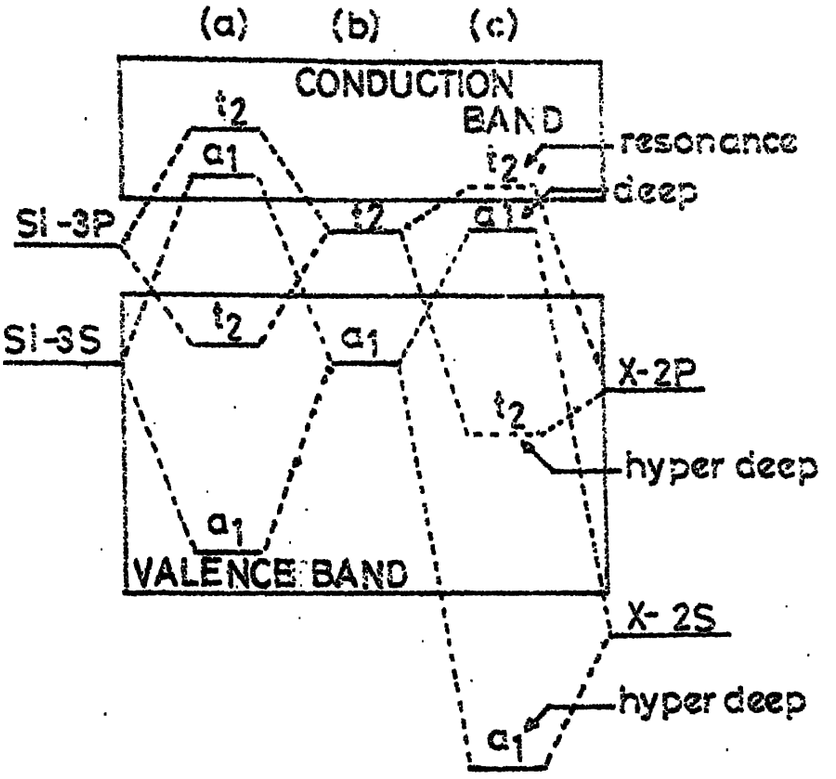

Fig.3.4

Schematic representation of vacancy-impurity(and vacancy-silicon interactions where(a) represents crystalline silicon,(b)the lattice vacancy,and(c) the substitutional impurity.

III.4 Defects in Indium Phosphide

The electronic structure of transition metal (TM) impurities in semiconductors are of much interest both from physical and technological points of view. These dopants are introduced deliberately as charge compensators. The 3d transition metal elements form localized states, called the deep impurity state, in the band gap of the host semiconductor. These states play an important role in modifying the electronic properties of these semiconductors. For example, Cr makes GaAs semi-insulating and Fe plays a similar role in InP. Cr doped GaAs is used as semi-insulating substrate for epitaxial growths and also in devices like field effect transistors and photoconductors. The TM doped InP have a very promising technological future since the devices made out of them are much faster than those made out of Si.

A battery of experimental tools such as electron paramagnetic resonance (EPR), luminescence, transient capacitance etc. are employed to study the TM impurities in semi-conductors [16]. But the results are difficult to analyze if no accurate energy level structures are available. The effective mass theory rightly accounts for the shallow impurity levels in the band gap but there is no such theory to take care of deep levels and the detailed understanding of TM impurity states has continued to elude us.

In this part of the thesis we discuss the electronic structures of the neutral, unrelaxed, transition metal impurities like Cr, Mn, Fe, Co, Ni and Cu in InP. It is well known from EPR experiments [16] that the TM atom occupies the cation site (In-site), due to chemical constraints, in III-V semiconductors with a minimal of lattice distortion. The case of single In vacancy in InP is also taken up.

The exchange parameters used in the MS X_α SCF calculations are due to Schwartz [14]. Table 3.3 gives the α-values of the host atoms and the impurity atoms.

TABLE 3.3

α -Values of the Atoms Used in Our Calculation [14]

Atom	α
In	0.70000
P	0.72620
Cr	0.71352
Mn	0.71279
Fe	0.71151
Co	0.71018
Ni	0.70897
Cu	0.70697

The bond length of InP is 4.08 a.u. [17] and so the central ion, ligand ion and the Watson sphere radii were fixed at 3.164 (muffin-tin radius of In [18]), 1.916 and 6.996 a.u., respectively.

To start with,we consider the 'perfect cluster' where the In is placed at the center of the cluster with four neighbouring P atoms placed in a tetrahedral configuration. Then a vacancy is created by removing the central In atom but without letting the P atoms to relax. The TM elements are put one after the other to study the electronic structure of the 'defect cluster'. There are 3 valence electrons available from In and 5 from each of the P atoms. Since each of the four In-P bonds uses two electrons of opposite spins, a net charge of (3 +4x5 -8=) 15 electrons is pushed up to the Watson sphere to maintain the electrical neutrality of the cluster. The uppermost filled level and the lowermost empty level correspond to the valence and conduction band edges. Since the bonding of the P atoms of the cluster with the second nearest neighbour remain unchanged for any substitutional impurity considered within the cluster, the charge on the Watson sphere was kept constant to simulate the solid.

The calculated energy level spectra of the clusters are shown in Figures 3.5 and 3.6, respectively. The clusters possess a tetrahedral symmetry and hence the

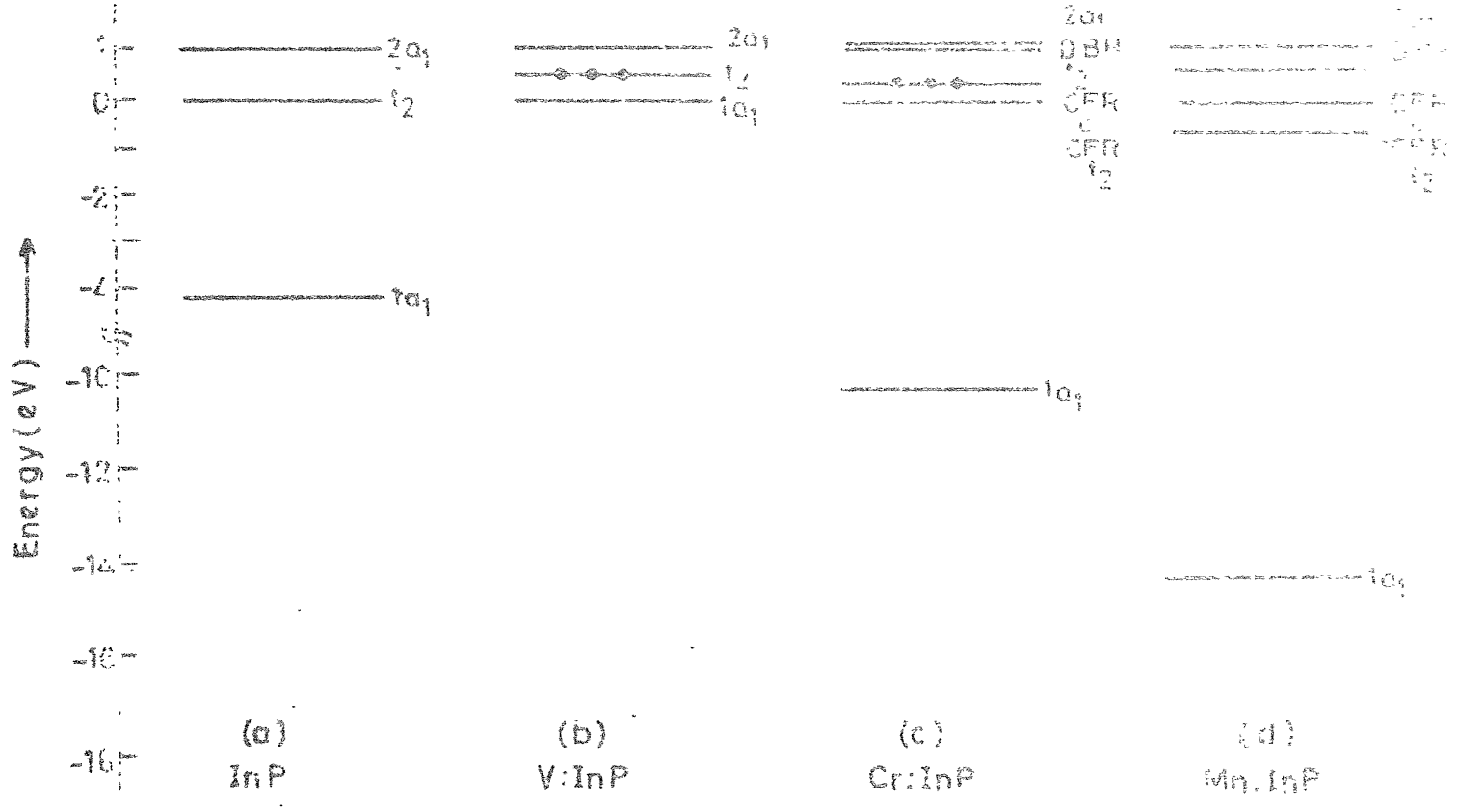

Fig. 3·5

Relative energy in eV for the different transition metal impurities in InP.

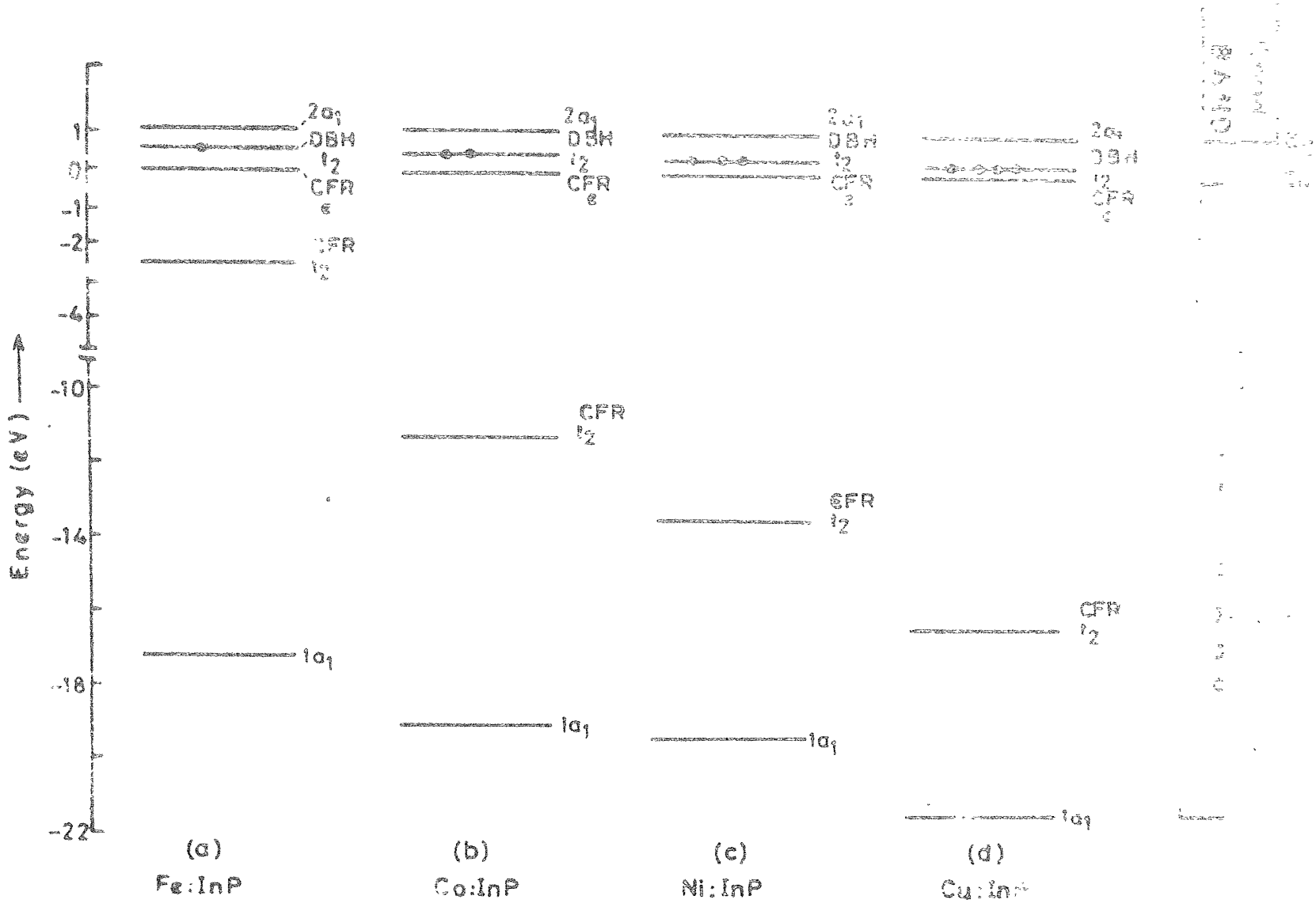

Fig. 3·6

Relative energy in eV for different transition metal impurities in InP.

energy levels are designated by the irreducible representation of the tetrahedral point group T_d. The energy levels are filled up in accordance with the Pauli exclusion principle. Figure 3.5(a) correspond to InP where the last filled level is of t_2-symmetry and the first empty level is of a_1-symmetry. This symmetry is also found in the bulk band structure calculations where the top of the valence band is p-like and the bottom of the conduction band is s-like. The difference in energy between these two levels, called the band gap, is 1.08 eV and is in reasonably good agreement with the experimental value of 1.35 eV [13]. It is important to note that the MS X_α SCF method, in which no empirical parameters are employed, is able to reproduce features of the bulk band structure. Similar accuracy has been reported by Hemstreet [7], Fazzio et.al. [19] and De Leo et al. [5]. This may be contrasted with the molecular orbital approaches [20-21], where the band gap is over estimated by atleast a factor of two inspite of empirical parametrization.

We now create a vacancy at the In-site. Figure 3.5(b) shows that the t_2-level moves up into the band gap from the valence band edge. This t_2-state is usually designated by t_2^{DBH}, the vacancy dangling bond hybrid. This six-fold degenerate t_2-level contains just three electrons as the three valence electrons are lost by the removal of central In

atom. This t_2-level is an acceptor level in the gap associated with the broken bonds due to creation of vacancy. The energy difference between the t_2^{DBH} level and the valence band edge is 0.4 eV. Theoretical calculations of vacancy in other semiconductors predict a partially occupied t_2^{DBH} level in the gap [5,19].

The vacancy created by the removal of In is now filled by Cr. The energy levels are shown in Figure 3.5(c). The atomic 3d-orbital of the TM is split due to the tetrahedral environment into two crystal field resonance (CFR) levels, t_2^{CFR} and e^{CFR}. This bonding t_2^{CFR} has an anti-bonding counterpart in the form of t_2^{DBH}. At the high Z-limit, where the atomic 3d levels lie far deeper than the anion derived host t_2 orbitals, there is little interaction between them. Hence the p-like anti-bonding t_2^{DBH} orbital is just above valence band maximum. We can see the appearance of these CFR levels in Cr doped InP (Figure 3.5(c)). Four of the six electrons of the Cr impurity are used up in healing the broken bonds created due to vacancy. The bonding orbital is now expected to acquire a s-d character in contrast to the s-p bonding in InP. But this is not very clear from our calculations. The partially filled e^{CFR} moves into the band gap while t_2^{CFR} is at the valence band edge. The unoccupied t_2^{DBH} level is pushed up almost into the conduction band. The e-level in the gap is at

E_v + 0.41 eV and the crystal field splitting is 0.68 eV (difference between partially filled e-level and the unoccupied t_2-level). The t_2^{DBH} level is just 0.14 eV below the unoccupied $2a_1$- level at the bottom of the conduction band.

When Cr is replaced by Mn, the unfilled e^{CFR} levels get filled and is pulled down to form the valence band edge (Figure 3.5(d)). The empty t_2^{DBH} level is at E_v + 0.65 eV.

Mn is then replaced by Fe. Figure 3.6(a) shows the $1a_1$- and the t_2^{CFR} levels to be pulled further down in the valence band compared to that of Mn. The t_2^{DBH} level in the band gap contains just one electron. The e^{CFR} and t_2^{DBH} energy difference is 0.54 eV, and the t_2^{DBH} and $2a_1$- are separated by 0.54 eV. So the t_2^{DBH} level lies exactly in the middle of the band gap and this provides a clue to the semi-insulating nature of Fe in InP [22].

The replacement of Fe by Co, Ni and Cu shows a monotonic trend in the energy level structure. Comparing Figures 3.6 (a,b,c,d) one finds that the energy difference between the two levels e^{CFR}- and $2a_1$- is almost same in all the cases. The occupation of t_2^{DBH} level increases from one to four as one goes from Fe to Cu. The $1a_1$- and t_2^{CFR} levels go deeper as the atomic number Z increases due to the increasingly attractive potential of the heavier TM impurities. The other notable feature is the gradual

change in position of the t_2^{DBH} level in the band gap. The energy difference between the e^{CFR}- and t_2^{DBH} level is 0.50 eV for Co while that for Ni and Cu are 0.41 and 0.30 eV, respectively. This shows that Cu is a shallow acceptor while Fe is a deep level. In the relative energy scale the position of the e^{CFR} level is found to be fixed. The e^{CFR} level forms a σ-bond with the second nearest neighbour. Our cluster does not have In as the second nearest neighbours. So there is no stabilizing mechanism in our calculation for e^{CFR} level. Hence it does not get pulled down in energy as opposed to a_1- and t_2^{CFR} levels.

A brief survey of other cluster calculations is worthwhile at this juncture. The study of TM impurities in Si [7,23], GaAs [19,24] and GaP [25] shows a similar trend as above the t_2^{DBH} level in the gap.

De Leo et.al. [5] have shown that the electronic structures appropriate of the Si 16 cluster are closely similar to those of the smaller Si 4 cluster. In fact there is very little change in a_1- and t_2- state positions relative to each other and valence band maxima in going from Si 4 to Si 16. A first principle calculation of Fe in InP [22] also predicts the impurity level (E_v + 0.7 eV) to be at the mid gap (E_g = 1.4 eV) which is consistent with our calculation (E_v + 0.54 eV with E_g = 1.08 eV). This proves that cluster truncation effects do not alter the electronic structure of

Fe in InP significantly. It provides confidence in our calculations.

Figure 3.7 shows the charge residing on the central ion, as obtained by MS X_αSCF calculation for any energy level (a measure of localization), for e^{CFR} and t_2^{DBH} states. When the localization is plotted against the atomic number, it becomes evident that the impurity levels of Cr have more atomic character than the other TM impurities. For example, the t_2^{DBH} level in Cr has a localization of 40% as contrasted to 2% for Cu. The reason is that for Cu, t_2^{DBH} is valence band like and hence the wave function may be expanded in terms of valence Bloch functions using effective mass theory. Interestingly, Fe marks the transition point. The localization of the wave function for t_2^{DBH} shows an abrupt variation at Fe.

Finally, Figure 3.8 shows the charge transferred from the central ion region to the ligands and/or into the intersphere region. The charge lost by the TM goes mainly to the intersphere region (30%) and less to the nearest neighbour P atoms (20%). The charge transferred to the P atoms from Fe, Co, Ni is constant ($\simeq$17.5%). This is in conformity with electronegativity (X) consideration. Fe, Co and Ni have the same electronegativity (X = 1.8) while P has a higher electronegativity (X = 2.1). Similarly, Mn which has X= 1.5 transfers a larger amount (25%) of its

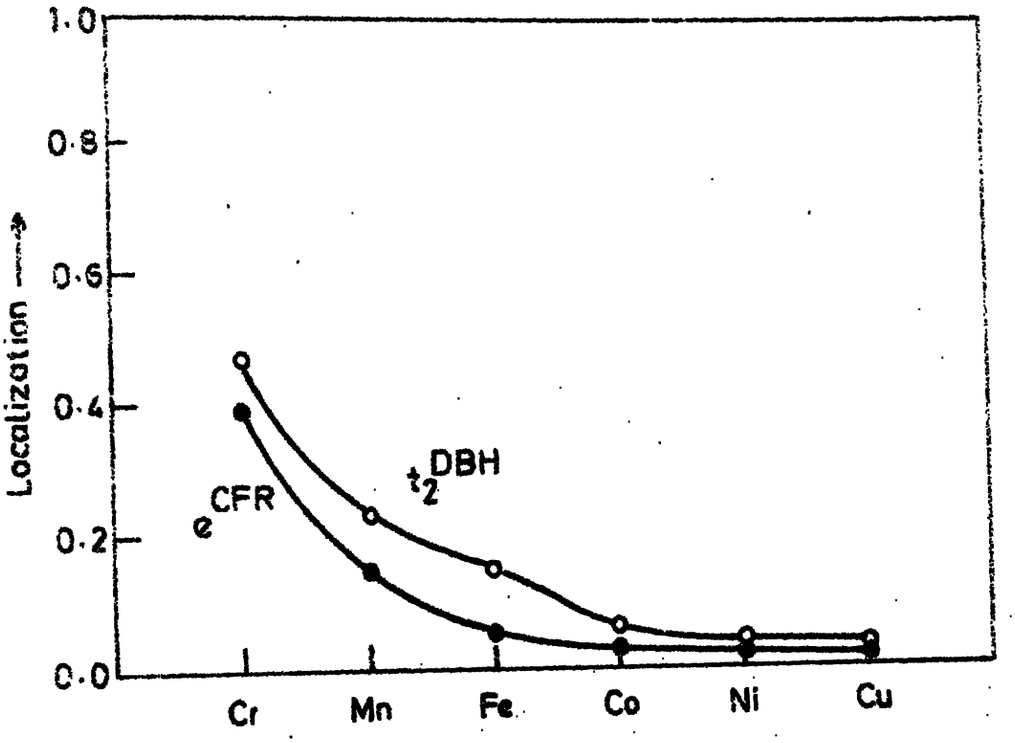

Fig. 3·7

Variation of localization for the different transition metal impurities in InP in arbitrary units.

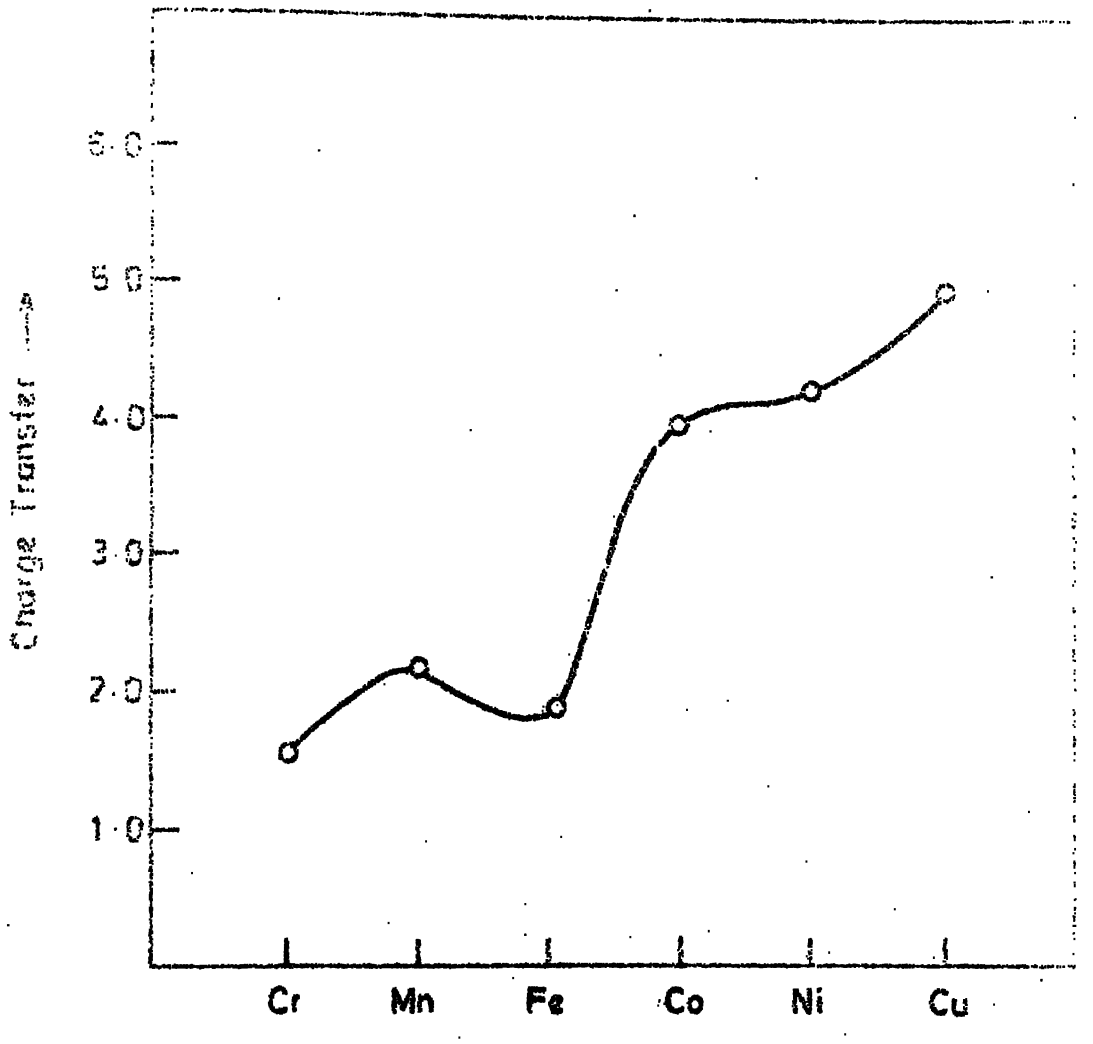

Fig. 3-8

Charge Transfer from the transition metal impurities in InP.

charge to P. This shows the itinerant character of the non-core electrons and it is interesting that even a simple cluster as ours could bring this out so well. Similar trends are shown by other TM impurities [22].

The charge transfer does not show a monotonic behaviour. It is small for Fe but larger for two neighbouring elements Mn and Co. This is certainly in conformity with the semi-insulating behaviour of Fe in InP. Our energy level calculations corroborate with this fact. The t_2^{DBH} level is in the mid-gap for Fe thus exhibiting extreme localization. The same t_2^{DBH} level is closer to conduction band edge for Mn and to the valence band edge for Co. They thus hybridize with the host and lose some of their charge.

In recent years careful electrical studies on Fe and Co doped InP have been conducted. The resistivity of Fe doped InP is $\geq 10^6$ Ω cm, while it is in the range 10^3-10^5 Ω cm for Co doped InP. This we attribute to the fact that the t_2^{DBH} level is in the mid-gap and hence highly localized for Fe while it is closer to the valence band edge for Co. Indeed, it is experimentally found that the main deep level is at E_v + 0.75 eV for Fe [26], while it is at E_v + 0.32 eV [27] for Co. Experiments show one more level in the band gap. These are not interpreted by our theory and we feel that these may be associated with the different charge states of Fe and Co.

We conclude by stating that we have successfully identified the main deep levels of Fe and Co doped InP and interpreted the basic features of their electronic structure and properties.

III.5 Different Charge States of Fe in InP

After finding out the electronic structure of TM impurities and comparing our results for Fe with other theoretical [22] and experimental results [26], we conclude that Fe makes InP semi-insulating. The obvious question arises what happens when Fe is present as an impurity in InP in different charge states? We shall now study the electronic level structure for the different charge states of Fe.

The central ion is linked with the ligands by sp^3 hybridization in these semiconductors. The different charge states correspond to different number of electrons in the outermost shell of the atom or ion. Keeping the sp^3 hybridization in mind, we designate the different charge states of Fe in InP as Fe^{1+} $(3d^7 4s^2)$, $Fe^{2+}(3d^6 4s^2)$, and Fe^{3+} $(3d^5 4s^2)$, respectively, e.g.

$$Fe(3d^7 4s^2) = Fe(3d^5 4s 4p^3) = Fe(3d^{6-5}) = Fe^{1+}$$

$$Fe(3d^5 4s^2) = Fe(3d^3 4s 4p^3) = Fe(3d^{6-3}) = Fe^{3+}$$

The notation $3d^{n+}$ merely implies that there are 6-n 3d wave functions centered on Fe. Similar nomenclature has been used for different charge states of Cr in GaAs [28,29].

The theoretical one electron spectrum of the different charge states of Fe in InP, calculated by us by MS $X\alpha$SCF method, is shown in Figure 3.9. The 3d level of Fe breaks up into e^{CFR} and t_2^{CFR} levels. The e^{CFR} level forms the valence band edge for all the three charge states of Fe in InP. The t_2^{DBH} level, arising due to the broken bonds, in the band gap contains 2,1 and 0 electrons for Fe^{1+}, Fe^{2+}, and Fe^{3+}, respectively. This level moves towards the valence band edge with increase in population and its position in the gap is at E_v + 0.97, E_v + 0.54 and E_v + 0.20 eV, respectively (Figure 3.9).

The normalized population density analysis (Figure 3.10) shows the localization, in arbitrary units, of t_2^{DBH} and e^{CFR} levels. This trend is similar to that shown by other TM elements used as dopants in III-V semiconductors [7,19,24,25] .

The semi-insulating behaviour for neutral Fe in InP has already been pointed out [22,30]. The study of the charge distribution in the different regions of the cluster (Table 3.4), shows a decrease in the central ion charge in going from Fe^{2+} to Fe^{1+} or Fe^{3+}. The ligand charge is found to remain almost constant. The charge transfer

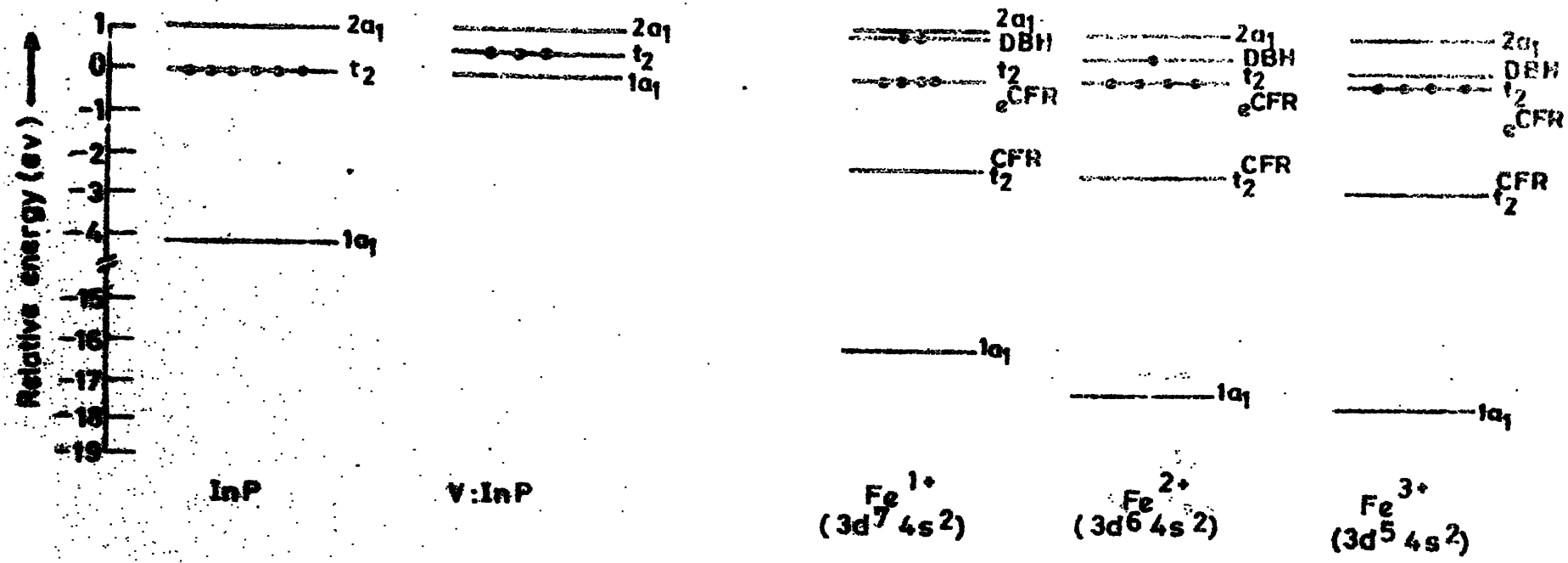

Fig 3-9

Relative energy in eV for pure InP, a vacancy at the In site and different charge states of Fe in InP. The filled circles denote the number of electrons in the particular level.

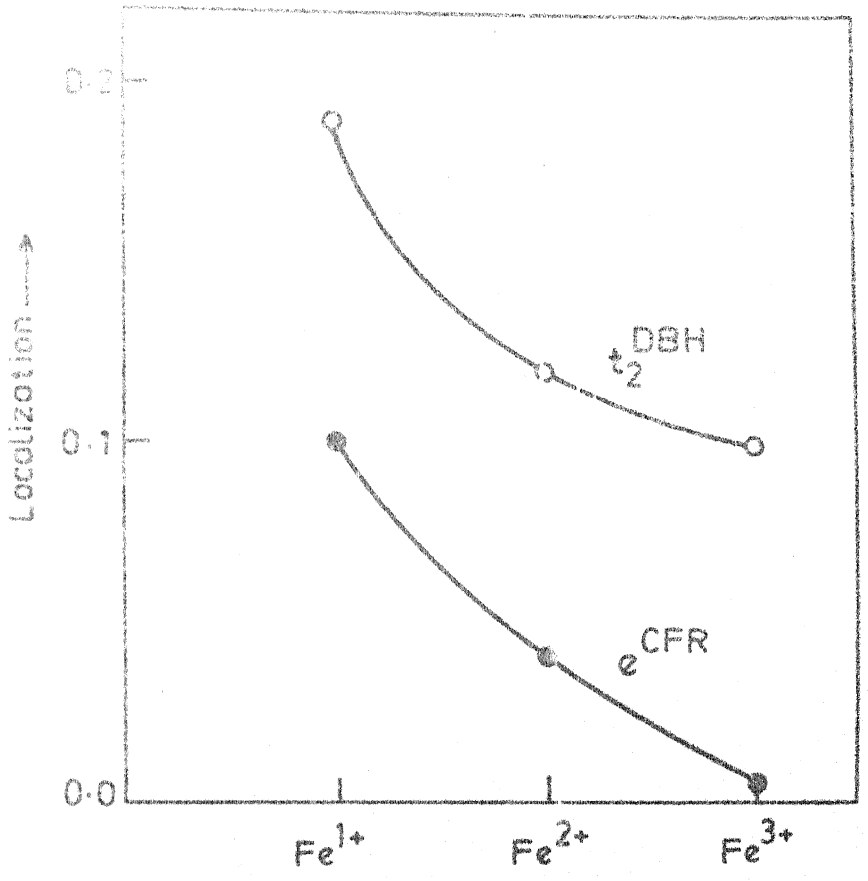

Fig. 3·10

Variation of localization for the different charge states of Fe in InP in arbitrary units.

from the central Fe atom to the nearest P atom is approximately constant (~18.5%) in all the three cases. The extra charge goes to the intersphere region.

TABLE 3.4

Charge Distribution for the Different Charge States of Fe in InP

Region	Fe^{1+}	Fe^{2+}	Fe^{3+}
Extramolecular	0.044	0.017	0.036
Central ion	20.908	24.234	20.063
Ligand ion	11.050	11.103	11.530
Intersphere	4.648	2.334	3.778

This proves that localization in Fe^{2+} is more than Fe^{1+} or Fe^{3+}.

In addition to these, the charge density at the origin was also determined and used to calculate the isomer shifts of the charge states Fe^{1+}, Fe^{2+} and Fe^{3+} of Fe in InP. As yet no Mössbauer data of Fe in InP is available. Table 3.5 shows the isomer shift of different charge states of Fe in InP calculated by us along with the experimental values of isomer shifts of Fe in various hosts

TABLE 3.5

Isomer Shift of Fe in Various Hosts

Theoretical (present calculation)		Experimental			
Fe^{1+} (in InP)	0.63	Co	0.04	Ge	0.331
Fe^{2+} (in InP)	0.37	Ni	0.02	In	0.410
Fe^{3+} (in InP)	0.62	Cu	0.225	Si	0.505

The theoretical as well as the experimental values are relative to metallic iron. The general trend is that for metallic hosts which are in the neighbourhood of Fe in the periodic table, the isomer shift is small compared to the case of semiconductors like Ge, In and Si. This is because the charge density distribution for Co and Ni should almost be identical to that of Fe because of their proximity in the periodic table. The semi-insulating nature of InP has already been pointed out with the t_2^{DBH}-level lying in the middle of the band gap. The charge on the central ion for Fe^{2+} (Table 3.4) shows that Fe retains more of its original atomic character. We know from neutron diffraction experiments that in the metallic iron, the iron charge distribution is substantially similar to its atomic counterpart [31]. Hence the isomer shift of Fe^{2+} in InP with respect to metallic iron would be expected to be small as

compared to Fe in In and Si. For the other two charge states, Fe^{1+} and Fe^{3+}, the t_2^{DBH} is either closer to the conduction band or the valence band edge. The wave functions in these two cases can then be expanded in terms of conduction band and valence band Bloch states. These Bloch states have mostly InP character and only marginally metallic iron character. Hence the isomer shift is large. We can look at it somewhat differently. A large amount of charge goes out of the central-ion (see Table 3.4) thus decreasing their contribution of charge density at the origin. Hence the isomer shift increases depending on the charge given out.

The low energy photoconductivity experiments [32] find the Fe^{1+} to Fe^{2+} transitions at 0.34 eV which is in excellent agreement with our calculated result of 0.36 eV. However, the Fe^{2+} to Fe^{3+} transition has an experimental value of 0.64 eV which is in contrast to our value of 0.33 eV. We expect that the detailed discrepancies may be removed by expanding the cluster to the second nearest neighbour of the impurity. An increase in the size of the cluster will no doubt change the band gap [5,33], but the general trend of the electronic levels is expected to remain identical. However, experiments like Hall effect and deep level transient spectroscopy [27] indicate additional

deep levels both in Fe and Co doped InP when the samples are subjected to heat treatment at 350°C for 1 minute. We feel that only a spin unrestricted calculation can lead to more than one state in the gap.

To the best of our knowledge, this is the first attempt made to understand the detailed electronic structure of the different charge states of Fe in InP. The above general agreement with the experimental data seem to be promising. We expect that calculated isomer shift results will stimulate further experimental activity in this area.

III.6 Electronic Structures of Substitutional Alkali-Metals in InP

The interaction of the alkali-metal impurities with defect dangling bonds in semiconductors is a subject of current interest and controversy. The importance of understanding the hydrogen vacancy interaction is clearly suggested by simple chemical reasoning: The vacancy or other defect dangling bonds, associated with defect electrical activity, could be passivated by appropriately located hydrogen impurities. In fact there is experimental evidence for the neutralization by atomic hydrogen dangling bond related electrical activity in Si [34]. This effect has importance in solar cell and electronic device technology. Such chemical reasoning and observations therefore suggest the following question: Can other group-I impurities with their characteristic

single unpaired s-electrons, also passivate defect-related dangling bonds in other semiconductors?

Alkali-metals are normally observed in semiconductors at the tetrahedral interstitial site [35], and when located there it is well understood. In irradiated material, however, impurities could be trapped at lattice vacancies. Therefore, one might expect to find a variety of alkali-metal-vacancy complexes. Experiments suggest the existance of alkali-metal-vacancy and other alkali-metal defect in complexes of Si[34]. As yet no experimental data for alkali-metal-vacancy complexes in InP exists.

We proceed here to explore these questions of electrical activity and dangling bond passivation by calculating the single particle electronic structures of substitutional Li, Na, and K in InP. Tetrahedral symmetry is preserved in all cases in these calculations.

According to the model proposed by Bernholc et.al.[36], dealing with Group-I substitutional impurities in Si, the group-I valence s-states tend to repair the broken a_1-symmetry dangling-bond combinations associated with the lattice vacancy. Lacking a 'p' valence electron, however, the t_2 electronic structure of the vacancy will tend to remain intact.

The electronic structures for the substitutional alkali impurities, Li, Na, and K, shown in Figure 3.11, have

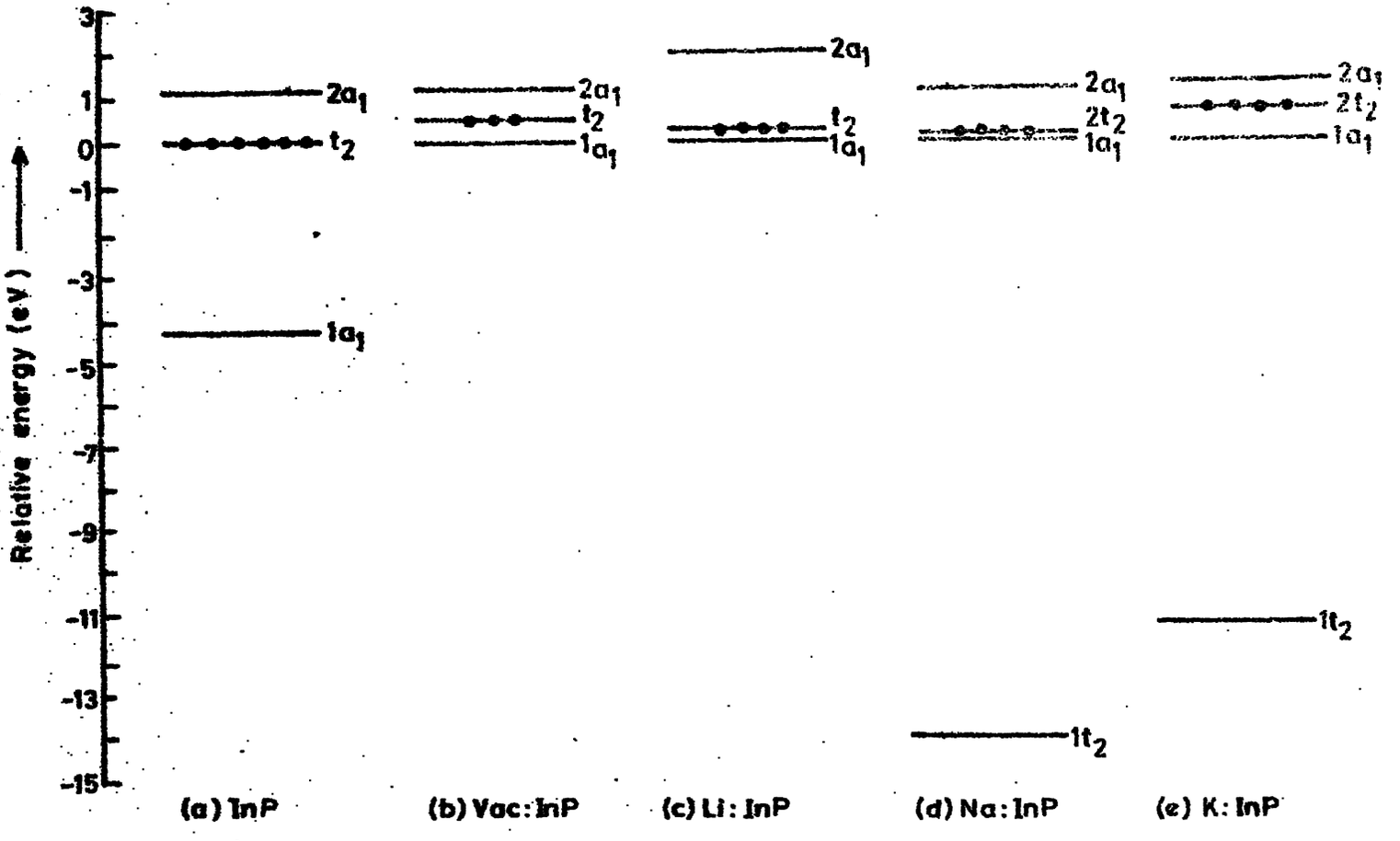

Fig. 3.11

Relative energy in eV for pure InP, a vacancy at the In-site and alkali-metal impurities like Li, Na and K in InP. The filled circles denote the number of electrons in the particular state.

certain similarities. We find here a vacancy like t_2-state in the gap which is occupied by four electrons. This, therefore, is similar to the case of a vacancy (Fig.3.11(b)) at the In-site. The extra electron in the t_2-gap state, as compared to the vacancy case, is provided by the s electron of the alkali-metals. The $1a_1$- state forms the valence band edge as in the vacancy case. This is in contrast to the $1a_1$-state in pure InP which is Bloch like. The position of t_2-gap levels are at $E_v + 0.4$, $E_v + 0.29$, $E_v + 0.14$, and $E_v + 0.71$ eV, for a vacancy at the In site. and respectively with Li, Na, K as impurities.

De Leo et al. [5] proposed a simple model for the alkali-metal impurity in Si , showing the change/shifts in the a_1- and t_2- levels (Figure 3.12). The computational results suggest that there is only a relatively weak interaction between the atomic valence ns and np states. These interactions are, therefore, similar to those of the vacancy-dangling-bond. The alkali-metal core states being substantially deeper, hardly play any role in the alkali-metal-vacancy interaction. Physically, we say that the defect state has been 'pinned' in the gap. If the impurity had introduced a near band gap 'p' state, then we would have expected to find the gap swept clean of the t_2 states as the impurity 'p' and vacancy t_2-states interacted [37,38]. Instead, we find that the vacancy t_2 state remains almost intact.

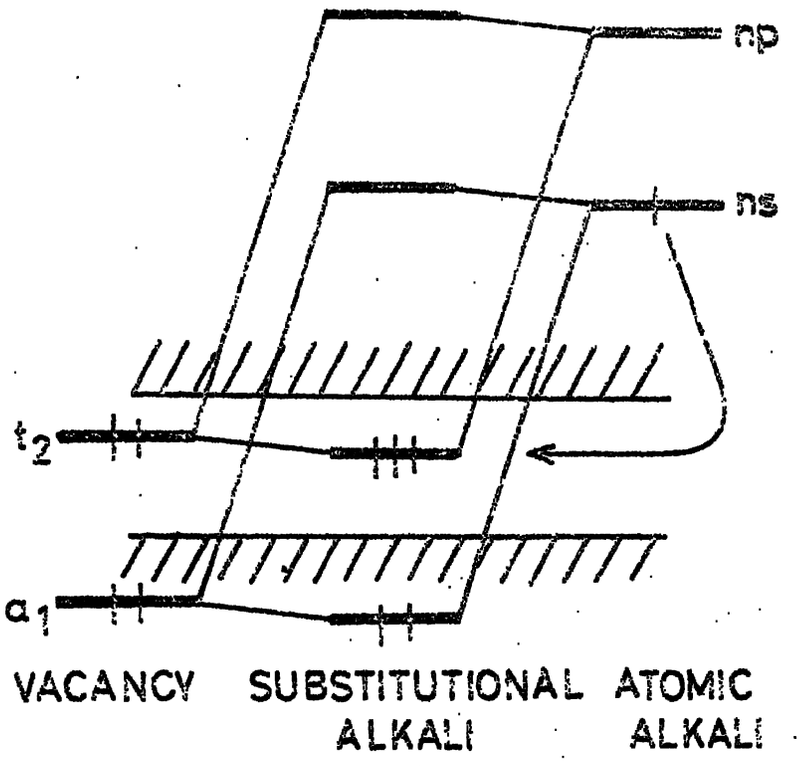

Fig.3·12

Ligand-field model for the electronic structure of the substitutional alkali-metal impurities in terms of the interactions between the vacancy orbitals and the alkali-metal-atom orbitals.

Table 3.6 shows the charge distribution in the different regions of the cluster. The charge on the ligands is almost constant for the different alkali-metals as impurities. The charges on Li and Na indicate that they tend to retain their atomic character. A major part of the charge transferred from K goes to the intersphere region. The intersphere charge increases as one goes from Li to K, through Na.

TABLE 3.6

The Total Electronic Charge in the Different Regions of the Cluster with Alkali-Metals as Impurities

Region	Li:InP	Na:InP	K:InP
Extra molecular	0.036	0.037	0.028
Central ion	3.038	10.173	15.099
Ligand ion	11.165	11.160	11.461
Inter sphere	0.226	1.098	3.029

The electronic structure and the charge distribution suggest that these impurities would not passivate the vacancy dangling bonds. In fact, the impurity system remain electrically active as a multiple donor.

REFERENCES

1. R.P.Messmer and G.D.Watkins, 1970, Phys.Rev.Lett. 25, 656.

2. F.P.Larkin, 1971, J. Phys. C 4, 3065, 3077.

3. B.Cartling, B.Ross and U.Wahlgren, 1973, Chem.Phys.Lett., 51, 380.

4. B.Cartling, 1975, J. Phys. C 8, 317, 3183.

5. Gary G.De Leo, W.B.Fowler and G.D.Watkins, 1984, Phys. Rev. B 29, 3193, 1819.

6. Gary G. De Leo, G.D.Watkins, W.B.Fowler, 1982 Phys. Rev. B 25, 4962, 4972.

7. L.A.Hemstreet, 1977, Phys. Rev. B. 15, 834.

8. T.Matsubara, 1982, The Structure and Properties of Matter (Springer-Verlag Berlin, Heidelberg, NY).

9. J.W.D.Connoly, H.Siegbahn, U.Belius and C.Nordling, 1973, J. Chem. Phys. 58, 4265.

10. J.Keller, 1971, J. Phys. C 4, L85.

11. A.R.Williams and J.Van W.Morgan, 1972, J. Phys. C 5, L293.

12. E.O.Kane, 1972, Phys. Rev. B5, 1493.

13. C.Kittel, 1977, Introduction to Solid State Physics, 5th Edition, p.210, Wiley Eastern Limited, New Delhi.

14. K.Schwartz, 1972, Phys. Rev. B 5, 2466.

15. G.B.Bachelet, G.B.Baraff and M.Schlüter, 1981, Phys. Rev. B 24, 4736.

16. U.Kaufmann and J.Schneider, 1980, Festkorper Probleme, 20, 8787.

17. H.F.Wolf, 1971, Semiconductors, Wiley Interscience, New York

18. V.L.Moruzzi, J.F.Janak and A.R.Williams, 1978, Calculated Electronic Properties of Metals, New York, Pergamon.

19. A.Fazzio, J.R.Liete, M.L.De Siqueira, 1979, J. Phys. C12, 513, 3469.

20. C.Weigel, D.Peak, J.W.Corbett, G.D.Watkins, and R.P. Messmer, 1973, Phys. Rev. B 8, 2096.

21. Vijay A.Singh, C.Weigel, J.W.Corbett and L.M.Roth, 1977, Phy. Stat. Sol. (b) 81, 637.

22. Vijay A.Singh and A.Zunger, 1983, Bull. Am. Phys. Soc., 28, 288.

23. R.Kleinhenz, Vijay A.Singh and J.W.Corbett 1979 (unpublished).

24. A.Fazzio and J.R.Liete, 1980, Phys. Rev. B 21, 4710.

25. N.Gemma, 1984, J. Phys. C 17, 2333.

26. S.Fung, R.J.Nicholas and R.A.Stradling, 1979, J. Phys. C 12, 5145.

27. M.S.Skolnick, R.G.Humphreys, P.R.Tapster, B.Cockayne and W.R.MacEwan, 1983, J. Phys. C 16, 7003.

28. J.J.Krebs and G.H.Stauss, 1977, Phys. Rev. B 15, 17.

29. L.A.Hemstreet and J.O.Dimmock, 1979, Phys.Rev. B 20, 1527.

30. P.K.Khowash, D.C.Khan and Vijay A.Singh (submitted).

31. W.Marshall and S.W.Lovesey, 1971, Theory of Thermal Neutron Scattering, Oxford, Clarendon Press.

32. L.Evas, A.W.Smith, P.J.Williams, B.Cockayne and W.R.MacEwam, 1981, J. Phys. C 14, 5036.

33. J.R.Liete, V.M.S.Gomes, L.V.C.Assali and L.M.R.Scolfaro, 1984, ICDS (Private communication).

34. J.L.Benton, C.J.Doherty, S.D.Ferris, D.L.Flamm, L.C.Kimerling and H.J.Leamy, 1980, Phys. Lett. 36, 670.

35. J.W.Corbett and G.D.Watkins, 1971, Radiation Effects in Semiconductors, Gordon and Breach, NY.

36. J.Bernholc, N.O.Lipari, S.T.Pantelides and M.Scheffler, 1982, Phys. Rev. B. 26, 5706.

37. HHP. Hialmarson, R.E.Allen, H.Buttner, and J.D.Dow, 1980, J. Vac. Sci. Technol. 17, 993.

38. H.P.Hialmarson, P.Vogl, D.J.Wolford and J.D.Dow, 1980,

CHAPTER IV

Conclusion

IV.1 Aim

The aim of the present work has been to study theoretically the electronic structure of a number of ionic, covalent and semiconductor solids, using MS X_α SCF method. The valence electron energy levels and the equilibrium charge distribution of all these systems have been analyzed to get informations on their bonding characteristics, optical properties and electrical conductivity.

The MS X_αSCF method considers a cluster scooped out of the solid and replaces the effect of the rest of the solid by putting proper charges on the boundary of the cluster. This is expected to simulate the localized physics of the solid to a good approximation. Hence the method is very suitable for the study of the bonding in the mixed ionic and covalent systems and the localization of the impurity levels in semiconductors.

IV.2 Achievements

We applied to MSX_αSCF method of calculation to systems like ionic solids (NaCl, LiF, NaF), perovskites (KMF_3 (M = Fe, Ni)), rutiles (MF_2 (M = Fe, Co, Ni, Zn)), metallic oxides (MgO, MnO, VO) and alloys (Fe-Te). Along with the SCF energies the charges within each atomic region

are also calculated. A charge transfer diagram was defined to get an understanding of the chemical bonding (ionic and/or covalent) in these systems. The 3d degenerate level in the cation breaks up into t_{2g} and e_g levels in the ligand field. This crystal field splitting, 10 Dq, was determined for all the crystals with 3d cation and compared with experiment wherever data were available. The transitions between two of the valence levels were calculated whenever we could locate the corresponding XPS or optical spectroscopic experimental data. Finally the Mössbauer isomer shifts were calculated for iron containing samples.

We started with some ionic solids, e.g. NaCl, NaF and LiF. The selfconsistent charge distribution study showed a transfer of charge from the central ion to the ligands along with some transfer to the interatomic region. This showed that these well known ionic compounds are not perfectly ionic but show a marginal covalent character. For NaCl the calculated charge distributions are in very good agreement with the experimental results. The energy levels of LiF and NaF have the characteristic that they bunch into two groups with predominantly F 2s and F 2p nature. The energy difference of the F 2s-like and F 2p-like states in LiF is 1.43 Ry as compared to the experimental result of 1.54 Ry obtained by X-ray photoelectron spectroscopy.

In the next stage the energy levels and the charge distributions were calculated for the fluorides and the oxides of different transition metals. The agreement of the energy difference of the F 2s like and F 2p like states in FeF_2, 1.36 Ry, with the XPS result 1.54 Ry was encouraging. The crystal field splitting, 10 Dq, has also been calculated for the transition metal fluorides. The Mg 2s and the Mg 2p levels were identified and their energy difference 2.85 Ry was found to be in fair agreement with the XPS data 2.38 Ry.

The Mössbauer isomer shifts in all the iron containing systems namely $KFeF_3$, FeF_2 and $Fe_{.4}Te_{.6}$ alloy were calculated and compared with the existing results from the experiments.

The first step towards the analysis of the covalent nature of the systems was to calculate the covalency parameter λ_σ from the coefficient of the ligand term in the extended eigen-function of upper most valence level. These values were matched with the λ_σ obtained from the analysis of the neutron diffraction and nuclear magnetic resonance experimental data in terms of the molecular orbital theory. We get satisfactory agreements for $KFeF_3$ and $KNiF_3$. For $KFeF_3$ our results are $\lambda_\sigma = 5.58\%$ as against the neutron diffraction result $\lambda_\sigma = 6.24\%$. For $KNiF_3$ they are 7.55% and 5.11% respectively. The value of λ_σ for MgO is 6.67 percent which is in good agreement with the ENDOR

value of 6.50 percent.

We then brought in the concept of pseudoatoms and calculated the charge transfer from and/or to these atoms and plot the charge transfer diagrams for all the solids studies by us. With the help of these diagrams we defined the measures of ionic bonding strength and covalent bonding strength for these systems. We showed that the natural state of the non-metallic solid is a mixed ionic-covalent state. In NaCl the ionic is the dominant bonding and covalent bonding is marginal whereas in FeF_2 the covalent bond strength is very large and ionic bonding is marginal. The transition metal perovskites and rutiles generally fall within these two limits. However, they are predominantly covalent. The oxides of transition metals also show very large values of covalent bond strength with different degrees of minor ionic character. MgO is an exception to this general character in that it has a small charge transfer from the anion to the cation. This type of charge transfer is typical of semiconductors and we have referred to it as inverse ionic character. MgO is known to behave as a semiconductor. Inverse ionic character along with large covalency was shown by all the semiconductors worked out by us, e.g. Si, InP and transition metal impurities in InP.

In the second part of the thesis MS X_αSCF method was applied to semiconductors, especially transition metal doped InP, with a view to study the localization of the levels within the band gap. The cluster model had been applied to the well known semiconductors, such as Si and GaAs. It was found that Cr makes GaAs semi-insulating. We expected that Fe plays a similar role in InP and worked out the selfconsistent field energy levels and their eigenfunctions. Our calculations did predict a highly localized impurity level for Fe in InP.

For the other transition metal impurities in InP we showed that the impurity level in the band gap moves closer to either valence band or conduction band edges. These states thus hybridize with the host and become delocalized as compared to Fe in InP. Very recent experiments on Fe and Co in InP confirms a higher localization of the former leading to a higher resistivity.

We also performed calculations on the different charge states of Fe in InP. We found that the t_2^{DBH} -levels arising due to broken bonds, is exactly in the middle of the band gap for neutral Fe, whereas it moves closer to the band edges for the other two charge states. The charge transfer is minimum for neutral Fe. The isomer shift for different charge states were calculated but unfortunately no experimental data are available to compare with. However, these results

also confirm that neutral Fe makes InP semiinsulating.

The electronic structure of the alkali metals as impurities in InP were also calculated. It was found out that they interact weakly with the host thus pinning the impurity level in the gap.

It is predicted that GaAs may soon supercede Si in technological importance. Since the devices made out of InP have proved to be much faster than those of Si, it is expected that InP is going to be a keen competitor to GaAs as a device material. Our work forms the theoretical basis for the analysis of the conductivity properties of transition metal doped in InP.

IV.3 Limitation of the Method

The cluster model is known to emphasize the localized physics. The long range effects may require clusters too large to be readily handled. Accurate values of bulk cohesive energies, work functions and many effects associated with the fermi surface are outside the scope of even a cluster as large as 50 atoms. Ideally a cluster study of a property should be supplemented with the investigation of the convergence of results as a function of cluster size. However, this makes the analysis very unwieldy and may not be within the computer economics of a researcher.

IV.4 Scope for Further Work

The present work concentrates on bonding characteristics and covalency in metallic compounds and deep levels in semiconductors. Since these are all localized physics, the consideration of nearest neighbours is justified. However, in semiconductors, the size of the cluster may be increased. By this the essential physics is not expected to change but the numerical values of the band gap will be in closer agreement with the experimental results. Hydrogen can be used, in the second nearest neighbour position, to saturate the dangling bonds, in semiconductors.

The muffin-tin form of potential can be improved by taking non-muffin-tin corrections as in DV X_α SCF method.

Apart from these, a spin polarized calculation, if performed, can lead to the actual magnetic state of the system. The magnetic form factor $f(\underline{k})$ can then be calculated by taking the Fourier transform of the difference of the two charge densities

$$f(\underline{k}) = \int dv \left[\rho_{\uparrow}(\underline{r}) - \rho_{\downarrow}(\underline{r})\right] e^{i\underline{k}.\underline{r}} \qquad (4.1)$$

The present activities of our group includes a spin polarized calculation for FeF_2. Also efforts are being made to extend the cluster to its second neighbours.

IV.5 Conclusions

We hope that the present work has extended our knowledge of the electronic structure of covalent solids and semiconductors with impurities. Quantitative measurements for the bonding characteristics have been developed for covalent solids and energy levels of the valence electrons have been determined forming the theoretical basis for optical studies. For semiconductors, the levels in the band gap with localized states have been studies in detail, interpreting photoelectric and electric conductivity.

PHY-[illegible] KHO THE